THESIS ON NATURAL AND EXACT SCIENCES B118

Selenization of Molybdenum as Contact Material in Solar Cells

LIINA KAUPMEES

TUT
PRESS

TALLINN UNIVERSITY OF TECHNOLOGY
Faculty of Chemistry and Materials Technology
Department of Materials Science
Chair of Semiconductor Materials Technology

Dissertation was accepted for the defence of the degree of Doctor of Philosophy in Natural and Exact Sciences on October 4, 2011.

Supervisor: Leading research scientist Mare Altosaar, Department of Materials Science, Tallinn University of Technology

Opponents: Dr. Alberto Bollero IMDEA Nanoscience, Ciudad Universitaria de Cantoblanco, Madrid

Dr. Ants Lõhmus, Institute of Physics, University of Tartu

Defence: December 1, 2011, at 14:00
Lecture hall: VII-226
Tallinn University of Technology, Ehitajate tee 5, Tallinn

Declaration:
Hereby I declare that this doctoral thesis, my original investigation and achievement, submitted for the doctoral degree at Tallinn University of Technology, has not been submitted for any academic degree.

/Liina Kaupmees/

ISSN 1406-4723
ISBN 978-9949-23-188-1 (publication)
ISBN 978-9949-23-189-8 (PDF)

LOODUS- JA TÄPPISTEADUSED B118

Molübdeeni kui päikesepatarei kontaktmaterjali seleniseerimine

LIINA KAUPMEES

TTÜ
KIRJASTUS

Table of Contents

LIST OF PUBLICATIONS

The present doctoral thesis is based on the following papers, which are referred to in the text by their Roman numerals.

I **L. Kaupmees**, M. Altosaar, O. Volobujeva, P. Barvinschi, "Study of Mo selenisation process on different Mo substrates". Thin-Film Compound Semiconductor Photovoltaics, 2009 MRS Spring Meeting, San Francisco, CA, April 13-17. Warrendale, PA, USA: Materials Research Society, 1165-M08-01. *Materials Research Society Symposium Proceedings* 1165 (2010) 289–294.

II **L. Kaupmees**, M. Altosaar, O. Volobujeva, T. Raadik, M. Grossberg, E Mellikov, M. Danilson, P. Barvinschi, "Isothermal and two-temperature-zone selenization of Mo layers". *Advances in Material Science and Engineering,* Accepted 6 October 2011, MS no. 345762, (see online: Articles in Press).

III O. Volobujeva, M. Altosaar, J. Raudoja, E. Mellikov, M. Grossberg, **L. Kaupmees**, P. Barvinsch, „SEM analysis and selenization of Cu–In alloy films produced by co-sputtering of metals". *Solar Energy Materials and Solar Cells* 93 (2009) 11 - 14.

VI M. Ganchev; **L. Kaupmees**; J. Iliyna; J. Raudoja; M. Altosaar; O. Volobujeva; E. Mellikov; T. Varema; H. Dikov, "Formation of $Cu_2ZnSnSe_4$ thin films by selenization of electrodeposited stacked binary alloy layers". Proceedigs of EMRS, Stasbourg, June 2009, *Energy Procedia* 2 (2010) 65–70.

V M. Ganchev, J. Iljina, **L. Kaupmees**, T. Raadik, O. Volobujeva, A. Mere, M. Altosaar, J. Raudoja, E. Mellikov, "Phase composition of selenized $Cu_2ZnSnSe_4$ thin flms determined by X-ray diffraction and Raman spectroscopy", *Thin Solid Films* 519 (2011) 7394–7398.

In Appendix A, copies of the papers are included.

Author's own contribution

The contribution by the author to the papers included in the thesis is as follows:

I Selenization of different origin of molybdenum substrates, analysis of $MoSe_2$ films, analysis of results and major part of writing.

II Selenization of Mo substrates, analysis of selenized Mo and Mo/Cu and Mo/In layers, analysis of results and major part of writing.

III Selenization of Mo/CuIn substrates, analysis of results and minor part of writing.

IV Selenization of electrochemically deposited Cu-Zn-Sn layers, analysis of CZTS layers (Spectrophotometer), analysis of results and minor part of writing.

V Selenization of electrochemically deposited Cu-Zn-Sn layers, analysis of results and minor part of writing.

List of abbreviations and symbols

PV	Photovoltaic
CIS (CISe)	Compound formed from Cu, In, Se; usually $CuInSe_2$
Si	Silicon
a-Si	Amorphous silicon
CIGS	Compound formed from Cu, In, Ga, Se, usually $Cu(In,Ga)Se_2$
CZTS	Compound formed from Cu, Zn, Sn, Se (S), usually $Cu_2ZnSnSe_4$
ITO	Indium tin oxide, In_2O_3:Sn
TCO	Transparent conducting oxide
ZSW	Zentrum für Sonnenenergie- und Wasserstoff-Forschung Baden-Württemberg
ED	Electrochemical deposition
SLG	Soda lime glass
CGS (CGSe)	Compound formed from Cu, Ga, Se; usually $CuGaSe_2$
HR-TEM	High-resolution transmission electron microscopy
TEM	Transmission electron microscopy
SEM	Scanning electron microscopy
EDX	Energy-dispersive X-ray analysis

XRD	X-ray diffraction
XPS	X-ray photoelectron spectroscopy
dc	Direct current
rf	Radio frequency
CVD	Chemical vapor deposition
XRF	X-ray fluorescence
I–V	Current-Voltage
CBD	Chemical bath deposition
CTO	Cadmium tin oxide
PLD	Pulsed laser deposition
DVT	Direct vapor transport method
T_{Sub}	Substrate temperature
η	Efficiency of a solar cell
FF	Fill Factor
J_{sc}	Short circuit current density
V_{oc}	Open circuit voltage
ppm	Parts per million, a way of quantifying small concentrations, usually mass
I-III-VI_2	Ternary compound, Cu, Ag, Au – In, Ga, Al – S, Se, Te
II-IV-V_2	Ternary compound, Zn, Cd - Sn, Ge, Si – As, P
I_2–II–IV–VI_4	Quaternary compound, Cu – Zn – Sn - Se(S)
VdW	Van der Waals
GW	Gigawatt
t	Time, duration
T_{sub}	Mo substrate temperature during the selenization
P_{Se}	Selenium pressure in the ampoule
T_{Se}	Temperature of Se zone

INTRODUCTION

Development of clean energy resources as an alternative to the fossil fuel has become one of the most important tasks assigned to the researchers engaged in modern science and technology in the 21st century. Among a wide variety of renewable energy sources, solar energy is the best alternative, suitable for meeting the energy demands of the modern society. In order to promote the use of photovoltaic (PV) devices, it is necessary to develop solar cells with low cost, high efficiency and that are less damaging to the environment.

The starting point of the research and development of solar cells was set by the discovery of the photovoltaic effect by the French experimental physicist Aléxandre Edmond Becquerel in 1839 [1]. The first "solar cell" was produced in 1877 by W. G. Adams and R. E. Day [2], who studied junctions formed by selenium plates and platinum wires. This "solar cell" as well as other varieties presented until the 1950s showed conversion efficiencies below 1%, and could not have been used as efficient sources of electrical energy. The first "modern" solar cell was produced at Bell Laboratories in the 1950s [3]. That device was a single-crystal silicon solar cell with diffused *p-n* junction, and it was first developed and used for electricity generation in space. The earliest terrestrial applications emerged in the 1970s. Silicon (Si) solar cells have dominated the PV market since then. In 1999, single-crystalline and polycrystalline Si shared about 80% of the sales between them [3].

On a large scale, three different generations of solar cells can be distinguished: 1) first generation cells consisting of a large area, high quality and single junction devices, like crystalline silicon cells; 2) second (or thin film) generation materials developed to address energy requirements and production costs of solar cells, like CdTe, $CuInSe_2$ (CIS) and amorphous silicon (a-Si) solar cells; 3) third generation technologies aimed to enhance poor electrical performance of the second generation while maintaining very low production costs, multi-junction (tandem) solar cells and concentrators [4]. CIS type solar cells belong to the group of the second generation, high efficiency and low-cost thin film material solar cells. Thin film solar cells based on a-Si, CdTe and $CuInGaSe_2$ (CIGS) have been successfully developed and are being commercialized [5]. During recent years, the development of thin film solar cells has made significant progress [6]. Vacuum deposited multi-crystalline layers of ternary compound CIS and its solid solutions with $CuGaSe_2$ (CGSe) - GIGS have shown as excellent absorber materials in thin film solar cells. The highest efficiency reported to date for CIGS-type solar cells is 20.3%, reported by ZSW in Stuttgart [7]. These CIGS films have been grown by physical vapor deposition in a three-stage co-evaporation process. In this process In, Ga and Se are evaporated in the first step; in the second step followed by Cu and Se co-evaporation and in the last step terminated by In, Ga and Se evaporation again.

Vacuum technologies are expensive. Among chemical methods the most popular is the electrochemical deposition (ED) of the components of a thin film

structure. The preparation of semiconductor thin films by the ED technique has some advantages over the other physical and chemical deposition techniques: it is easy and economical, as semiconductors with no or small waste of materials could be prepared. Because of the purification effect, which often results from ED, there is no requirement to have very pure starting materials, as it is the case for other methods. The semiconductor properties, like *n*- or *p*- type conductivity, band-gap variation, control of stoichiometry, doping and other properties could be controlled with a reasonable accuracy. However, as the electrodeposition is a low temperature process, the as deposited layers have to be subjected to a post heat-treatment to improve the crystallinity and phase composition. Selenization of as deposited layers at elevated temperatures is a widely used possibility. As several conductive substrates (ITO or Mo covered glasses) are used in ED, chemical interaction between substrate material and Se in the post-deposition annealing in the Se vapor has its impact on the properties of the multilayer structure.

The present thesis ”**Selenization of molybdenum as contact material in solar cells**” is focused on the formation of $MoSe_2$ thin films on pure Mo layers as well as on Mo covered with components for CIS and its In-free analog $Cu(ZnSn)Se_2$. This thesis is divided into four chapters. Following the introduction, the literature review is given in Chapter 1, CIS and CZTSe-type absorber materials and back contact materials for solar cells are covered. In the experimental part in Chapter 2 the preparation of materials and experimental methods are presented. Chapters 3 and 4 focus on the $MoSe_2$ formation by the selenization of pure Mo and Mo through different metallic stacked layers. Selenization of electrodeposited layers is described in Chapter 4. Finally, main results are summarized in the conclusions of the thesis. Chapters 2 and 3 deal with an investigation of $MoSe_2$ formation by the direct selenization of Mo with Se vapor under various conditions, to define optimum parameters for the growth of a $MoSe_2$ buffer on back contact. Different parameters of the $MoSe_2$ growth were varied in order to optimize the compositional, chemical and structural properties of $MoSe_2$. The formation of $MoSe_2$ by the selenization of polycrystalline Mo layers on glass and Mo foil were studied. For all the $MoSe_2$ layers a hexagonal crystal structure was found. The orientation of the Mo substrate has no influence on the preferred orientation of $MoSe_2$. In order to achieve the desired semi-conducting properties, the electro-deposited precursor films need to be thermally annealed. Changing of annealing conditions (temperature, time and atmosphere of annealing) allows the morphology and optical and electrical properties of annealed films to be controlled and films and later solar cells structures with tailored technical parameters to be prepared. The structure and morphology of CIS and CZTSe thin films depend on the precursor film composition, annealing temperature and the pressure of the Se vapor.

1. LITERATURE REVIEW AND AIM OF THE WORK

1.1. Solar cell structure

A solar cell (also called a photovoltaic cell or a photoelectric cell) is a solid state device that converts the energy of sunlight directly into electricity by the photovoltaic effect. The basic component of a CIS and a CZTS-type ($Cu_2ZnSnSe_4$ or Cu_2ZnSnS_4) solar cell (see Fig. 1) is the absorber layer, where the conversion of photons (with an energy greater than the band-gap energy of CIS/CZTS into electron-hole pairs takes place.

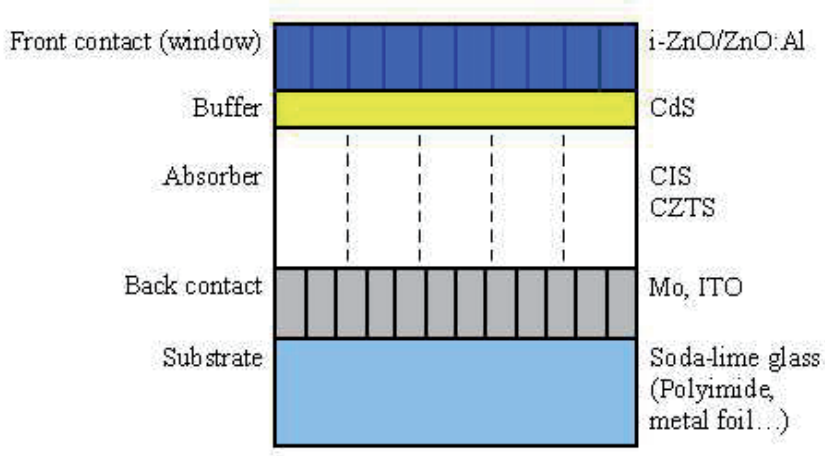

Figure 1. Schematic representation of a CIS/CZTS-type solar cell structure.

For thin film cells, a polycrystalline, slightly Cu-deficient *p*-type CIS or CZTS material is used. An *n*-type semiconductor film, often called a "buffer" layer, on top of the absorber layer is required to establish an electric field in the working regime at the *p-n junction* (depletion or space-charge region). The band gap of the buffer layer should be wide, such that most of the incoming radiation can be transmitted to the absorber. For efficient transport of the photo-generated carriers, ohmic front and back contact layers with high conductivities are required. The front contact (on top of the buffer layer, also called "window" layer) should be as transparent to the incoming radiation as possible. The back contact consists usually of an opaque metal film, unless a semi-transparent cell (tandem device) is desired.

1.2. Back contact materials, Mo and its behaviour in the selenization process

Mo back contact – a historical approach

Various metal contacts to *p-type* CIS were examined by Matson et al. [8] who concluded that only Au and Ni ensure an ohmic contact between the absorber material and the back contact layer. Orgassa et al. [9] fabricated CIGS solar cells with different back-contact materials and found that W and Mo contacts provide the best CIGS/back contact interface passivation. Nowadays, Mo grown by sputtering or electron-beam evaporation is the most commonly used back contact for CIGS solar cells.

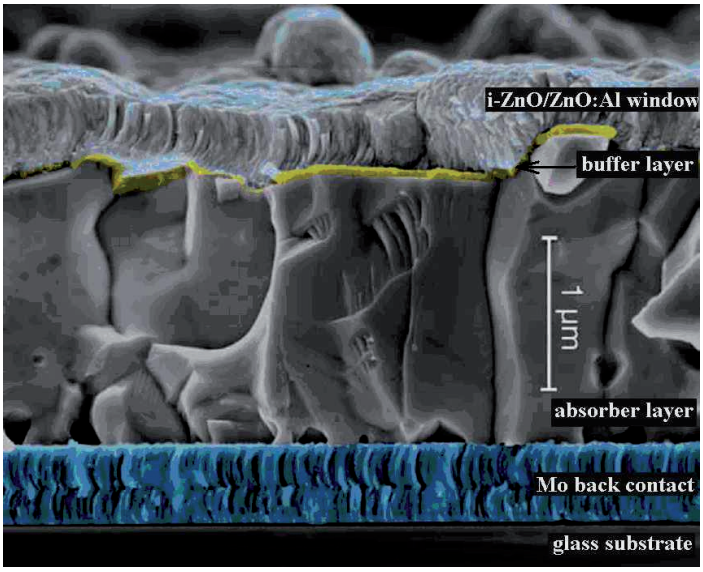

Figure 2. Typical thin-film solar cell structure.

Early results by Russell et al. [10] suggested that Mo back contacts for the CIS form a Schottky-type barrier. Also, Jaegaermann et al. [11] reported that the Mo/CIGS contact, consisting of the Mo film and the CIS crystal, is the Schottky-type. However, Shafarman et al. [12] who analyzed the Mo/CIS interface showed that the contact was ohmic, probably because of the formation of a $MoSe_2$ layer between Mo and CIS [13]. The ohmic behaviour of $MoSe_2$ at the CIGS/Mo interface makes the $MoSe_2$ formation an important issue. $MoSe_2$ could be considered as a buffer layer between Mo and CIS, which leads to a better energy-band alignment and thus to an improved electrical contact. Kohara et al. [14] also found that the CIGS/Mo hetero contact, including the $MoSe_2$ layer, was not a Schottky-type but a favorable ohmic contact [14]. They found that the solar

cell made from the CIGS/Mo/SiO_2/glass structure (without the $MoSe_2$ layer) showed a conversion efficiency of 9 %. By measuring the low-temperature *I–V* curves at different temperatures they found that the slope at the forward current region was depressed with lowering temperature (see Fig. 3(a)) due to a barrier at the interface of semiconductor/metal electrode (Schottky-type contact). The solar cell with the CIGS/Mo/$MoSe_2$/glass structure showed a conversion efficiency of 14 %. The dark *I–V* curves measured at 298 and 120 K are shown in Fig. 3(b). These curves have the typical diode character of a *p-n junction* and have a similar slope in the forward current (positive voltage) region. The results indicate that the CIGS/Mo hetero contact with the $MoSe_2$ layer is an ohmic type contact. Furthermore, the $MoSe_2$ layer forms the back surface field due to the wider band gap than that of a CIGS film. Thus, the existence of the interface layer with the wider band gap of $MoSe_2$ improves the CIGS/Mo hetero contact.

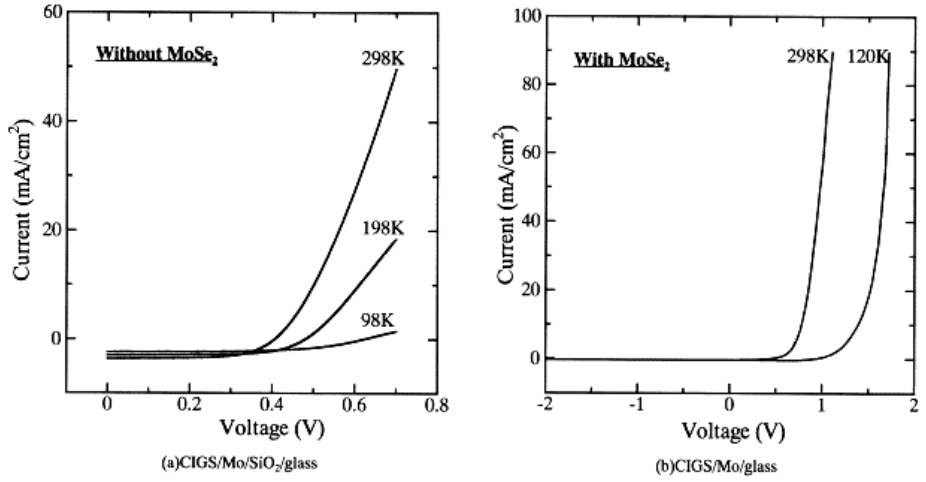

Figure 3. Temperature dependant behaviour of *I–V* characteristics of CIGS/Mo/glass structure solar cells without $MoSe_2$ (a) and with $MoSe_2$ (b) [14].

Mo back contact deposition

Mo is usually deposited by direct current (dc) magnetron sputtering or by electron-beam evaporation methods. The stress state of Mo thin films is known to depend strongly on the deposition conditions. It had been shown already in [15] that Mo films sputtered at a single pressure step did not possess simultaneously low resistivity and good adhesion, properties necessary for fabricating good back contact in CIGS based solar cells. In order to circumvent this problem, a two-pressure deposition process was proposed by Scofield et al. [15]. Films sputtered with high argon pressure adhere well to the glass, but are resistive. When produced by sputtering, the layer properties are varied primarily

by changing the sputter power, resulting in different kinetic energies of the sputtered Mo atoms arriving at the substrate. For a high sputter power (e.g., 2 kW), the adhesion of the Mo and soda lime glass (SLG) substrate is enhanced compared with low-power (e.g., 0.3 kW) films. However, continuous sputtering at high sputter power exhibit Mo films with larger resistivity as compared with low-power films. Therefore, commonly, a Mo bi-layer is applied as back contact in solar cells. First, a thinner layer is deposited at high sputter power (e.g., thickness of 100 nm), then a thicker layer is deposited at a low sputter power (e.g., 850 nm).

It is known that the high-pressure Mo films have smaller grains, a more open grain structure (i.e., larger gaps between grains), and the films are more porous than the low pressure Mo films. This leads to greater inclusion of oxygen (probably in the grain boundaries), higher resistivity, higher Na levels, and more rapid impurity diffusion in high pressure sputtered Mo films. The morphology of the high-pressure Mo provides a greater number of nucleation sites for the absorber layer, leading to better absorber adhesion and smaller, less faceted absorber grains. These differences lead to the higher selenization rate of the high pressure Mo during absorber formation [16].

$MoSe_2$ properties

According to the equilibrium phase diagram of the Mo-Se system [17], only two stable Mo-Se compounds exist: $MoSe_2$ and Mo_3Se_4. If excess supply of the Se is given during the selenization, generally, only $MoSe_2$ as a reaction product is formed [18]. When Se is available only at limited concentrations, predominantly Mo_3Se_4 forms [19].

$MoSe_2$ is a class of compounds called layered transition metal dichalcogenides. Layered transition metal dichalcogenides have been extensively studied because they have two interesting physical properties - superconductivity and the ability to form many derivates of these compounds via intercalation reactions [20]. Molybdenum dichalcogenides have interesting sandwich structure layers of Se-Mo-Se, which interact with each other through Van der Waals (VdW) forces. The hexagonal crystal structure of $MoSe_2$ is presented in Fig. 4. A hexagonal multilayer structure of $MoSe_2$, through the process of intercalation enables the introduction of foreign atoms in the interlayer space. The intercalation changes the electric properties of the semiconductor. $MoSe_2$ has been reported as an efficient compound for the photo-electrochemical conversion of solar energy [21]. $MoSe_2$ compound in the form of a polycrystalline thin films, though less perfect than a single crystal, nevertheless (after adequate doping) becomes an attractive semiconductor compound for electronics [22].

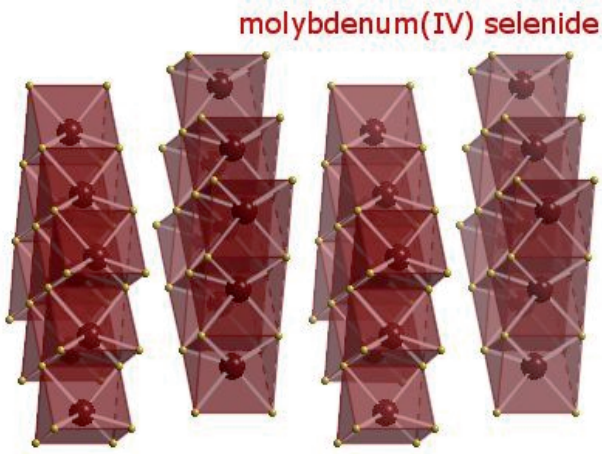

Figure 4. Layered hexagonal crystal structure of $MoSe_2$ [23].

Sienicki [22] published a preparation of $MoSe_2$ intercalated with atoms of the group III-A elements gallium, indium and tallium. The synthesis was performed in closed vacuum ampoules at 950-1000 ^oC for 10 days. The compounds were grown in the form of hexagonal thin plates and exhibited the *p*-type conductivity. The intercalates obtained had an increased specific conductivity and reduced energy gaps in comparison with pure $MoSe_2$. No dramatic increase in the absorption coefficient caused by the dopants was observed. It was proposed that the atoms introduced into the interlayer spaces do not behave at room temperature like typical dopants, but appear to form with $MoSe_2$ a semiconductor material of a specific band structure. In [24] indium intercalated $MoSe_2$ single crystals with different In content $In_{1-x}Mo_xSe_2$ ($0.5 \leq x \leq 1$) were grown by the direct vapor transport technique (DVT). After intercalation the band-gap values of $In_{1-x}Mo_xSe_2$ ($0.5 \leq x \leq 1$) were changed and they all were *p-type*. Deshpande et al. [25] described the transport and optical properties in indium intercalated $MoSe_2$ single crystals and as reported in [26], they have grown transition metal dichalcogenide single crystals $Mo_xW_{1-x}Se_2$ series, with x = 0.3, 0.4, 0.85 and 0.9 by the DVT technique. All the samples were found to be of *p*-type conductivity and with different transport properties in different crystallograpic directions.

The *n*-type $MoSe_2$ is mainly produced by low temperature methods: by chemical bath deposition [27], by radio frequency (rf) magnetron sputtering [28] or by chemical vapor transport at high temperature [29, 31]. The introduction of impurities does not alter conductivity type but alters the width of the band gap [22, 24, 25, 29, 30, 32].

The role of $MoSe_2$ in a solar cell

An understanding of the $MoSe_2$ formation is vital to develop low resistance electrical back contacts for high efficiency CIGS solar cells, since the thickness and crystallographic orientation of the $MoSe_2$ layer determine the adhesion and electrical properties of the CIGS-Mo interface. The formation and properties of the $MoSe_2$ layer depend on the CIGS deposition method and growth recipes [13]. In CIGS solar cells $MoSe_2$ is regularly found in the hexagonal phase, which consists of Se-Mo-Se sheets oriented perpendicular to the *c*-axis of $MoSe_2$. From the anisotropic crystal structure of $MoSe_2$, similarly to MoS_2, possible applications as a lubricant arise [33] due to the atomically flat surface. So, the adhesivity of an absorber layer on Mo in a solar cell structure is dependent on the crystallographic orientation of the formed $MoSe_2$ layer.

The formation of a thin *p*-type $MoSe_2$ layer between Mo and the absorber that occurs during the absorber preparation at sufficiently high temperatures under $(In,Ga)_xSe_y$-rich growth conditions [34, 35] is beneficial for the cell performance for several reasons:

- it forms a proper ohmic back contact;
- the adhesion of the absorber to the Mo back contact is improved;
- since the band gap of $MoSe_2$ is wider (about 1.4 eV [34]) than that of a typical CIGS absorber, it forms a back surface field for the photo-generated electrons [34, 36, 37], providing simultaneously a low-resistivity contact for holes [36]. The back surface field reduces recombination at the back contact since the insertion of a wider band-gap layer (of the same conductivity type as the absorber) between the back contact and the absorber creates a potential barrier that confines minority carrier in the absorber [38].
- $MoSe_2$ layer prevents further reactions between CIGS and Mo [39].

- In electrodeposition of absorber layers, Mo film electrodes are sensitive to exposure to aqueous alkaline and acidic electrolyte environments and readily form oxide coatings. Therefore, when Mo substrates are employed reproducibility problems may occur. The new methodology based on $MoSe_2$ coated Mo film electrodes is amendable to scaling up. Thin films of $MoSe_2$ produced by the selenization of sputter coated Mo films provide excellent substrates for ED. The $Mo/MoSe_2$ heterostructure is chemically robust and electrochemically active. Irreproducibility problems encountered when using Mo-metal films can be avoided [40].

Formation of $MoSe_2$

The formation of $MoSe_2$ by the selenization of polycrystalline Mo layers and Mo single crystals has been studied in dependence of the substrate temperature, the Mo crystal orientation and the Na concentration by Abou-Ras et al. [41]. For all $MoSe_2$ layers, the hexagonal crystal structure was found. It was shown that

$MoSe_2$ formed at 450 °C had the *c*-axis oriented preferably perpendicular to the Mo surface, whereas at 580 °C, the *c*-axis was oriented preferably parallel to the Mo surface. The formation of a thinner $MoSe_2$ layer at 450 °C was explained by impeded Se diffusion through $MoSe_2$ with *c*-axis orientation perpendicular to the Mo surface. Na was found to induce the growth of $MoSe_2$ with *c*-axis orientation perpendicular to the Mo surface. The initial orientation of the Mo grains in the substrate was found to have no influence on the preferred orientation of $MoSe_2$. Both the $MoSe_2$ layer thickness and the Mo grain size were affected by the oxygen concentration in Mo prior to the selenization [41].

An important issue in the $MoSe_2$ growth is the $MoSe_2$ *c*-axis orientation with respect to the Mo surface. Several authors have reported different *c*-axis orientations for different growth conditions, i.e., the *c*-axis may be oriented on average parallel or perpendicular to the Mo surface. When a $MoSe_2$ layer with a certain thickness has already formed on Mo, Se atoms or molecules have to diffuse through this $MoSe_2$ layer to the $MoSe_2$/Mo interface in order to contribute to the further $MoSe_2$ growth. Se diffusion is facilitated when the $MoSe_2$ *c*-axis is oriented parallel to the Mo surface, since Se atoms or molecules can diffuse through the channels of the layered $MoSe_2$ structure to the $MoSe_2$/Mo interface. For the *c*-axis orientation perpendicular to the Mo surface, the Se diffusion through $MoSe_2$ is impeded. Under certain growth conditions the diffusion rate of Se through the $MoSe_2$ layer can be the limiting factor of the $MoSe_2$ layer thickness growth. The *c*-axis orientation affects also mechanical and electrical properties of $MoSe_2$. The adhesion is deteriorated when $MoSe_2$ forms with the *c*-axis on average perpendicular to the Mo surface. This leads to the delamination between Mo/$MoSe_2$ and the absorber, as it often occurs when mechanical stress is applied on a SLG/Mo/$MoSe_2$/CIGS stack [42].

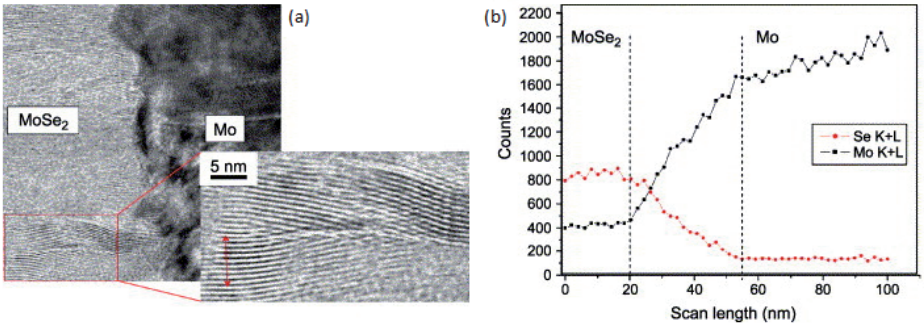

Figure 5. (a) HR-TEM photo of the Mo/$MoSe_2$ interface; in the magnified part, the distance of the layers corresponds to the *c*-value of the hexagonal $MoSe_2$ crystal structure. (b) Line scan obtained by EDX applied on the cross-section; on the $MoSe_2$ side of the interface, the Se signal is twice as large as the Mo signal [42].

In [42] the Mo/Mo–Se interface was investigated by high-resolution transmission electron microscopy (HR-TEM) (Fig. 5(a)). The Mo–Se compound in this figure was identified as $MoSe_2$. The $MoSe_2$ layer shows the *c*-axis parallel to the Mo surface. By means of an energy-dispersive X-ray spectroscopy (EDX) line scan across the Mo/Mo–Se compound interface (Fig. 5(b)), the Mo–Se compound was also identified as $MoSe_2$ [42].

The influence of absorber layer deposition on $MoSe_2$ formation

The thickness of the interface $MoSe_2$ layers was found to depend on the deposition conditions of the Mo layers [13, 43]. On the other hand, the formation of $MoSe_2$ is also affected by the sequence of deposition of absorber precursor layers.

Nishiwaki et al. [43] compared the formation of $MoSe_2$ on different substrates at 550 °C. Their results show that the $MoSe_2$ formation and *c*-axis orientation do not depend only on the state of Mo prior to selenization but also on the medium of selenization – pure Se vapor or Se mixed with In- and Cu-species can make a difference. $MoSe_2$ forms easily under In, Ga- and Se-rich conditions at high temperatures. Cu-rich conditions impede the formation of $MoSe_2$ [34].

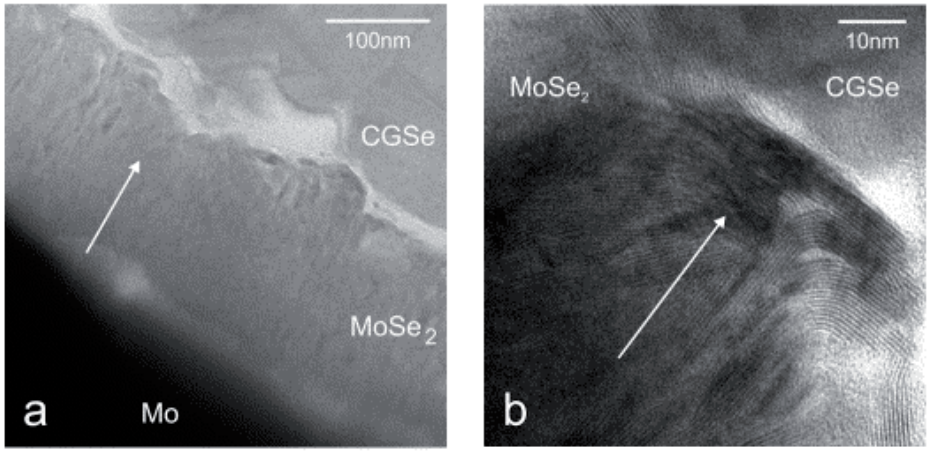

Figure 6. (a) TEM-picture of a two-stage sample, showing a 170 nm thick $MoSe_2$ interface layer at the Mo/$CuGaSe_2$ interface; (b) zoom of (a) at the $MoSe_2$/$CuGaSe_2$ interface; the arrow shows the surface normal direction of the Mo layer [44].

Sodium has been suggested to aid the formation of the beneficial $MoSe_2$ layer between Mo and CIGS. High reaction temperatures also facilitate the formation of $MoSe_2$ [34]. It was found that for the Cu-Se/Mo and Cu-rich Cu-In-Ga-Se/Mo structures, the thicknesses of the $MoSe_2$ layers were small. For the case of the In-Ga-Se/Mo structure, a much thicker interfacial $MoSe_2$ layer was observed

with *c*-axis oriented parallel to the Mo surface [43]. In [44] CGSe thin films grown by the chemical vapor deposition (CVD) method on Mo coated glass exhibited an interfacial $MoSe_2$ layer. The $MoSe_2$ sheets were oriented almost perpendicular to the Mo surface. The orientation of the $MoSe_2$ sheets changed from almost perpendicular to parallel directly at the $MoSe_2$/CGSe interface (Fig. 6). The $MoSe_2$ growth rate was found to increase with the Ga content in the gas phase during growth. The poor adhesion of CGSe layers on Na free substrates was attributed to a higher degree of parallel oriented $MoSe_2$ sheets in comparison with the $MoSe_2$ layers on SLG [44].

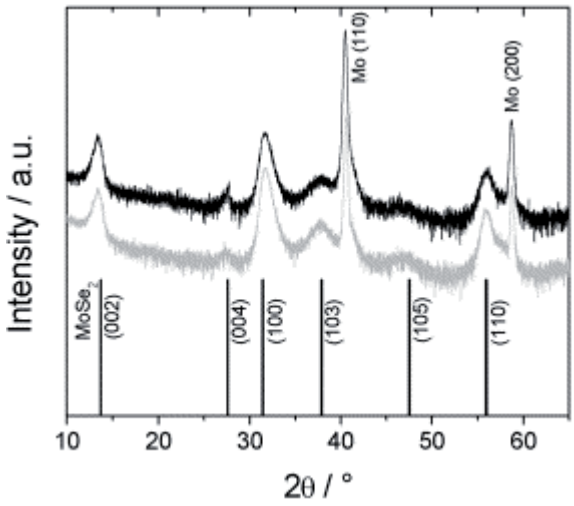

Figure 7. XRD measurement of a two-stage sample on Mo coated SLG (black curve) and Na free glass (grey curve); the lines mark $MoSe_2$-peak positions according to Ref. [JCPDS card n. 29-914].

The orientation of the $MoSe_2$ layers has been investigated also by means of XRD in the grazing incidence mode. In order to obtain better $MoSe_2$ signal intensity the CGSe layer was removed with a glue stripe from the samples on Mo coated SLG. It was confirmed by XRF, that only the CGSe layer peeled off with the glue stripe while the $MoSe_2$ completely remained on the Mo coated substrate. Fig. 7 shows the diffraction pattern of two-stage samples grown on SLG (top black curve in Fig. 7) and on Na free glass (bottom grey curve in Fig. 7).

The most intense $MoSe_2$ (100) and (110)-peaks are related to the layers that are oriented perpendicular to the Mo back contact surface. The (002)-peak with less intensity and the (004)-peak just emerging from the background level correspond to $MoSe_2$ layers with parallel orientation to the Mo surface, which are mainly situated at the $MoSe_2$/CGSe interface (Fig. 6(b)). The (103)-peak at 37.9 ° and the (105)-peak just emerging out of the background level could be

attributed to that part of the $MoSe_2$ layer, where the layers bend from the perpendicular to the parallel orientation. So the XRD measurements highly confirmed the TEM results. From the XRD investigation they could not find any difference in the structure of the interfacial $MoSe_2$ layers grown on SLG and Na free glass, although they observed a huge difference in the adhesion of the studied thin film CGSe absorbers. CGSe films grown on Mo coated Na free glass revealed only very small adhesion since they completely peeled off for a film thickness greater than approximately 400 nm, whereas they adhered well on plain Na free glass and Mo coated SLG. The poor adhesion of CGSe thin films onto the $MoSe_2$ interfacial layers grown on Mo coated Na free glass substrate could be caused by an enhanced portion of parallel oriented $MoSe_2$ sheets directly at the interface $MoSe_2$/CGSe. In the last case the CGSe film would be only weakly bonded by the VdW forces toward the parallel oriented $MoSe_2$. This explanation cannot be supported by the XRD measurement (Fig. 7), as the peak intensity for the $MoSe_2$ (002)-peak for the sample on Mo coated Na free glass is comparable to that of the sample on a Mo coated SLG [44].

The film morphology is strongly influenced by the substrate temperature. The crystallite size increases considerably with increasing substrate temperature. Topographical and cross-sectional investigations reveal a dense lamellar microstructure with the basal plane of the $MoSe_2$ crystallites perpendicular to the substrate but randomly oriented. The growth characteristics of the material do not seem to depend on the substrate. In particular, for films deposited onto $MoSe_2$ single-crystal substrates the basal plane of the crystallites is also perpendicular to the substrate, i.e. parallel with the *c*-axis of the crystal substrate. Epitaxial growth never occurred even at higher temperatures [45]. In [46] the CIGS/Mo and the Mo/glass interfaces in high efficiency thin film solar cells were investigated by surface-sensitive photoelectron spectroscopy and bulk-sensitive x-ray emission spectroscopy. The interfaces were accessed by a suitable lift-off technique. The experiments showed a strong Se diffusion from the absorber into the Mo film, suggesting the formation of a $MoSe_2$ layer in the surface-near region of the back contact. In addition, a Ga diffusion into the Mo back contact was found, while no diffusion of In and Cu occurred.

1.3. CIS-type thin film solar cells

1.3.1. Requirements for back contact materials of $Cu(In,Ga)Se_2$ solar cells

The requirements for a good back contact material for CIGS solar cells are manifold. A certain inertness of the contact material is the prerequisite for reproducible CIGS absorber growth in the highly corrosive process atmosphere during the CIGS deposition. The contact layer must function as a barrier that hinders diffusion of impurities from the substrate into the absorber. For good

electronic device properties, the formation of an ohmic contact for the majority carriers (holes) from the *p*-type CIGS and a low recombination rate for the minority carriers (electrons) at the CIGS/BC interface is essential. Finally, a high optical reflectance is necessary to minimize optical losses.

Molybdenum, the 'historical' back contact material for CIGS solar cells, complies well with most of the requirements. Mo is inert during the deposition, allows for the growth of large grains, and forms an ohmic contact via an intermediate $MoSe_2$ layer [13]. More detailed information about Mo back contact material is given in Chapter 1.2.

The following part of the chapter gives a brief overview of a possible transparent candidate of a back contact material as ITO (indium tin oxide).

Transparent back contact materials

ITO (In_2O_3-SnO_2) is widely used as a transparent conducting material in the panel liquid crystal displays [47], flat panel electroluminescent displays [48], electrochromic devices [49], solar cells [50], and antistatic coatings [51].

Sputtering deposition method, which easily gives a uniform film over a large area, is widely used for ITO film deposition. In general, a post annealing is necessary for ITO films to decrease the resistivity and increase the transmittance in the visible light region [52]. The key material properties of ITO films for such applications are low resistivity (< 200 μΩ cm) and high transmittance (>90%) in the visible light range.

The properties of ITO films are strongly dependent on the deposition conditions, most significantly on the substrate temperature, the oxygen partial pressure, and the distance between the target and the substrate.

Qiao et al. [53] reported that the microstructure and electrical properties of the ITO film change with the film thickness: the electrical carrier density increases with increasing film thickness, and thus the electrical resistivity decreases with increasing film thickness. They attribute the differences in the properties of the thin and thick films to a change of the film's microstructure taking place at 0.3 - 0.5 μm, with a lower deposition rate and more oxygen incorporation in the thinner films. Effects from chemical treatments of ITO on its properties have been investigated in [48, 54]. Bianchi et al. [55] have studied the electrical, chemical, and optical characteristics of ITO films deposited on glass substrates and submitted to aqua regia treatments. The properties investigated include the refractive index, roughness, thickness, work function, conductivity, indium and tin contents on the surface, contact angle, and surface energy. The chemical treatment with H_2SO_4 for shorter times was reported to have no significant effect on the ITO properties, it was found only to decrease its thickness. Etching for a longer time (more than 30 min), although the work function and In/Sn ratio were not affected, conductivity, roughness, and the absorption spectra and the refraction index were greatly affected.

The influence of different degreasing and activating techniques of the ITO surface on the electrochemical deposition process of copper has been studied by Altosaar et al. [56].

First solar cells on the ITO back contact with intentionally grown $MoSe_2$ intermediate layer clearly showed a better photovoltaic performance than without the $MoSe_2$ intermediate layer, and efficiencies of up to 11.8% were achieved. The details of the PV parameters gained are given in Table 3. These results prove that $MoSe_2$ layers can be used as a buffer layer for quasi-ohmic contact and to develop high-efficiency CIGS solar cells on a variety of back contact materials. CIGS solar cells on a transparent back contact (ITO) by the application of the $MoSe_2$ layer improve the efficiency from 2% to >10% [57].

Table 3. Photovoltaic parameters for solar cells with and without intermediate $MoSe_2$ layer between [57].

ITO back contact and CIGS	ITO/$MoSe_2$	ITO/$MoSe_2$	ITO
selenization temp. [°C]	450	580	580
V_{oc} [mV]	585	559	314
J_{sc} [mA/cm^2]	29.3	27.1	21.6
FF [%]	68.9	60.8	29.6
η [%]	**11.8**	9.8	2.0

1.3.2. Absorber materials and their properties in CIS-type thin film solar cells

The chalcopyrite-type semiconductor I-III-VI_2 compounds are used as absorber materials in thin film solar cells. Among these compounds, $Cu(Ga,In)Se_2$ solid solutions have optimum band gaps of 1.2-1.5 eV for solar cells, and many preparation methods of the thin films have been reported by many authors. A conversion efficiency of solar cells of 20.3 % has been achieved by using thin films as absorber layers. Furthermore, many studies focus on finding new materials better than these solid solutions. The ternary and quaternary compounds can be designed by various combinations of elements in the vicinity of the group IV element. Such tetrahedrally coordinated semiconductors, for example, defect chalcopyrite, spinel, stannite and famatinite, have been suggested [58]. To examine the possibility of the above semiconductors for useful devices is very important for novel material development.

CIS type solar cells belong to the group of the second generation, high-efficiency and low-cost thin film solar cells. Most widely investigated absorber materials are $CuInSe_2$, $CuInS_2$, $CuGaSe_2$ and $Cu(In,Ga)SSe_2$. Quaternary compounds Cu_2ZnSnS_4 and $Cu_2ZnSnSe_4$ in which expensive indium (gallium) is substituted by more common elements like tin and zinc have been proposed

recently. All of them are stable semiconductor materials, with a direct band gap 1.0 - 1.65 eV, resulting theoretically in high efficiency of solar cells.

General features of the absorber materials are:

- semiconductor with a direct band gap of around 1.4 eV, (1.1 – 1.5 eV);
- high absorption coefficient;
- consisting of abundant and non-toxic materials;
- suitable for large area thin film deposition with simple methods;
- should yield long term stable and high efficiency cells.

$CuInSe_2$ has certain exceptional semiconductor characteristics, such as band gap width (1.04 eV), absorption coefficient (close to 10^5 cm^{-1}) and minority carrier diffusion length, which are particularly suitable for photovoltaic and photo-electrochemical device applications [59].

The electrical and optical properties of $CuInSe_2$, $CuInS_2$, $CuGaSe_2$ and their alloys can be controlled by adjusting the stoichiometry and molecularity of the materials, sometimes by small amounts, as in the case of the chalcogene constituent, sometimes by large amounts, as in the case of the copper content. The main motivation for research of these materials is their promise as the active semiconductor of thin film photovoltaic solar cells. The paper [60] reviews investigations of the effects of stoichiometry on the properties of these materials and on their performance in solar cells.

Quaternary compounds CZTS and CZTSe as absorber materials

Many existing solar cell technologies that play an important role in the present sub-gigawatt (GW) energy production levels, are affected by several material shortages. The scarcity of tellurium and indium is the showstopper that would prevent the scale-up of CdTe and CIGS based thin film solar cells technologies to the terawatt range [61]. For the future, the substitution of indium is an important issue. The supply of the rare metal indium in the mass production stage of the CIS thin-film solar cell in the near future is troublesome. Thumm et al. showed that 30 tons of indium is necessary to produce 1 GW of electricity power as the estimated calculations for a CIS thin film solar cell [62]. It can be considered that this is an amount that is only about 10% of the aggregate demand of indium in Japan, and those amounts exist without problems at all if the recycling technology is essentially available. However, the apprehension for the sudden rise of the cost of indium by the extensive liquid crystal business may exist in the future according to the rising demand for a transparent conduction substrate of ITO.

The substitution of In(Ga) atoms in $CuIn(Ga)(S,Se)_2$ by an isoelectronic pair of (II–IV) atoms is proposed: (II–IV) being {Zn, Cd} and {Sn, Ge, Si, Zr, Ti}, respectively. Among these possible compounds very few of them have been synthesized and characterized. Cu_2ZnSnS_4 (CZTS) and $Cu_2ZnSnSe_4$ (CZTSe**)** are

the only compounds used as novel absorber materials due to their *p*-type conductivity, high absorption coefficients ($>10^4$ cm^{-1}) and direct band gap ranging from 0.96 to 1.63 eV [63, 64, 65, 66]. Most of their elemental constituents are abundant on the earth's crust. The development of CZTS thin film solar cells started in 1988 by K. Ito and T. Nakazawa [64]. An overview of progress in the development of CZTS solar cells is given by H. Katagiri [67]. During the recent years the studies on CZTS solar cells have been intensified. The CZTS record cell showed 6.7 % of efficiency [68] and the best $Cu_2ZnSnSSe_4$ 9.66 % [69].

CZTS thin films can be prepared by a variety of methods, like vacuum evaporation [67, 70], spray pyrolysis [71, 72], CBD, and ED [73, 74, 75]. Among these, ED deserves special attention since it provides an inexpensive, low temperature and non-polluting production method.

1.3.3. Electrodeposited absorber layers and their post-treatments

One of the main challenges in solar energy research is to find a fabrication method that results in high-quality thin films at low cost and of easy scalability [76]. Electrodeposition is a simple and economical method that can be used for the preparation of metal, semiconductor and conducting oxide thin films. Its advantages include feasibility of upscaling to large substrate areas and production volumes [77]. Moreover, the deposition equipment is relatively simple and the deposition temperatures are considerably lower than in many other methods. These features make ED a low-cost deposition method. Thus, the fact that the solar cell efficiencies achieved with electrodeposited films are generally somewhat lower than those achieved by the more expensive gas-phase methods is not necessarily a major drawback, since it is compensated by the lower process costs.

Electrodeposition is a liquid phase thin film deposition method that is based on electrochemical reactions (reductions or oxidations) carried out using an external power supply. ED is the process of producing a coating, usually metallic, on a surface by the action of electric current. The deposition of a metallic coating onto an object is achieved by putting a negative charge on the object to be coated and immersing it into a solution which contains a salt of the metal to be deposited. In addition to the power supply, at least two electrodes are needed, between which the current flows in the deposition solution. One of the electrodes is a working electrode or substrate on which the film grows, and the other one is a counter electrode. The film growth occurs most often via reduction reactions, i.e., the working electrode is a cathode. Usually a three-electrode setup is used where the third electrode is a reference electrode with respect to which the electrochemical potential of the working electrode is controlled or measured [78, 79]. If the potential of the working electrode is controlled, the resulting current may be measured, and vice versa. Deposition is often carried out at a constant potential (potentiostatically) or at a

constant current (galvanostatically), but voltage and current waveforms or pulses can be used too.

The structure, chemical composition and surface morphology of the films and their evolution are related to the variation in preparation parameters, such as the applied potential, deposition time, solution temperature, solution pH, and composition

It is well known that annealing in different atmospheres can improve morphology and composition of absorber materials substantially. This comprises firstly the re-crystallization and combination of a material and secondly the formation of defect structures. Factors that can influence the process are:

- temperature and annealing time;
- stoichiometrical composition of a non-annealed (precursor) film;
- velocity of cooling a sample;
- composition of a vapor phase.

Selenium is known to produce various allotropic modifications with different crystalline and amorphous structures showing red, grey and black colours. It melts at 220 ºC and boils at 685 ºC. Selenium vapor consists of Se_n molecules (n = 2-10) with a molecular size distribution that depends on the vapor temperature. Higher temperature shifts the distribution to low atomic molecules, which have higher enthalpies of formation than the higher atomic molecules. The existence of different vapor compositions is supposed to influence reproducibility [80].

Chalcogenization of as-grown CIS films

Electrodeposited CIS and CIGS films are usually amorphous or of poor crystallinity and consist of small grains. They tend to be Cu-rich and contain frequently degenerate $Cu_{2-x}Se$ phases that are detrimental to the device performance. Cu-rich films have generally larger grain sizes than stoichiometric or In-rich films. The films may also contain impurities that originate from the aqueous deposition solution or from the complexing agents. For the above reasons, the films require at least annealing under an inert atmosphere prior to completing the device preparation. Very often the films stoichiometry needs to be correlated too, for instance by annealing under a Se-containing atmosphere and/or by selective etching in cyanide-containing solutions.

Selenization is most often carried out under a selenium-containing atmosphere at high temperatures, typically above 400 °C. Selenium may be present either as H_2Se [81, 82], most often diluted by Ar, or elemental Se [82, 83, 84, 85, 86]. Selenization time depends on thickness, structure, and composition of the film, as well as on the reaction temperature and selenium source. Generally, the formation of CIS by selenization is faster and occurs at lower temperatures than for CGSe [83, 87]. As a result, CIGS films may contain CIS and CGSe as separate phases if the reaction temperature is too low or the

time is too short [81]. High reaction temperatures also facilitate the formation of $MoSe_2$ [34, 82]. The chalcogenization method offers also a possibility of forming $CuIn(S,Se)_2$ thin films by introducing both Se and S precursors into an annealing atmosphere [85].

In the paper [88] the CIS films were successfully deposited on ITO coated glass substrate using an electrochemical technique. The structural, morphological and optical properties of CIS films were studied in terms of annealing time. It was found that the annealing time plays an important role in the evolution of CIS properties. Before annealing, the XRD spectra show only the ITO phase peaks and after annealing at 300 °C, all the resulting films show the tetragonal chalcopyrite $CuInSe_2$. The average grain size of the films increases linearly with the annealing time. The film annealed during 45 min exhibits better crystallinity, higher intensity ratio and good optical properties and it can be used as an absorber layer in the fabrication of thin film solar cells [88].

Our research group has found [89] that morphology and composition of co-electrodeposited $CuInSe_2$ layers on an ITO substrate do not depend only on the deposition temperature and the potential, but also on the direction of potential change in the two-potential deposition process developed by our group. The potential change from lower negative values to higher ones resulted in layers with low adhesivity. Alternatively, in the deposition process from higher potential to lower potential, homogeneous, well structured adhesive and smooth layers could be deposited. Modifying deposition periods in a two-step process, the chemical composition of the films can be tailored. ITO on substrates was found not to be inert in acidic deposition solutions in the range of pH values $1.7<pH<1.9$. In more acidic solutions an ITO layer probably dissolves and takes part in the co-deposition process. This could be the reason of high scattering and low reproducibility of the chemical composition of the deposited layers at $pH < 1.7$.

Influence of annealing temperature on deposited films for CZTSe layers

One of the most common preparation methods is electrodeposition [75, 90, 91]. As in the practical part of this work, some of the deposited films were prepared by the electrodeposition technique, thus major attention has been paid to the annealing of electrodeposited films. The metal precursors are often deposited at near room temperature, but higher temperatures have been used as well. In order to facilitate the interdiffusion of the metal precursors and alloy formation between them, the metal precursors can be pre-annealed at lower temperatures [75, 90].

In [92] metal films were sequentially deposited on Mo/SLG by vacuum evaporation and selenized by annealing in the temperature interval 250 -520 °C [92]. The authors found that selenization started with the formation of binary Cu-selenides with their composition varying by temperature. The selenization of

Sn-Zn-Cu films at temperatures higher than 370 °C resulted always in multi-phase ($MoSe_2$, $SnSe_2$) films that consist of high quality CZTSe crystals with sizes of up to 2 μm and a separate phase of ZnSe. Where precursor films were obtained by magnetron sputtering and later annealed at 250 – 400 °C, crystallization of the thin films occurred at annealing above 250 °C [93]. The major diffraction peaks of the CZTSe thin films corresponded to (112), (200), and (220), (312) planes. The crystal structure of the thin films was identified as the kesterite structure. The intensity of the (112) preferred orientation was stronger where the annealing temperature was increased. Both studies [92, 93] have shown interdependency between the degree of crystallinity and the annealing temperature.

1.4. Summary of the literature review and objectives of the research

From the literature review it can be summarized that Mo is the most widely used back contact material in thin film solar cells. During the formation process of solar cell structures, preparation conditions have a huge impact on the back contact properties and also the back contact and absorber materials interact with each other. In order to obtain high quality structures a thorough understanding of the basic structural, optical and electrical properties of the materials deposited under various conditions is essential.

The formation of a thin *p*-type $MoSe_2$ layer between Mo and the absorber that occurs during the absorber preparation at sufficiently high temperatures under $(In,Ga)_xSe_y$-rich growth conditions [34, 35] is beneficial for the cell performance.

An understanding of the $MoSe_2$ formation is vital for the development of low resistance electrical back contacts for high efficiency CIGS solar cells, since thickness and crystallographic orientation of $MoSe_2$ layer determine the adhesion and electrical properties of the CIGS-Mo interface. The formation and properties of $MoSe_2$ layer may depend on the CIGS deposition method and growth recipes [13].

While the efficiencies of the "best" small-area cells have steadily improved, uncontrolled factors continue to thwart the reproducibility of these cells, and to a greater extent, degrade the quality and through-put of large-area CIGS and CZT(S,Se) module fabrication efforts. In connection with these problems, a variety of suspect areas have been suggested; these include 1) the nature and importance of surface defects on the glass substrates, 2) substrate cleaning processes, 3) the possible formation of $MoSe_2$ near the Mo/absorber layer interface, 4) the possible importance of sodium diffusion into the absorber layer, 5) the softening of the glass substrate at the high processing temperatures, and 6) adhesion failures at the Mo/glass and/or Mo/absorber interfaces. A number of these issues appear to be related to the properties of the Mo back contact layer

universally employed for CIGS and CZT(S,Se) devices. At most institutions, considerable fabrication efforts have been devoted to improving the properties of the absorber layer. In contrast, significantly less effort has been devoted to understanding and shaping the properties of the Mo layer. In many cases, the Mo layer has been deposited by whatever means were available, with the only property of concern being the Mo sheet resistance. Only recently have we recognized the importance of the Mo layer as the substrate upon which the CIGS absorber layer is grown and that it may have a significant impact on the absorber layer nucleation, growth, and morphology. The electrical and mechanical properties of sputtered refractory metal films are known to vary with sputter pressure [94].

In the present work we have used different origin of Mo layers. In order to shed light on some of the questions raised above we have subjected these Mo films to our usual solar cell processing stages, including the high-temperature selenization of CIS and CZTSe.

Several groups [42**,** 95] have reported that solar cells on a transparent conducting oxide (TCO) back contact with intentionally grown $MoSe_2$ intermediate layer show a better photovoltaic performance than without the $MoSe_2$ intermediate layer. So, it is necessary to make separate experiments with Mo substrates of different origin with and without other layers on top, to find out the parameters, which control the growing process and lead to the desired $MoSe_2$ thin layer. From the literature review it is obvious that there is little or inconsistent information about $MoSe_2$ formation depending on the Se vapor pressure and temperature. Also, the formation of $MoSe_2$ on differently deposited Mo substrates and on TCO layers is not thoroughly understood. It is partly understood how the substrate temperature affects the $MoSe_2$ growth and orientation and that the orientation of Mo grains in the Mo layer plays no role.

Because of the adhesion problems between Mo back contact and absorber material a detailed study is necessary to find out selenization parameters that provide good adhesion and give continuous $MoSe_2$ layers.

On the bases of the findings summarized above and due to the very important role of $MoSe_2$ in solar cell performance, the objectives of the present doctoral thesis were set as follows:

- To investigate the selenization processes of Mo of different origin and Mo layers covered with different precursors.
- To investigate how the various parameters, such as Mo layer pre-treatment, annealing temperature and duration, Se vapor pressure and different origin of Mo substrates affect the formation of $MoSe_2$, influence the Mo-Se film phase composition, structure and morphology and many other properties.
- To find out optimum selenization conditions which give continuous and smooth layers of $MoSe_2$ without cracks and with desired properties suitable

for solar cells - *p*-type $MoSe_2$ with *c*-axis orientated parallel to the Mo surface.

- To find out the influence of any metal/metal stack coverage on the $MoSe_2$ growth process. In order to apply $MoSe_2$ as a buffer between back contact and CIS or CZTSe, variations of different parameters have been performed and studied: the influence of Cu, In, Cu-In and Cu-Zn-Sn on the $MoSe_2$ growth.

EXPERIMENTAL

The main experimental features are briefly presented in this section. For details of the experiments, see publications I –V.

2. Synthesis of $MoSe_2$ films

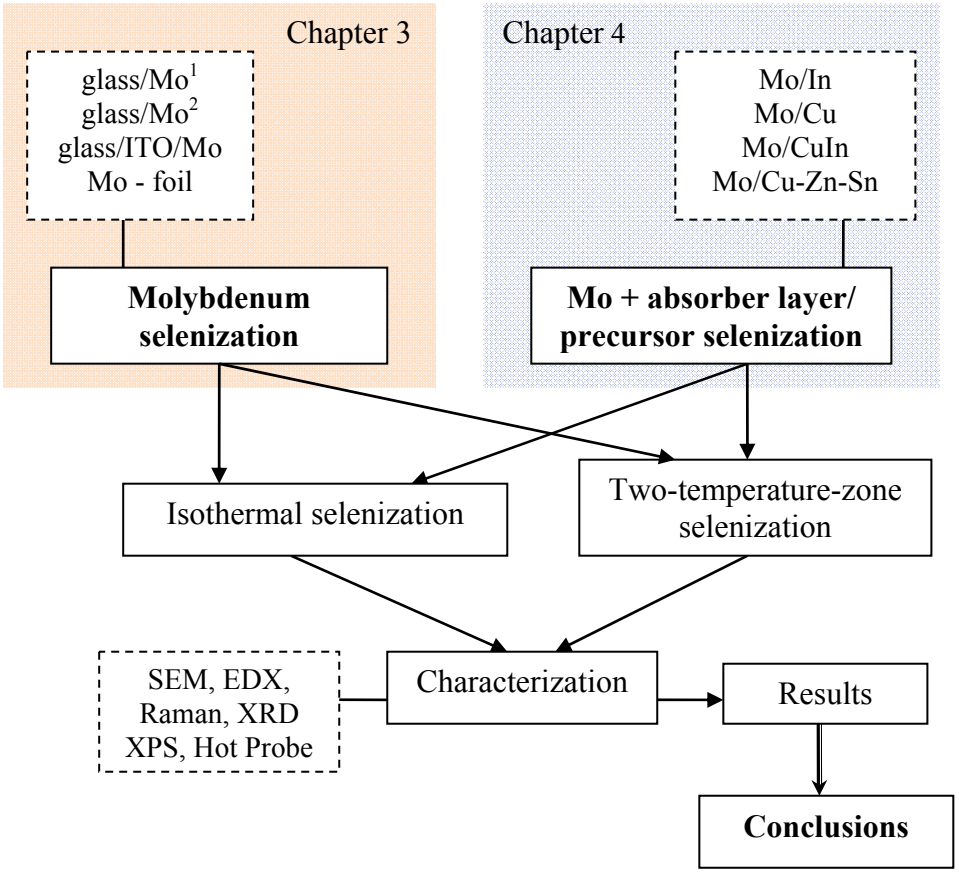

The background of our studies is given in the literature review, Chapter 1.2. Schematic diagram of the experimental work is presented here on page 31. Temperature profiles of $MoSe_2$ films preparation are shown in Fig. 8. More detailed explanation is presented in Chapter 3.

2.1. Preparation of samples

Precursor Mo layers

The investigations are based on four types of Mo samples of different origin (see Fig. 12):
Mo-foil (99.95 %, 250 μm thick) from Strem Chemicals Inc.;
Sputtered Mo[1]. 1 mm thick soda lime glass substrates covered with 1 μm thick Mo[1] layer, rf. sputtered (Mo target 99.997 %, short step: high power deposition for 30 sec, 3 kW, 200 Pa Ar and long step: low power deposition for 5 minutes, 0.7 kW, 500 Pa Ar) in ETH Zurich (Eidgenössische Technische Hochschule Zürich),
Sputtered Mo[2]. 1 mm thick glass substrates covered with 1 μm thick Mo[2] layer, dc. sputtered in ZSW (Zentrum für Sonnenenergie- und Wasserstoff-Forschung, Stuttgart), (sputtered as for CIGS solar cell production process in ZSW);
Sputtered Mo[2] on ITO. 1 mm thick glass substrates covered with 500 nm ITO with 70 nm Mo layers on it, dc. sputtered in ZSW. A very thin $MoSe_2$ layer may be grown on an ITO layer, acting as a tunnelling quasi-ohmic contact, the $MoSe_2$ layer acts as a buffer between ITO and the absorber layer.

Deposition of stacked Cu-In alloy layers on Mo

Cu-In alloy films on Mo covered soda-lime glass substrates were deposited by magnetron sputtering of Cu-In alloy targets in Scheuten Glassgroup at ambient temperature. High purity (99.998%) argon plasma was used in the co-sputtering process. The applied power density was 0.8 watt/cm^2.

Deposition of In and Cu on Mo

In on sputtered Mo[2]. Surface cleaning by dry plasma etching for 10 minutes under standard conditions (see Chapter 2.2) was used prior to electron gun thermal evaporation of 200 and 500 nm thick layer of In (by Dr. Tiit Varema).
Cu on sputtered Mo[2] (50 and 100 nm). Mo surface was cleaned by plasma etching for 10 minutes under standard condition (see Chapter 2.2). Cu deposition was done at the substrate temperature of 120 °C. Other conditions: initial vacuum 2.6 x 10^{-4} Pa, vacuum during the deposition 8 x 10^{-4} Pa, deposition time 32 min., chamber was filled with argon. BOC Edwards Auto 500 System was used by Dr. Sergei Bereznev.

Selenization and characterization of those films is reviewed in Chapter 4

2.2. Selenization of precursor Mo samples

Cleaning procedure of Mo samples - following results of different cleaning procedures of Mo samples (see Chapter 3.1.), only dry plasma etching of Mo before the selenization processes was used. The substrates were plasma etched in Ar for 5 minutes (40 Pa, 100 W).

Polycrystalline Mo layers were selenized under various conditions. The varied parameters were: the selenization duration (t); Mo substrate temperature during the selenization (T_{sub}); selenium pressure in the ampoule (P_{Se}); the use or absence of Ar gas; the use of copper or indium layers on Mo/glass substrates; the use of two-zone selenization; isothermal selenization.

To form $MoSe_2$ on Mo layers by selenization, Se atoms or molecules react first with the Mo surface atoms, and then the Se gas has to diffuse through the already formed $MoSe_2$ layer to the $MoSe_2$/Mo interface. Mo substrates were selenized with various durations at different temperatures, using the following selenization methods:

a) Isothermal selenization. In the isothermal arrangement, the Mo sample (0.75 x 2.5 cm^2) and selenium were heated in the same temperature zone. The selenization process was performed in sealed quartz ampoules, in which the Se pressure is determined by the used temperature. Mo samples were selenized at 375, 470, 500, 530 and 580 °C for 30 or/and 60 minutes in the isothermal sealed quartz ampoules.
b) Samples were annealed in a preheated two-temperature-zone quartz tubular vacuum reactor where temperatures of the Se source and the reaction zone can be independently controlled. The molybdenum substrate was heated in the higher temperature zone, while in the other zone the selenium source was heated to produce a reactive Se vapor atmosphere. The vapor pressure of Se in ampoules was determined by the temperature of the inexhaustible Se source.

Figures 8 and 9 show the temperature profiles and a photo of the furnaces.
Cooling. In both cases, after annealing the ampoules were taken out of the furnace and cooled down on a ceramic plate at room temperature.
Se source. Se pellets served as a source of Se vapor.
Quartz ampoules. The used quartz ampoules (1 cm in diameter and 7 cm (isothermal selenization) or 35 cm (2-zone selenization) in length) were etched with the mixture of concentrated HF + HNO_3 (1:1), rinsed with DI water and heated in the flame of C_3H_8 + O_2 gas. The ampoules with precursor samples and Se were evacuated down to $13 \cdot 10^{-3}$ Pa and sealed. The sealed ampoules were inserted into a preheated tubular furnace.

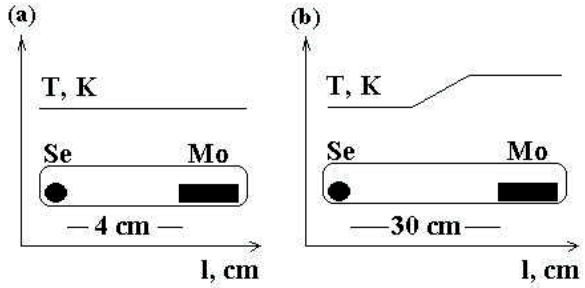

Figure 8. Temperature profile in the one-zone (a) and two-zone (b) tubular furnaces.

Figure 9. Photo of the used furnaces, a) for the isothermal arrangement, b) for the two-zone arrangement.

Annealing temperature - when the heating temperature is low, Mo reacts with Se at very low speed. The higher temperature limit is determined by glass substrates - temperatures higher than 600 °C cannot be used, because of the formation of thermal stresses in the glass after cooling, resulting in cracked or curved glass.

Annealing duration – when the Mo layers of different thicknesses are used, it is important to ensure the necessary amount of chalcogen (selenium) to avoid the situation where the whole source of Se is consumed for a short selenization time and no true time dependence can be gained. One possibility to hold back a high

reaction speed in the isothermal arrangement is to use the overpressure of some inert gas (argon). In some cases we used the Ar environment.

2.3. Methods of characterization

Table 4 summarizes the analytical techniques used for the characterization of the selenized layers. More detailed information about the instrumentation and measurements can be found in the experimental sections.

Table 4. Analytical techniques used for the characterization of the selenized films

Characterization method	**Material properties**	**Equipment –** details of the method	**Operator**	**Ref.**
SEM – Scanning electron microscopy	film morphology and thickness	**Zeiss Ultra 55** scanning electron microscope	Dr. Olga Volobujeva	I - V
EDX – energy dispersive x-ray spectroscopy	film composition	RÖNTEC EDX XFlash 3001	Dr. Olga Volobujeva	I- V
XRD – X-ray diffraction	phase composition, crystallinity	**Bruker D8 Advance diffractometer,**	Dr. Paul Barvinschi	I-III
		Rigaku Ultima IV diffractometer	Dr. Arvo Mere	IV-V
Raman spectroscopy	phase composition	**Horiba LabRam 800**	Dr. Maarja Grossberg, MSc.Taavi Raadik	II - V
XPS – X-ray photoelectron spectroscopy	surface and bulk chemical composition	**AXIS Ultra^{DLD}**	MSc. Mati Danilson	II
Hot Probe	Conductivity type		MSc. Liina Kaupmees	I, II

3. Results and discussion

3.1. Cleaning of Mo samples prior to selenization

Selenization of differently cleaned Mo samples was studied to ascertain an optimal substrate cleaning method. Mo-coated glass substrates (0.8x0.8 cm^2) were processed with aqueous solutions of 10 % KOH, 0.1 M H_2SeO_3 (etching time of 10 – 30 minutes at 25 °C), with 5 % laboratory cleaning agent Decon 90 (pH = 13) and with ethanol. The substrates were also etched in Ar plasma for 5 minutes (40 Pa, 100 W).

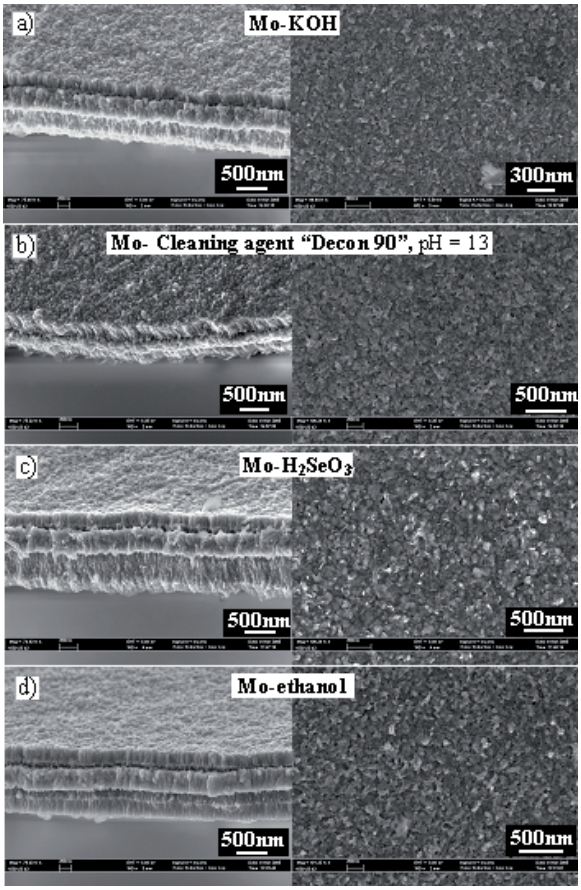

Figure 10. SEM images of differently cleaned Mo samples after selenization in a two-temperature-zone furnace for 20 minutes at 530 °C under the selenium vapor pressure of $4.4 \cdot 10^3$ Pa (T_{Se}= 500 °C): a) etched in 10 % KOH; b) etched in the cleaning agent Decon 90 (pH = 13); c) treated in 0.1 M H_2SeO_3 aqueous solution; d) degreased in ethanol.

After different cleaning procedures the Mo samples were selenized in a two-temperature-zone furnace for 20 minutes at 530 °C under the selenium vapor pressure of $4.4 \cdot 10^3$ Pa (T_{Se}= 500 °C). SEM images of selenized samples are presented in Fig. 10. SEM studies of selenized Mo layers revealed that the etching with aqueous etching solutions and also with ethanol prior to selenization destroyed the initial compact Mo layer.

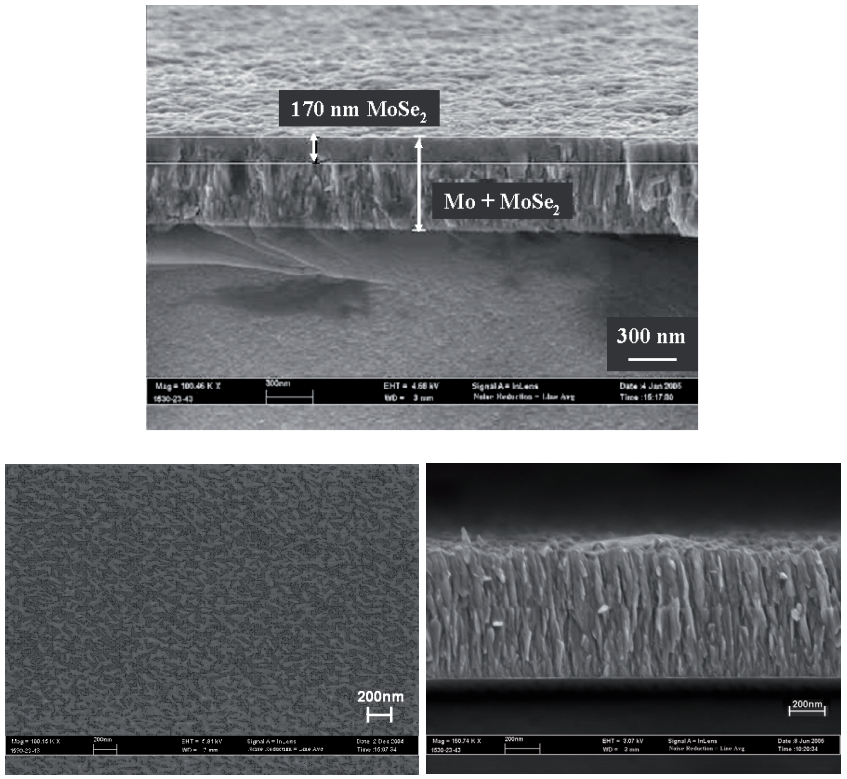

Figure 11. SEM images of a selenized Mo sample cleaned by dry plasma etching for 5 minutes prior to selenization: overview (upper image), surface (lower left image) and cross-section (lower right image). Selenization conditions - 20 minutes at 530 °C in a two-zone ampoule under the selenium vapor pressure of $4.4 \cdot 10^3$ Pa (T_{Se}= 500 °C).

After the selenization the smoothest surface of $MoSe_2$ was obtained with dry plasma etched Mo samples (see Fig. 11). The formation of $MoSe_2$ was confirmed by EDX. All the $MoSe_2$ films formed had *p-type* conductivity.

3.2. $MoSe_2$ by the selenization of Mo substrates of different origin

This section describes the selenization of Mo substrates of different origin for different durations ranging from 5 to 100 minutes using the two-zone and isothermal selenization methods. Results are published in [I] and [II].

3.2.1. Morphology of different Mo films before and after selenization

SEM image of Mo samples used for selenization studies are presented in Fig. 12. The cross-sectional micrographs of selenized Mo samples (Fig. 12 (a)-(d)) show that the formed polycrystalline $MoSe_2$ films have a columnar structure.

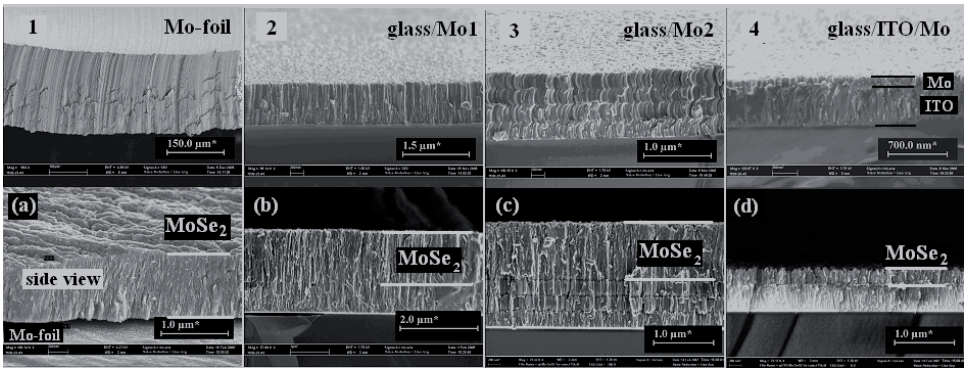

Figure 12. Side views and cross-sectional SEM images of different Mo samples before (1, 2, 3, 4) and after (a, b, c, d) the two-zone selenization process (T_{Mo}= 530 °C; T_{Se}= 365 °C , t = 20 minutes): (1) 250 µm thick Mo-foil; (2) 1 µm Mo^1/glass; (3) 1 µm Mo^2/glass; (4) glass/ITO/Mo (70 nm thick Mo layer on 500 nm thick ITO).

The layered structure of $MoSe_2$ follows the basic initial layered Mo structure deposited by a multi-step process. However, in the case of the two-zone arrangement, the surface morphology revealed the existence of longitudinal cracks on the surface. By using glass/Mo^1 samples, the surfaces of $MoSe_2$ layers were full of cracks in the case of the Se vapor pressure higher than $1.3 \cdot 10^3$ Pa (T_{Se}= 450 °C), probably due to the tensions in the thick formed $MoSe_2$ layers. The cracks were not visible from the cross-sectional images. Annealing of Mo under low Se vapor pressures (lower temperatures of Se source) resulted in smooth $MoSe_2$ surfaces and uniform dense layers. The adherence of Mo/$MoSe_2$ was found to depend on the quality of precursor Mo and also on the rate of selenization. The important conclusion made was based on fact that all the fully selenized Mo/$MoSe_2$ layers peeled off from glass substrates: the adherence depends on the extent of the selenization of the Mo layer.

In summary, it was found that it is important to examine both the surface and the cross-section of the formed Mo/$MoSe_2$ structures to acquire a complete overview of the morphology of the formed layers. Sometimes the selenization in the isothermal arrangement results in a perfect surface without any cracks. At the same time the cross-sectional view indicated longitudial cracks. To obtain an overall picture of the formed layers both the overview and the cross-sectional view must be studied. On the bases of the selenization results of four different Mo samples, we found that Mo^2 (produced by the ZSW technology) gave the most defectless $MoSe_2$ layers and in the following studies we used only Mo^2 samples.

3.2.2. Identification of phase composition

According to the equilibrium phase diagram of the Mo-Se system, only two stable Mo-Se compounds exist: $MoSe_2$ and Mo_3Se_4. If an excess supply of Se is given during the selenization, generally, only $MoSe_2$ as a reaction product was found. When Se is available only at limited concentrations, predominantly Mo_3Se_4 forms [19].

Table 6. Elemental composition of Mo-Se films selenized at T_{Mo}= 530 °C for t = 20 minutes in selenium vapors of 130 and 4400 Pa (corresponding to T_{Se}= 365 °C and T_{Se}= 500 °C in the Se side of ampoule) (EDX data).

Sample	$\mathbf{P_{Se}}$ (Pa)	**[Mo]** (at %)	**[Se]** (at %)
Mo-foil	$1.3 \cdot 10^2$	35.2	64.8
Mo-foil	$4.4 \cdot 10^3$	34.1	65.9
glass/Mo^1	$1.3 \cdot 10^2$	35.1	64.9
glass/Mo^1	$4.4 \cdot 10^3$	32.9	67.1
glass/Mo^2	$1.3 \cdot 10^2$	35.4	64.6

In our experiments, both the XRD and EDX measurements suggest that the formed Mo_xSe_y compound can be identified as $MoSe_2$ (see Table 6). XRD patterns of selenized Mo-foil, glass/Mo and glass/ITO/Mo samples are shown in Fig. 13. There are only two peaks corresponding to the hexagonal $MoSe_2$ phase in the XRD patterns [JCPDS cards 29-0914; 77-1715 and 87-2419] that indicate a strong preferred orientation of $MoSe_2$ with respect to the Mo substrate: the average orientation of the *c*-axis is parallel to the Mo surface (in other words, the layers of hexagonal $MoSe_2$ are situated perpendicular to the Mo surface) [42]. Despite of the fact that the orientation of Mo grains in Mo-foil was more random compared with oriented sputtered Mo grains on glass, the $MoSe_2$ phase on both substrates was grown in the same crystallographic direction (this is seen from the presence of only two reflections (100) and (110) in the XRD patterns of the samples discussed here).

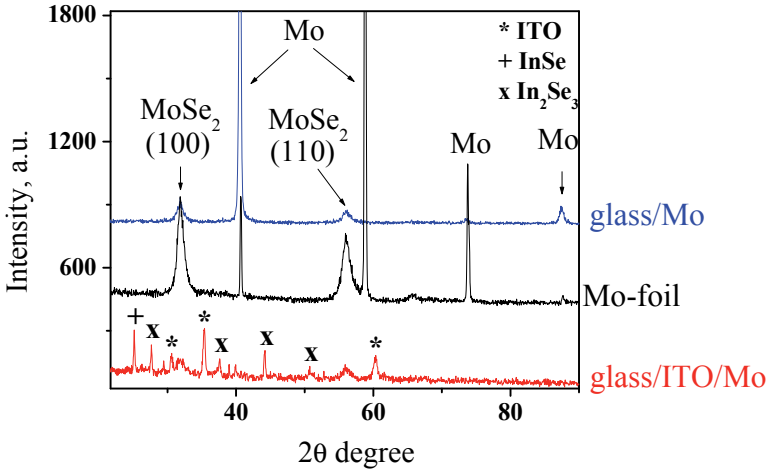

Figure 13. X-ray diffraction patterns of glass/ITO/Mo, Mo-foil and glass/Mo[1,2] films selenized at 530 °C for 20 minutes in two-zone conditions, where T_{Se} = 365 °C (P_{Se}= 130 Pa).

3.3. Isothermal selenization of Mo layers

In the analysis of the selenization of four different Mo samples (Chapters 3.2.1. and 3.2.2.) we found that Mo[2] (produced by the ZSW technology) resulted in the most perfect $MoSe_2$ layers and we used only Mo[2] samples in the following studies.

Selenization in the isothermal process arrangement at higher temperatures (530 and 580 °C) causes intense selenization of Mo corresponding to a relatively high selenium pressures determined by the used temperatures. SEM cross-sectional images of Mo/$MoSe_2$ samples annealed in the isothermal conditions at 530 °C for 60 minutes and at 580 °C for 30 minutes under Ar over-pressure are presented in Fig. 14, indicating that all the layers are full of cracks.

XRD patterns indicate also to the existance of un-reacted Mo in selenized samples and to Mo preferred orientation in the (110) direction [JCPDS card 42-1120] (see Fig. 15). According to XRD patterns (Figs. 15 and 17), the $MoSe_2$ films prepared in the isothermal selenization at 470, 530 and 580 °C show two main peaks related to $MoSe_2$ [JCPDS cards 29-0914; 77-1715 and 87-2419], that indicates to the preferential growth of hexagonal $MoSe_2$ in the (100) and (110) direction. This may facilitate the diffusion of Se through the already formed $MoSe_2$, thus leading to thicker $MoSe_2$ layers. The preferred orientation in (100) and (110) direction, i.e. the average orientation of the *c*-axis of the $MoSe_2$ layer parallel to the Mo surface, becomes more pronounced for $MoSe_2$ layers grown at 530 and 580 °C for 60 and 30 minutes, respectively.

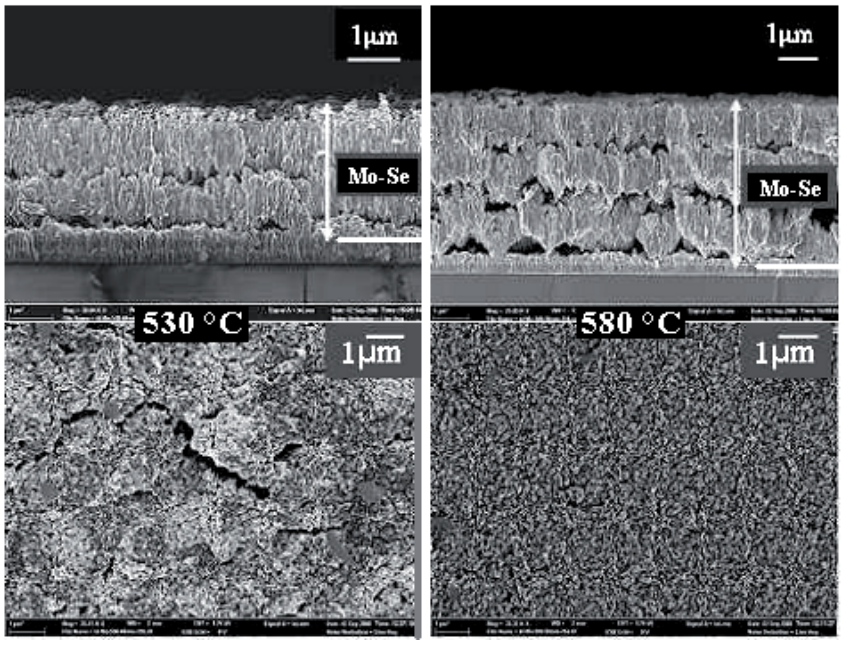

Figure 14. SEM cross-sectional and surface photos of $Mo^2/MoSe_2$ samples annealed in the isothermal conditions at 530 °C for 60 minutes (left) and at 580 °C for 30 minutes (right) under Ar over-pressure.

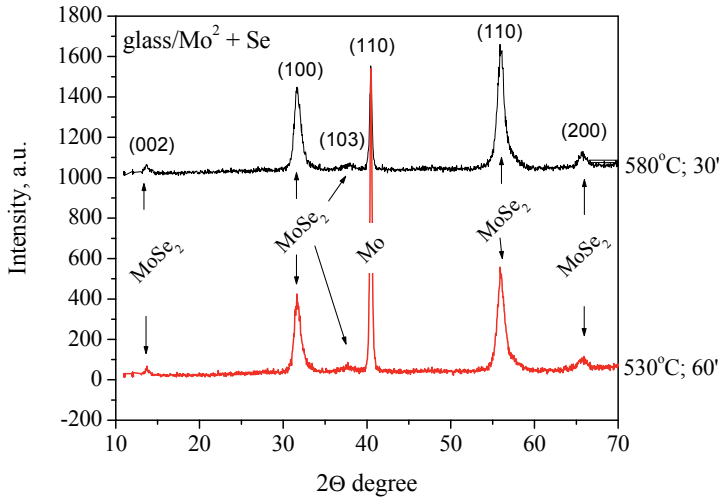

Figure 15. XRD patterns of $Mo^2/MoSe_2$ samples annealed under isothermal conditions at 530 °C for 60 minutes (lower) and at 580 °C for 30 minutes (upper) under Ar over-pressure.

Correspondence between the results of SEM and XRD analysis. From SEM micrographs (see Fig. 16) it is visible that the top layer's (surface's) orientation is different from the orientation of the middle layers with less pronounced $MoSe_2$ texture. This result is in good accordance with XRD results (Fig. 17). We found that by rising the selenization temperature the thickness of the top layer of $MoSe_2$ can be reduced. We assume that at heating temperatures below 530 °C, the orientation of the *c*-axis of the $MoSe_2$ layer may be perpendicular to the Mo surface, thus reducing the Se diffusion through the layered $MoSe_2$ structure and leading to the formation of thinner $MoSe_2$ layers.

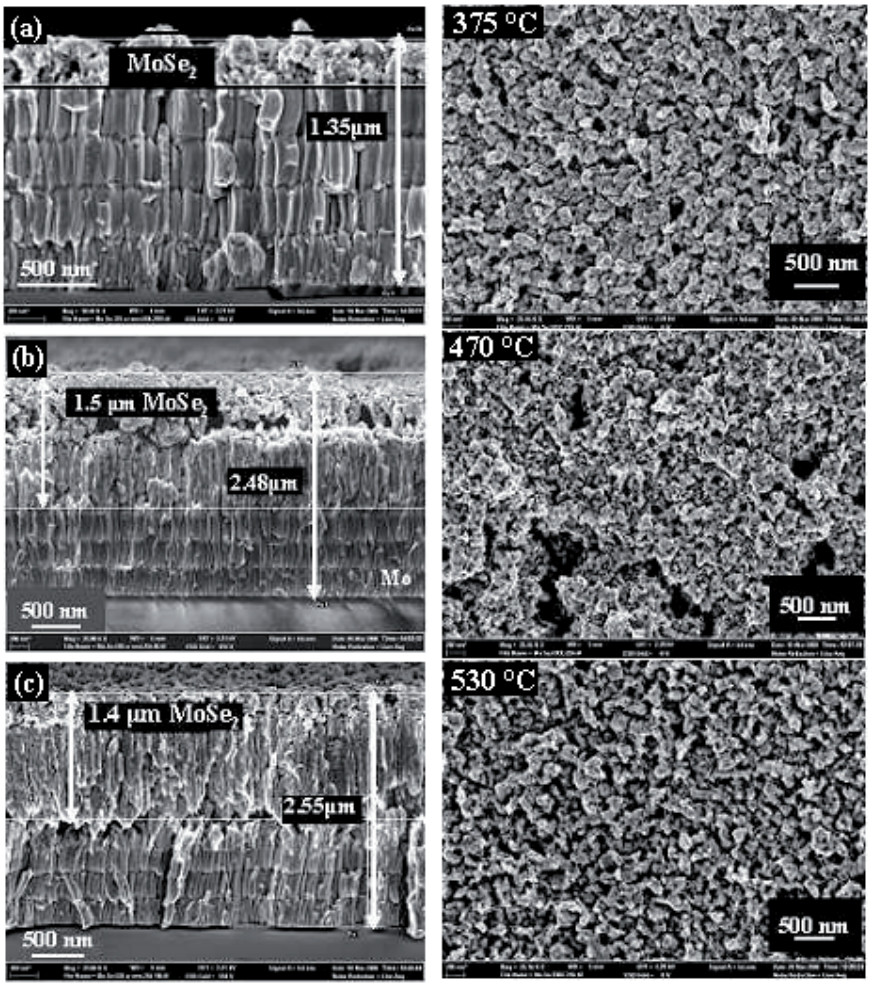

Figure 16. SEM images of cross-sections and surfaces of $MoSe_2$ layers on glass/Mo^2 substrates. Selenization process under isothermal conditions for 30 minutes at: (a) 375 °C, (b) 470 °C and (c) 530 °C.

Resulting from the analysis of $MoSe_2$ samples selenized for 30 minutes at different temperatures under isothermal conditions (Fig. 16), the following features can be drawn out:

a) $MoSe_2$ grown at 375 °C was non-orientated; the surface was neither smooth nor dense and porous. The total thickness of the Mo/$MoSe_2$ layers was about 1.3 μm, wherefrom the $MoSe_2$ layer thickness was determined to be approximately 250 nm.
b) Annealing at 470 °C resulted in $MoSe_2$, composed of two layers, the top layer was similar to the previously described 375 °C layer and the next layer under the top layer (following the initial layered structure of as deposited Mo) was orientated with the *c*-axis parallel to the Mo surface. The total thickness of the formed $MoSe_2$ was around 1.5 μm, with thicknesses of the two layers described above being 700 and 800 nm, respectively. According to the SEM analysis, thickness of the upper non-orientated layer of $MoSe_2$ diminished with increasing the selenization temperature.
c) Selenization at 530 °C was found to be a breaking point from where (at higher temperatures) mainly $MoSe_2$ with *c*-axis parallel to Mo surface grows. Still the 30-minute selenization resulted in a mixture of $MoSe_2$ with *c*-axis parallel and perpendicular to the Mo layer. The surface layer was quite thin, about 330 nm, and is expected to disappear in a prolonged process.

With an increase of the selenization temperature from 470 to 530 °C, the orientation of the $MoSe_2$ layers changes from perpendicular to an almost parallel alignment with respect to the Mo substrate plane. If the *c*-axis orientation of the top $MoSe_2$ layer is perpendicular to the Mo substrate, the growth rate of $MoSe_2$ thickness is low due to the low diffusion rates of Se through the formed $MoSe_2$ layer with *c*-axis perpendicular to the Mo substrate. The reason for the evolution of the described top layer of $MoSe_2$ in the isothermal selenization process, where the Se source and the Mo sample are placed into the close vicinity of each other, could be the rapid selenium flow from the Se source to the Mo sample surface at the beginning of the process when occurs the temperature difference between the colder sample and the hotter ampoule walls, and before Na, diffusing from the glass, reaches to the reaction zone. The role of sodium in the re-orientation of MoS_2 was analysed in [96]. The authors connected the change in MoS_2 orientation with the formation of an intermediate solid solution Na_2S_x-MoS_2 (x=1–6≠5) at temperatures higher than 550 °C. Similar behavior can be proposed in the case of $MoSe_2$ because of the close values of electronic affinities of Se and S (2.4 and 2.5, respectively). From the literature it is known that O and Na impurities in Mo influence the selenization process. The only sodium source in our case can be the used glass substrates. Na out-diffusion from a SLG substrate plays an important role also in the fabrication of CIGS based solar cells enabling the growth of the crystals of the absorber material [97]. As it is known that sputtered Mo layers contain molybdenum oxides in Mo grain boundaries [96, 98,

99] that create efficient channels for Na diffusion [98]. By XPS measurements they found that Na is bound with Se rather than with O in grain boundaries of Mo. The diffusion of Na in metallic Mo is very slow ($D_{Na} = 2.3x10^{-10}$ cm^2/s for 800 ^oC [98]). Mo oxides between Mo grains are responsible for the rapid diffusion and high solubility of Na in the sputter-deposited Mo films [99]. It is very probable that sodium poly-selenides formed at lower temperatures are the mediators for the formation of $MoSe_2$ at higher temperatures. From the Na-Se phase diagram [100] it is seen that at around 495 ^oC there occurs a peritectic transformation of Na_2Se_2 to Na_2Se and liquid Se forms. The latter can act as a liquid flux for the recrystallization of both the CIGS absorber material and $MoSe_2$ crystals. At low Se partial pressure the formation of Na_2Se_x (x=1) dominates and no Se is available. This was used to explain the lowered selenization of Mo in the presence of Na at low Se partial pressure [101]. At high Se partial pressures the formation of Na_2Se_x (x>1) dominates and Se is available for Mo selenization and also as flux for recrystallisation and growth at temperatures higher than 495 °C.

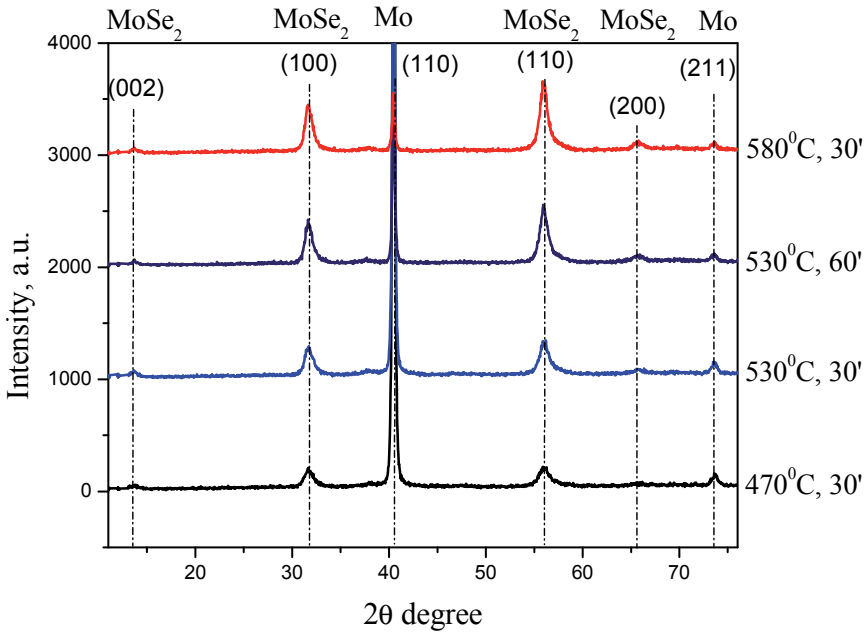

Figure 17. XRD patterns of $Mo/MoSe_2$ samples annealed in the isothermal conditions at 470, 530 and 580 °C for 30 and 60 minutes. Two upper patterns belong to samples selenized under Ar over-pressure.

In the case of the isothermal arrangement at high temperatures (530 and 580 °C), which corresponds to quite high selenium pressures ($8 \cdot 10^3$ Pa and $22 \cdot 10^3$ Pa) respectively [102]) and causes rapid selenization, the two samples placed

into the ampoule with their backs facing each other tended to stick together with selenium condensed between the glasses so that a sublimation process in vacuum was needed to remove the extra selenium on top and between of the layers. After that we annealed the samples in argon atmosphere to hold back the speed of the process and to prevent the total "adhesion" between the two layers.

Using the argon environment during the selenization in a closed isothermal system we can inhibit the process and decrease the condensation of a massive amount of selenium on the surfaces of the samples. At the beginning of the process, clearly, some amount of selenium is depositing to the substrate surface (selenium condensation). However, it is consumed in the further process, when the temperatures are converged and the diffusion process takes place. This results in more homogeneous layers. In this case the amorphous Se phase does not remain on the surface and the subsequent sublimation process is not required.

3.4. Two–zone selenization of Mo layers

Mo samples were selenized at 470, 530 and 580 °C for different periods (20 to 100 minutes) to understand the formation process of $MoSe_2$. Selenium zone temperatures were fixed at 300, 365, 450 and 500 °C that correspond to the Se vapor pressures of 10, 130, 1330 and 4400 Pa, respectively [102, 103].

Selenization of glass/ITO/Mo samples

On glass/ITO/Mo samples, even on a short period of selenization, thin molybdenum layers were fully selenized. The analysis of XRD patterns of the selenized glass/ITO/Mo substrates revealed that several phases - $MoSe_2$, ITO and In_2Se_3 and InSe - were formed by the selenization of ITO-on-Mo layers (see Fig. 13).

Selenization of glass/Mo^2 substrates

Selenization of glass/Mo^2 substrates for 60 minutes at 530 and 580 °C under the selenium vapor pressure of 4400 Pa (T_{Se}= 500 °C) resulted in dense and thick layers of $MoSe_2$ (see Fig. 19). The comparison of XRD patterns (Fig. 18) shows that $MoSe_2$ layers selenized at 580 °C consist of grains with a larger size and better crystallinity (XRD peaks are narrower and higher in the difractograms) but the Mo layer is selenized thoroughly (Mo peak disappeared in the XRD pattern).

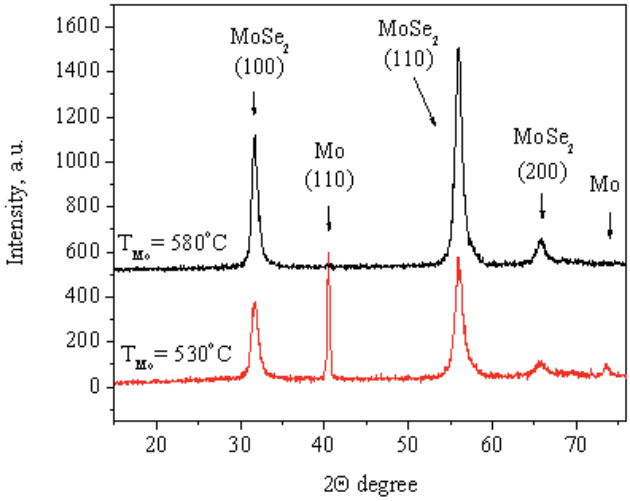

Figure 18. XRD patterns of glass/Mo[2] samples selenized for 1 h at 530 and 580 °C in two-zone ampoules under the selenium vapor pressure of 4400 Pa (T_{Se}= 500 °C).

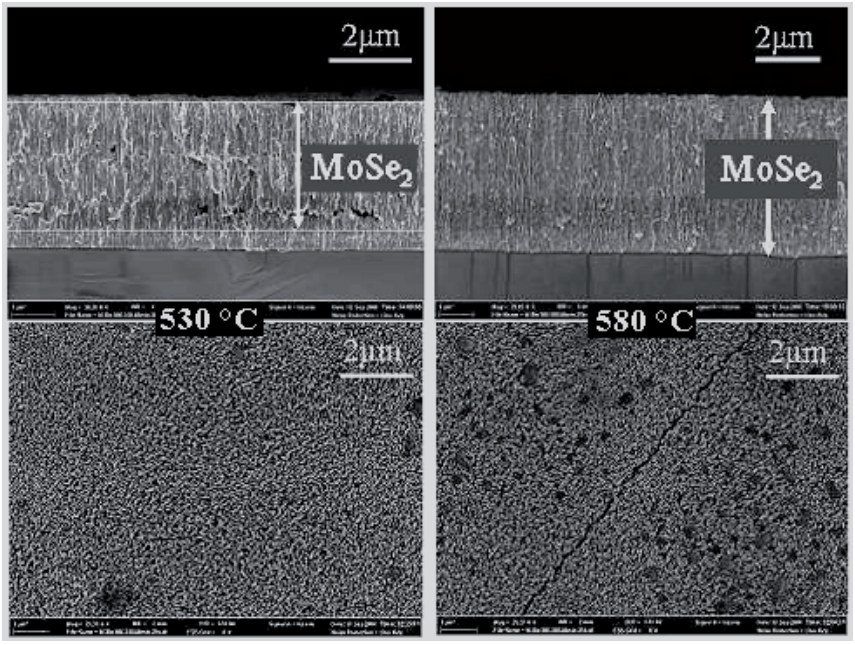

Figure 19. SEM cross-sectional and surface images of glass/Mo[2] samples selenized for 1 h at 530 °C (on the left) and 580 °C (on the right) in two-zone ampoules under the selenium vapor pressure of 4400 Pa (T_{Se}= 500 °C).

3.4.1. Growth rate of $MoSe_2$

$MoSe_2$ layers on substrates selenized at 470 °C were thinner compared with the samples selenized at 530 °C. Their thickness increased with increasing temperature and duration. The dependences of Mo-Se layer thickness on the selenization time and the Se vapor pressure are presented in Fig. 20. The growth rates of $MoSe_2$ films on Mo layers of various origin were different. Fig. 20(a) shows that the thickness of $MoSe_2$ layer on Mo-foil selenized at 530 °C in the Se vapor of 4400 Pa increases linearly with increasing selenization time.

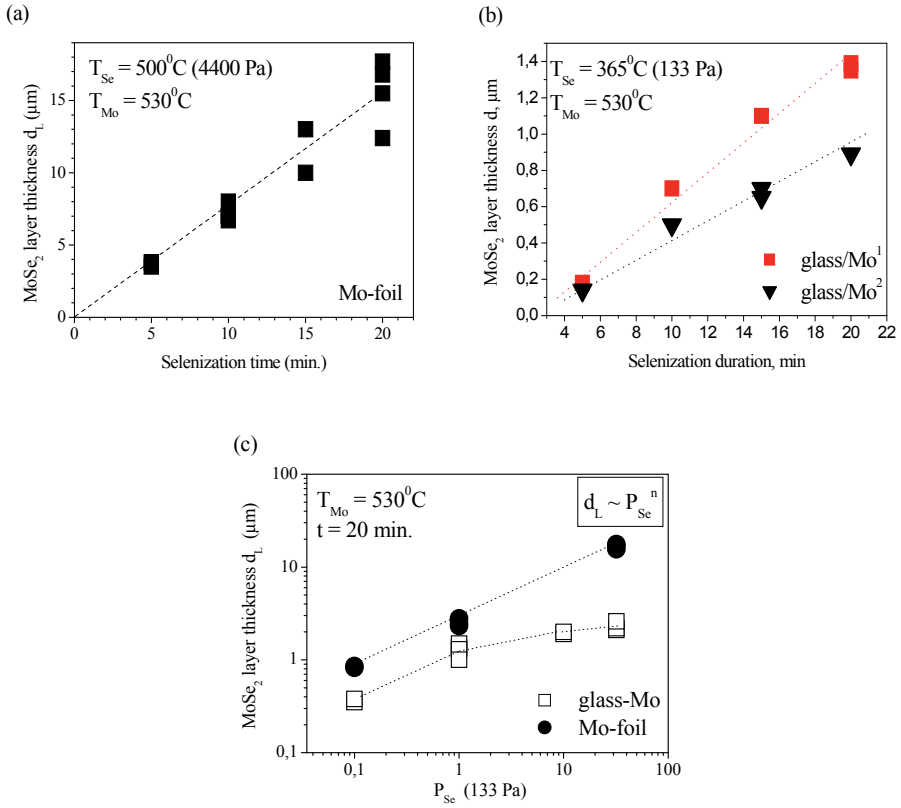

Figure 20. Dependence of the thickness of the $MoSe_2$ layer on the selenization time ((a)- Mo-foil and (b)- glass/Mo^1 and glass/Mo^2)) and on the Se vapor pressure (c).

The growth rate of the thickness is about 0.7 μm per minute on Mo-foil. The $MoSe_2$ film thickness of sputtered glass/Mo samples of various origin (ETH Zurich and ZSW Stuttgart) was different under the same conditions. For example, after annealing for 20 minutes at 530 °C under the selenium pressure of 130 Pa, the thickness of $MoSe_2$ on the glass/Mo^1 samples was about 1.5 times

higher than that on the glass/Mo[2] substrates, resulting in the growth rate of about 1.3 μm (65 nm/min.) and 0.9 μm (45 nm/min.), respectively (Fig. 20(b)).

The growth rate in our experiments is much higher than it was found in [42] (3 nm/min.) for dc. sputtered Mo on Si substrates, where the selenization was also performed in the two-zone arrangement at 577 °C, but in a carrier gas stream, where the process rate was suppressed by the inflow of Se. The authors of the work [42] explained the growth of the $MoSe_2$ layer thickness as a process limited by the diffusion of Se atoms through the grown $MoSe_2$ layer and they fitted the experimental data with $D=x^2/2t$ and estimated the value of the diffusion coefficient from the same dependence, where x means the thickness of the $MoSe_2$ layer (in the present study *thickness of the $MoSe_2$ layer is marked by* d_L) and t is the selenization time. From the above given equation, x is equal to $x=\sqrt{2Dt}$. It means that thickness should increase on time in the square root function dependence. This fitting does not coincide very well with all the experimental data of the work [42] (see Fig. 21). In view of all the experimental data of [42] in Fig. 21, the linear fitting would match much better. In our experiments $MoSe_2$ layer thickness increased linearly with the selenization time in the all cases, as it is realistic also in the work [42].

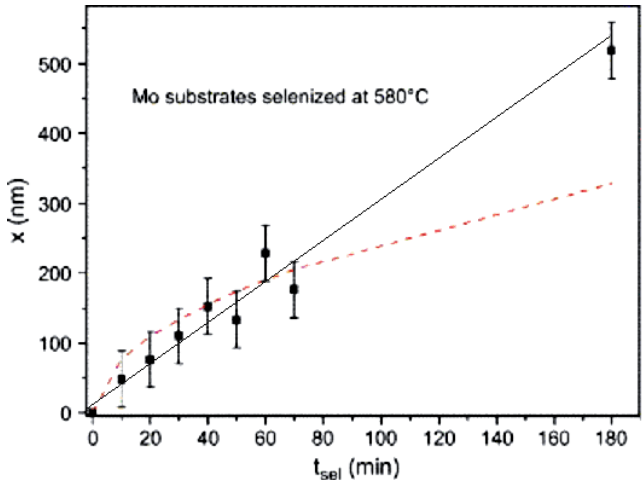

Figure 21. The $MoSe_2$ layer thickness x versus the selenization duration t_{sel}, obtained at a substrate temperature of 580 °C; the dashed curve gives the $x(t_{sel})$ square root dependence with $D=5\times10^{-14}$ cm^2/s. [42].

The dependences of the $MoSe_2$ layer thickness on the selenium vapor pressure both for Mo-foil and for sputtered Mo/glass samples are presented in Fig. 20(c). The growth of $MoSe_2$ layer thickness d_L on Mo-foil depending on the Se vapor pressure can be described as a power function: $d_L \sim P_{Se}^{1/2}$. In view of

the vapor phase of selenium at temperatures used in the present work consists of molecules given in Table 7, from where it can be seen that Se_2 and Se_5 molecules (weight average around 4 atoms) prevail in the used temperature range, the formation process of $MoSe_2$ at constant temperature can be written as follows:

$$\mathbf{Mo + 1/2Se_{4\ (weight\ average)} \rightarrow MoSe_2.} \quad (1)$$

On the basis of the reaction (1), the growth of the thickness of $MoSe_2$ layer d_L on Se vapor pressure can be described as:

$$\boldsymbol{d_L \sim k\, P_{Se}^{1/2}}, \quad (2)$$

where k is the velocity constant of the reaction (1). On this analytical basis we can conclude that the diffusion of Se does not inhibit the growth rate of $MoSe_2$ on Mo foil and it is limited by selenium availability on the Mo surface.

Table 7. Partial pressure (atm.) of different Se molecules in the vapor phase of Se [103]

T, K	**T**, deg.C	**∑Pse**, atm.	**Se_2**	**Se_3**	**Se_5**	**Se_6**	**Se_7**	**Se_8**
650	**377**	2.46 x10^{-3}	5.54 x10^{-4}	1.32 x10^{-5}	1.32 x10^{-3}	3.89 x10^{-4}	1.55 x10^{-4}	2.75 x10^{-5}
Partial load (%)		100	22.5	0.54	53.66	15.8	6.3	1.1
800	**527**	9.2 x10^{-2}	2,35 x10^{-2}	1.26 x10^{-4}	5.76 x10^{-2}	6.92 x10^{-3}	3.23 x10^{-3}	5.88 x10^{-4}
Partial load (%)		100	25.54	0.14	62.61	7.52	3.51	0.64

The selenization process of the sputtered Mo layer differs from the process of Mo-foil. The similar, $d_L \sim P_{Se}^{1/2}$, behavior is visible only in the low Se vapor pressure region (Fig. 20(c)). The growth of the $MoSe_2$ layer proceeds due to the diffusion of selenium atoms or molecules through the layered structure of $MoSe_2$ followed by their subsequent interaction with molybdenum atoms at the Mo-$MoSe_2$ interface. The straggling Mo grains in Mo-foil compared with dense sputtered Mo on glass could enable faster diffusion of Se atoms through the grown $MoSe_2$ layer. As ΔG of the reaction $Mo+Se_2 \rightarrow MoSe_2$ is negative at 530 °C: ΔG = - 145 kJ, we can conclude that difference in the density of Mo in substrates of various origin could be the reason for different packing density of the columnar structure of $MoSe_2$ as well, and this is the reason of different growth rates under the same processing conditions.

3.5. Comparison of the isothermal and two-zone arrangements of the Mo selenization process

In the isotermal arrangement the selenium source and the Mo sample are situated in the vicinity of each other in the same temperature range. Fast formation of a relatively high vapor pressure of Se in the vicinity of the Mo sample (determined by the heat treatment temperature) allows faster start of the $MoSe_2$ formation reaction in comparison with the two-temperature zone arrangement where the Se source is at a distance of about 30 cm from the reaction zone and the Se vapor pressure can be tuned by the lower temperature of the Se source. In the isothermal arrangement the vapor pressures of Se is determined by annealing temperature. The extent of the selenization of Mo can be tailored by the amount of Se in the reaction ampoule. For example: heating for one hour at 530 °C resulted in thoroughly consumed Se and Mo layers with the final thickness of the $Mo/MoSe_2$ layer of about 3 μm (possible maximum thickness being 4.4 μm, achievable at the same time in the two-zone process with an inexhaustible Se source). XRD analysis confirmed the existence of un-reacted Mo and $MoSe_2$ phases. SEM investigations of surface morphology did not show any cracks. However, after the 30-minute process at 580 °C, nearly the same thickness of $MoSe_2$ layer was gained with the same amount of Se. This means that the amount of Se was limiting the process of selenization in the isothermal arrangement.

Experiments showed that the optimum selenization temperature of Mo layers is 530 °C. At higher temperatures, the tensions between the layers were remarkable and thermal stresses resulted in cracks. If the layer is growing too fast, or the Mo layer is thoroughly selenized to $MoSe_2$, there can occur adhesion problems - peeling off either from glass or $MoSe_2$/Mo interface.

4. Selenization of Mo through different metallic layers

4.1. Characterization of isothermally selenized stacked Mo/Cu and Mo/In layers

The results of research in this field have been published and described in [II]. Influence of In and Cu coverage on molybdenum in the selenization process of Mo was investigated. The structural evolution of layers is illustrated in Fig. 22. In the case of In coverage (see left side photos in Fig. 22) at 300 ^{o}C Mo is covered with a polycrystalline core of formed In-Se compounds. At higher temperatures little crystals of In-Se are sparsely standing in the layer, allowing an easy Se molecule penetration to the layer. Cu on Mo (see right side photos in

Fig. 22) forms a compact continuous layer with large sintered crystals at lower temperatures. At higher temperatures the crystals in the layer grow larger and at the highest used temperatures gather to large single aggregates.

The native logarithmic dependences of the thicknesses of the $MoSe_2$ films as a function of reciprocal temperature are shown in Fig. 23. The thickness of $MoSe_2$ on uncovered Mo follows the Arrhenius equation (see Fig. 23). So, when a reaction has a rate constant (k) that obeys the Arrhenius equation, a plot of ln (k) versus T^{-1} (temperature) gives a straight line, whose slope and intercept can be used to determine E_a (activation energy) and A (pre-exponential factor, constant). This procedure has become so common in experimental chemical kinetics that it is widely used to define the activation energy for a reaction or some process. [104]:

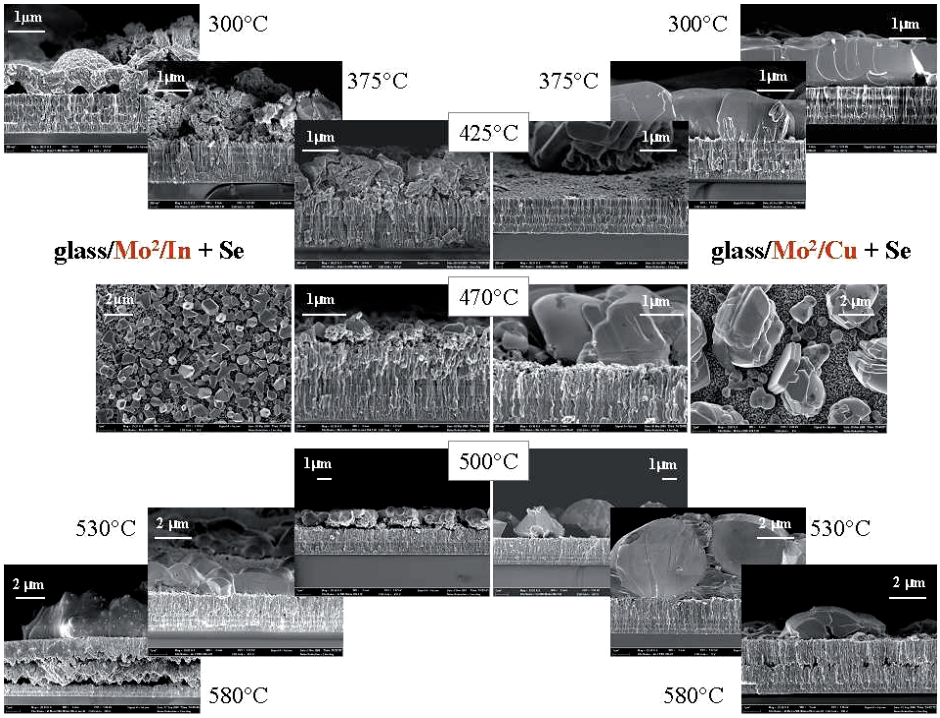

Figure 22. SEM micrographs of glass/Mo/In and glass/Mo/Cu substrates selenized at different temperatures.

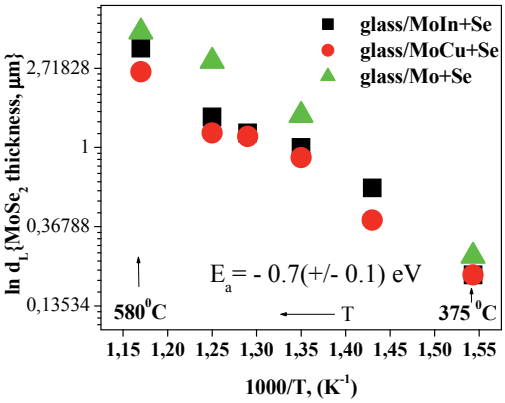

Figure 23. Dependence of the thickness of $MoSe_2$ on glass/Mo, glass/Mo/In and glass/Mo/Cu on the reciprocal selenization temperature.

From the Arrhenius plot the activation energy of the layer growth process was found to be - E_a = - 0.7 ± 0.1 eV that is close to the activation energy found in [105].

Clearly, the Cu and In layers on Mo impede the growth of $MoSe_2$ in comparison with uncovered Mo samples (see Fig. 23), while samples with indium gave thicker $MoSe_2$ layers than those with copper. The former is understandable in view that CuSe forms a compact continuous coverage on Mo (Fig. 22) that inhibits the access of Se molecules to Mo.

The formed $MoSe_2$ interlayer is clearly seen on the SEM images (Figs. 22 and 25) and its existence was confirmed by the EDS line scanning profiles (Fig. 26), XRD (Fig. 24) and Raman analysis (Fig. 27).

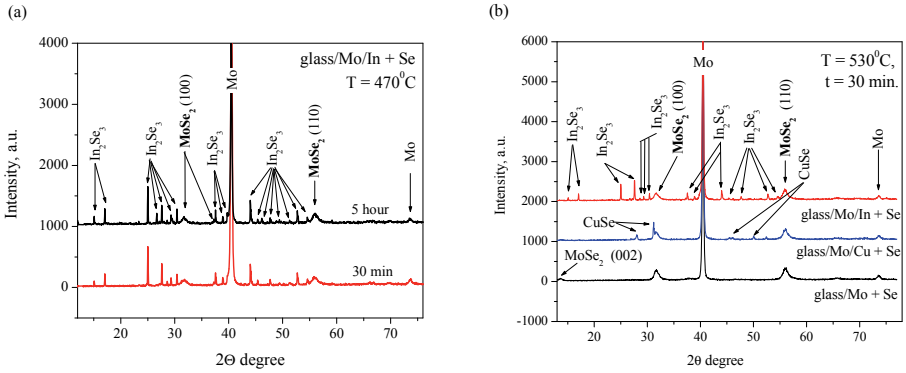

Figure 24. XRD patterns of glass/Mo, glass/Mo/In and glass/Mo/Cu layers selenized at 470 and 530 °C for 30 to 300 minutes.

The XRD analyses confirm that in addition to the hexagonal $MoSe_2$ [JCDPS card 29-0914] phase, large CuSe crystals [JCDPS card 34-0171, 20-1020] and In_2Se_3 [JCDPS card 40-1407] as agglomerated rounded crystals on the surface (Figs. 22 and 25(a, b) are presented in selenized $MoSe_2$ films. The formation of CuSe only is understandable in view that in closed ampoules the applied Se overpressure avoids the thermal decomposition of CuSe to Cu_2Se and Se, the process is being presumptive by the Cu-Se phase diagram [106]. Fig. 24(a) shows that the crystallinity of In_2Se_3 had not improved by prolonging the selenization time from 30 minutes to 300 minutes.

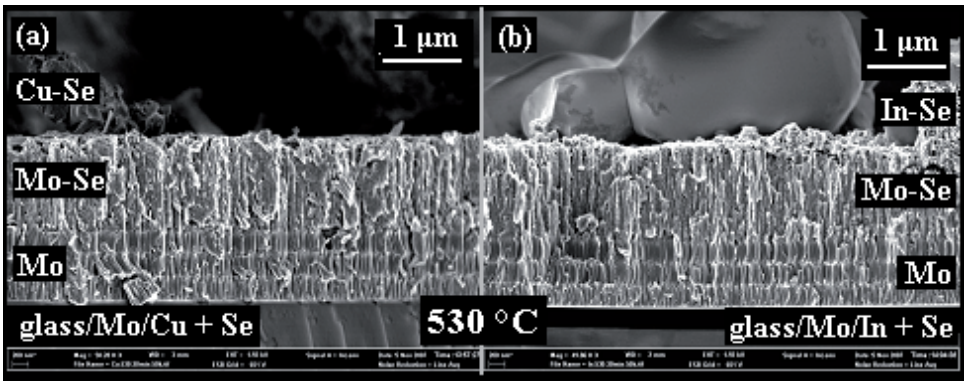

Figure 25. SEM micrographs of Mo/Cu (a) and Mo/In (b) layers selenized at 530 °C for 30 minutes.

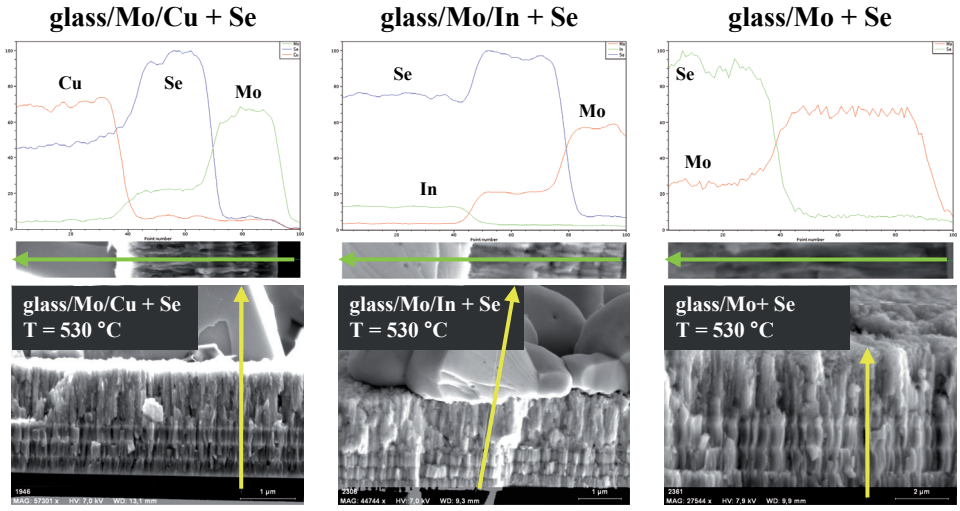

Figure 26. EDS line scanning profile of the cross-section of glass/Mo, glass/Mo/In and glass/Mo/Cu layers selenized at 530 °C for 30 minutes.

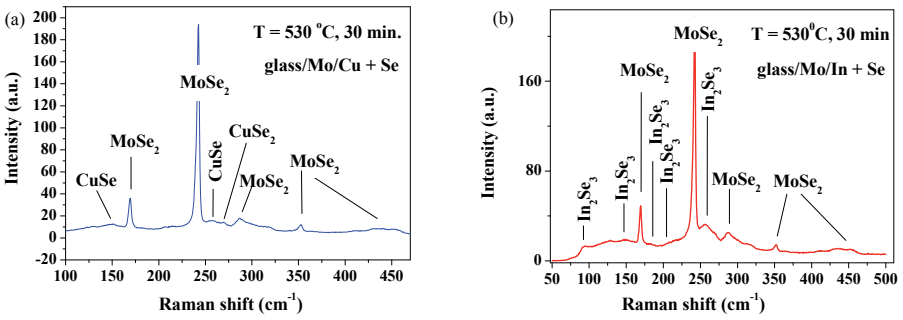

Figure 27. Raman spectra of (a) glass/Mo/Cu layers and (b) of glass/Mo/In layers selenized at 530 °C for 30 minutes.

Micro-Raman spectra in Figs. 27(a) and 27(b) of selenized Mo-In and Mo-Cu samples show the peaks at 169, 240, 280 and 350 cm^{-1} characteristic of $MoSe_2$ [107, 108]. Analysis of the Raman spectrum (Fig. 27(a)) of the glass/Mo/Cu layer selenized at 530 °C for 30 minutes shows the existence of different Cu-Se phases - Raman peaks at 147 and 260 cm^{-1} belong to CuSe [109, 110] and a peak at 270 cm^{-1}can be associated with Cu_2Se or $CuSe_2$ [111]. Analysis of the Raman spectrum of the glass/Mo/In layer selenized at 530 °C for 30 minutes (Fig. 27(b)) reveals besides $MoSe_2$ the existence of different phases – In_2Se_3 (Raman peaks at 91, 148, 182, 204 and 256 cm^{-1} [112, 113].

XPS study of glass/Mo/Cu and glass/Mo/In layers selenized by isothermal and two-temperature zone arrangement

The XPS depth profiles of selenized glass/Mo/Cu and glass/Mo/In layers are presented in Fig. 28. It is seen that Cu and In were diffused into Mo-Se layer. After etching off the surface layer, besides copper and indium, the bulk of the Mo-Se layer also contains oxygen.

It is known that as deposited Mo films sputtered without intentional substrate heating contain a significant amount of oxygen bound as MoO_2 and MoO_3 [96, 98]. In the work [98] the oxygen content of rf sputtered Mo films was 8 at%, as determined by RBS. It is important to point out that during the selenization in a two-temperature zone arrangement; the concentration level of oxygen in the layers is diminished in comparison with the isothermal selenization. This can be explained by the formation of SeO_2 that has remarkable vapor pressure at the applied temperatures and condensates in the lower temperature zone due to the difference of SeO_2 vapor pressures at 500 and 530 °C [103] (melting point of solid SeO_2 is 340-350 °C [114].

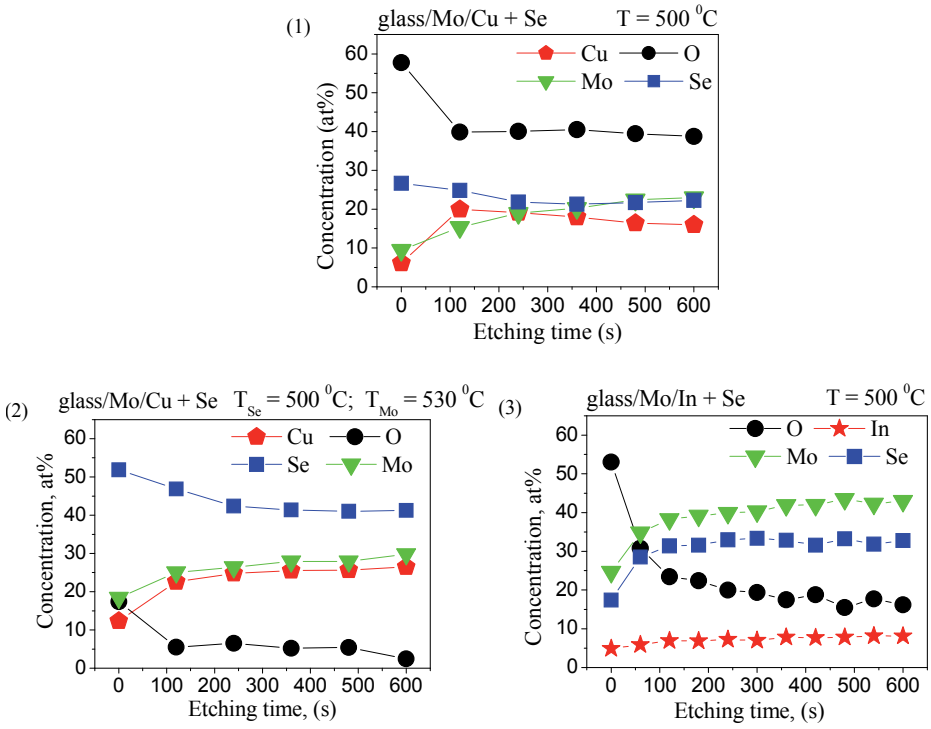

Figure 28. XPS depth profiles of glass/Mo/Cu substrates selenized under (1) isothermal and (2) two-temperature zone arrangement, (3) XPS depth profile of glass/Mo/In substrates selenized under (1) isothermal arrangement.

4.2. Characterization of the two-zone selenization process of Mo/CuIn films

Precursor CuIn alloy films on Mo exhibit a rough bilayer structure of the surface in which island-type crystals were formed. The cross-sectional SEM image of a CuIn alloy film (Fig. 29) indicates that island-type crystals extend through the matrix layer down to the Mo layer. The XRD pattern of as-sputtered metallic precursors is shown in Fig. 29. Before selenization the dominant $Cu_{11}In_9$ phase (matrix) and secondary In and $CuIn_2$ phases (island-type crystals) are present. The overall atomic ratio of as-sputtered metallic precursors was Cu:In = 0.88. Results are published in [III].

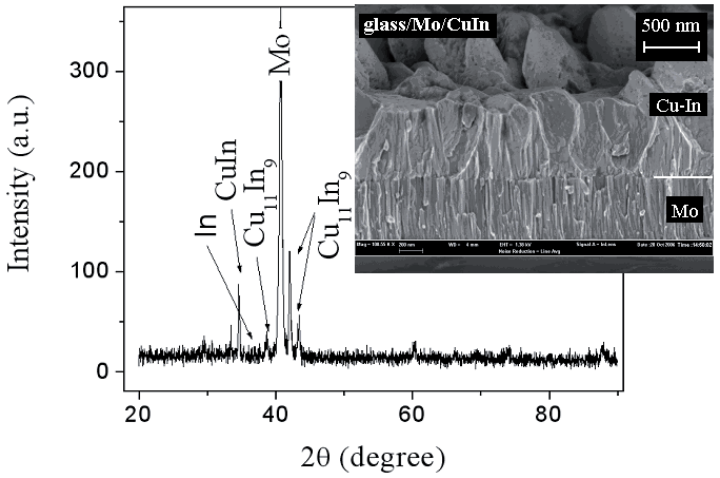

Figure 29. XRD pattern and SEM micrograph of as-sputtered metallic precursors.

Thickness of the Mo layer (500 nm) and Cu-In film (about 1000 nm) were measured on SEM images. The XRD pattern of glass/Mo/CuIn samples selenized at 470 ºC for 1 hour under selenium pressure of 130 Pa is shown in Fig. 30. The peaks of chalcopyrite $CuInSe_2$ (112) [JCPDS card 87-2265], Mo [card 42-1120], and hexagonal $MoSe_2$ [JCPDS cards 72-1420] are seen. The presence of a large number of peaks indicates that the films are polycrystalline in nature. The cross-sectional SEM micrographs of films selenized at 470 and 530 ºC for 1 hour are shown in Figs. 31(a) and 30(b). It is seen that the most part of Mo is transformed to $MoSe_2$ at 530 ºC.

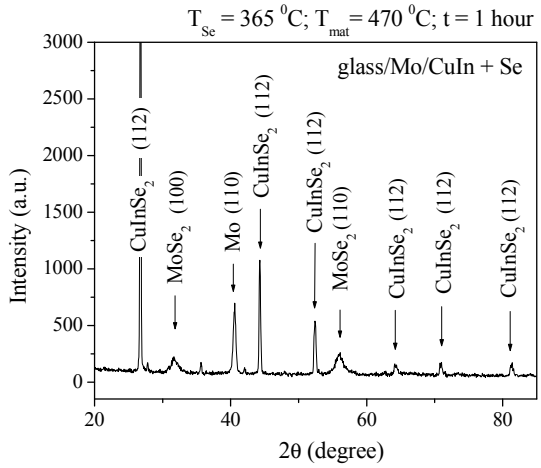

Figure 30. XRD pattern of glass/Mo/CuIn substrates selenized at 470 ºC for 1 hour under Se vapor pressure of 130 Pa.

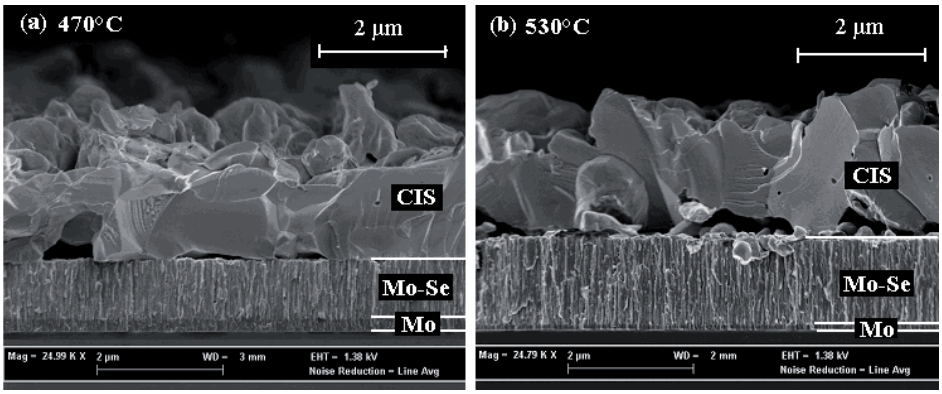

Figure 31. Cross-section SEM micrographs of selenized glass/Mo/CuIn films at (a) 470 °C and (b) 530 °C under selenium pressure 130 Pa for 1 hour.

The cross-sectional SEM images (Fig. 31) of layers selenized at 470 °C exhibit uniform, large and densely packed $CuInSe_2$ crystals with sizes of about 2 µm. The surface of the films is relatively smooth, providing good starting conditions for their use as absorber layers. The results of XRD analysis confirm that the layers selenized at 470 °C were single phase $CuInSe_2$. Preferred (112) orientation of crystals was observed for all the films. The thickness of well-grown CIS films is about three times larger than that of precursor layers. The thickness of the formed $MoSe_2$ layer was 0.9 µm at 470 °C and 1.4 µm at 530 °C.

4.3. Formation of $Cu_2ZnSnSe_4$ absorber films by selenization of electrodeposited Cu-Zn-Sn stacked layers on Mo substrates

The aim of this part of the work was to investigate $Cu_2ZnSnSe_4$ thin absorber film formation by selenizing electrochemically deposited Cu-Zn-Cu layers on glass/Mo substrates. Two different ways of sequential electrodeposition were used:

1) electrodeposition of Cu-Zn followed by the deposition of the Cu-Sn alloy;
2) electrodeposition of Cu-Zn followed by the deposition of a Sn layer.

Precursors were electrodeposited from aqueous pyrophosphate solutions containing sulphate salts of Cu^{2+}, Zn^{2+} and Sn^{2+}. More detailed information about the deposition conditions is given in [IV] and [V].

Electrochemically deposited and thermally treated films were investigated by different methods to identify the composition of the films and to clarify the existence of secondary phases in selenized films. The morphology and the

thickness of the films were observed and studied as well. The electrodeposited metallic precursor films were selenized under isothermal conditions for 15 to 60 minutes at different temperatures: 450, 490, 530 and 560 °C [115]. Table 8 (in Appendix B) presents the composition of electrodeposited precursor films and selenized films as determined by EDX.

4.3.1. Investigation of Cu-Zn and Cu-Sn stacked layers

Fig. 32 presents XRD patterns of samples 36-8/4 and 36-5/8. Sample 36-8/4 passed additionally the homogenization step in vacuum at 400 °C for 1 hour, after that those films were isothermally selenized at 560 °C for 1 hour. Sample 36-5/8 was selenized at 530 °C for 15 minutes and then cooled down slowly.

In both cases, main reflexes of CZTSe are seen, signals are strong and peaks sharp, indicating well-crystallized CZTSe [JCDPS 01-070-8930]. Well-defined reflexes from molybdenum substrate layer are detected. Also, we can see reflexes (11.54, 31.66 and 56 °) which belong to the $MoSe_2$ phase [JCDPS 03-0653481].

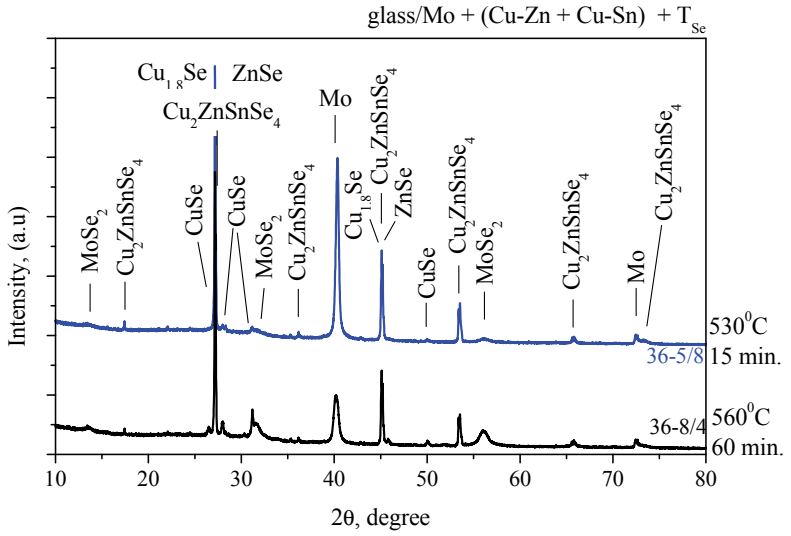

Figure 32. X-ray diffraction patterns of $Cu_2ZnSnSe_4$ thin layers annealed in different regimes: Sample 36-5/8 – selenization for 15 minutes at 530 °C and 20 minutes slow cooling down; 36-8/4 – 1 hour annealing in vacuum and 1 hour selenization at 560 °C.

In both cases, detailed structural analysis has revealed multiphase thin film materials. There are minor well distinguished reflexes related to CuSe [JCDPS 01-070-8576]. ZnSe [JCDPS 01-080-0021] is difficult to determine due to the

coincident with the CZTSe peaks. In addition, scrupulous analysis supposes existence of another phase – $Cu_{1.8}Se$ [JCDPS 01-071-0044]. Comparing the data in Fig. 32 it is possible to conclude that a longer annealing time is favourable for the formation of well-crystallized $Cu_2ZnSnSe_4$. Also, Raman spectra showed well-formed CZTSe phases (see article IV).

Fig. 33 presents a SEM cross-sectional CZTSe and surface views of a sample, which was annealed in vacuum for 1 hour at 400 °C and then selenized at 560 °C for another hour. CZTSe thin layer consists of large grains with a size of about 1 μm or more.

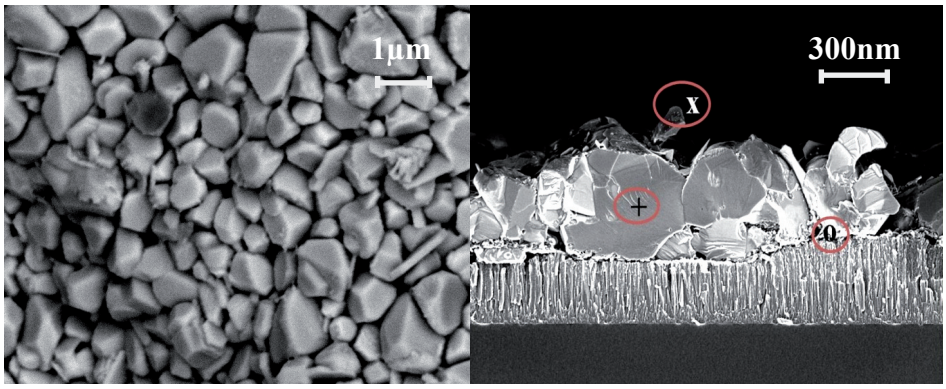

Figure 33. Surface overview (left) and SEM cross-sectional view (right) of a CZTSe thin film annealed in vacuum for 1 hour, followed by selenization at 560 °C for 1 hour. + indicates a slightly Sn rich CZTSe crystal, **o** presents the ZnSe phase, **x** corresponds to the CuSe.

The band gap of the CZTSe thin films was determined by optical measurements as 1.31 ± 0.01 eV. This value is larger than determined for CZTSe [116] by now. It can be explained by the existence of ZnSe in films, as it was shown in [117] (see article IV).

4.3.2. Selenization of Sn on Cu-Zn stacked films

Cu-rich, stoichiometric and Cu-poor layers were selenized at 450 °C to find out the influence of the film initial composition on the produced CZTSe properties. After that the following selenization experiments at different temperatures (490, 530 and 560 °C) were done with Cu-poor samples of CZTSe. The composition of layers and selenization parameters for all the samples used are presented in Table 9 (in Appendix B). According to the XRD analysis, $Cu_2ZnSnSe_4$ Mo and $MoSe_2$ (reflections at 11.5, 31.6 and 56.0 °) were detected, also several secondary phases ZnSe, CuSe and also Cu_2SnSe_3 and Cu_2SnSe_4 ternaries were found in the selenized layers [118]. By increasing the selenization temperature,

the number of secondary phases decreases and ZnSe prevails. Raman measurements also confirm the existence of CZTSe and ZnSe phases. In all samples, according to Raman measurement, the dominating phase is CZTSe. More detailed information is presented in [V].

Fig. 34 shows the morphology of a CZTSe film annealed at 530 °C (Fig. 34(a)) and its cross-sectional view (Fig. 34(b)). The layer is uniform, dense and well crystallized with a grain size of about 1 μm. On the borders of grains small hexagonal crystals of some secondary phase are seen. Thickness of $MoSe_2$ is approximately 1.3 μm, which coincides with the results obtained by selenizing glass/Mo substrates with In and Cu layers under similar conditions.

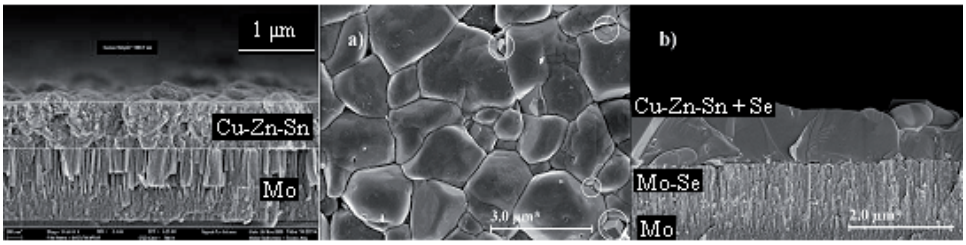

Figure 34. High resolution SEM cross-sectional micrograph of an as deposited Cu-Zn-Sn layer (on the left), (**a**) surface view of a thin CZTS layer selenized at 530 °C for 30 min in isothermal conditions and (**b**) – cross-section of the selenized film. Hexagonal secondary phases on grain boundaries are marked by circles.

CONCLUSIONS

The main objective of this thesis was to form $MoSe_2$ layers on different Mo substrates by the selenization method. The results comprise two parts and can be presented as follows:

$MoSe_2$ at the isothermal and two-temperature-zone selenization of Mo substrates of different origin

- Differences in the density of Mo in the substrates of various origins are the reason for different packing density of the columnar structure of $MoSe_2$ and this is the reason of different growth rates of $MoSe_2$ under the same processing conditions.
- The formation of $MoSe_2$ of *p*-type conductivity on Mo substrates was found in the temperature range from 375 to 580 °C under applied selenium vapor pressures and used annealing durations.
- The optimum selenization temperature was 530 °C, which resulted in uniform $MoSe_2$ layers with the *c*-axis orientation parallel to the Mo surface.

At higher temperatures, the tension between the layers was found to be remarkable and resulted in cracks and poor adhesion.

- The thickness of $MoSe_2$ on rf. sputtered glass/Mo samples follows the Arrhenius equation - the thickness (in a native logarithmic scale) of the formed $MoSe_2$ layer increases linearly with the reciprocal selenization temperature. The activation energy of the process was found as $E_a = - 0.7 \pm 0.1$ eV.
- In the two-zone arrangement the thickness of the formed $MoSe_2$ layer d_L on Mo-foil depends on the selenization duration t linearly and on the Se vapor pressure P_{Se} as a function $d_L \sim P_{Se}^{1/2}$. Isothermal arrangement allows a faster start of the $MoSe_2$ formation in comparison with a two-temperature zone arrangement. We can conclude that the selenization process in the isothermal arrangement can be controlled by the annealing duration and temperature if the added amount of elemental Se is unlimited or by the limited amount of Se.
- It was found that the selenization in the two-temperature zone arrangement allows the concentration of oxygen in the $MoSe_2$ layers to be reduced in comparision with the isothermal selenization due to the possibility to condensate the formed SeO_2 (g) to the lower temperature zone as SeO_2 (l, s).

Selenization of Mo through different metallic stacked layers

- Cu and In layers on Mo were found to impede the growth of $MoSe_2$ as compared with uncovered Mo samples. The thickness of $MoSe_2$ layer was higher on the glass/Mo/In samples than on glass/Mo/Cu samples under the same selenization conditions due to the faster penetration of Se molecules through the formed In_2Se_3 with smaller crystals in contrast to the formed compact continuous coverage of CuSe.
- The structural evolution of selenized films was analyzed, all samples showed the formation of $MoSe_2$ interlayer, with thickness increasing by the duration and temperature of the selenization process. Thickness of the grown $MoSe_2$ layer corresponds approximately to the value which has been achieved under similar selenization conditions without stacked metal layers.
- $CuInSe_2$ films were prepared by the selenization of the glass/Mo/CuIn precursors. It is shown that the selenization of co-sputtered Cu–In alloy films at high temperatures results in high-quality dense chalcopyrite CIS films with crystals of about 2 μm and with a preferred orientation of the crystals in the (112) direction.
- Selenization of electrodeposited Cu-Zn-Se stacked layers at high temperatures (530 °C and more) results in a highly crystallized and well-ordered material with a grain size of about 1 - 1.5 μm. Films selenized during 15 minutes at high temperatures already presented a well-crystallized $Cu_2ZnSnSe_4$ phase.

ACKNOWLEDGEMENT

This thesis is based on the experimental work carried out at the Department of Materials Science, Tallinn University of Technology.

I am sincerely thankful to my supervisor, Dr. Mare Altosaar, whose encouragement, guidance and support from the initial to the final level enabled me to develop an understanding of the subject, for fruitful discussions and interesting ideas and for guiding me all through those years.

I would also like to thank Prof. Enn Mellikov, Head of the Department of Material Science at TUT, for his support throughout the time in his laboratory. It is a pleasure to thank those who made this thesis possible, Dr. Olga Volobujeva for the SEM and EDX analysis, Prof. Paul Barvinschi, MSc., Rainer Traksmaa and Dr. Arvo Mere for the XRD analysis, Dr. Maarja Grossberg and PhD student Taavi Raadik for the Raman analysis. Special thanks go to Dr. Jaan Raudoja and Dr. Karin Kerm. I would like to express my gratitude to all my colleagues for their contribution to this work. Dr. Kaia Ernits has made available her support in a number of ways.

Financial support from Estonian Science Foundation (under contacts № 6160, 6179, 8147 and 8964), Estonian Doctoral School of Materials Science and Materials Technology (MMTDK), Graduate School on Functional Materials and Technologies (GSFMT), University of Tartu and Tallinn University of Technology, EU Social Funds Project 1.2.0401.09-0079, the financial support of the European Union Energy Programme and European Social Fund Fund's Doctoral Studies and Internationalisation Programme DoRa are gratefully acknowledged.

My warmest and deepest gratitude belongs to my family.

Tallinn, October 2011

Liina Kaupmees

ABSTRACT

Selenization of molybdenum as contact material in solar cells

This study focuses on the selenization process of Mo samples prepared by different methods and different coverages: sputtered glass/Mo, Mo-foil, glass/ITO/Mo, glass/Mo/In, glass/Mo/Cu, glass/Mo/Cu-In and glass/Mo/Cu-Zn-Se were used as substrates to study the $MoSe_2$ layer formation. Dependence of the selenization process of Mo on the temperature and time was studied by the two-temperature zone and the isothermal one-zone selenization methods. Thickness, structure, morphology and composition of $MoSe_2$ were determined. Samples were characterized by EDX, SEM, XRD, XPS, Raman and the Hot Probe method.

The formation of $MoSe_2$ of *p*-type conductivity on Mo was found in the used temperature range from 375 to 580 °C under the applied selenium vapor pressures and used annealing durations. It was found that in the case of isothermal arrangement, quick formation of a relatively high vapor pressure of Se in the vicinity of the Mo sample (determined by the heat treatment temperature) allows a faster start of the $MoSe_2$ formation in comparison with the two-temperature zone arrangement. The growth rates of $MoSe_2$ films on the Mo layers of various origin were different. The thickness of $MoSe_2$ on rf. sputtered glass/Mo samples follows the Arrhenius equation - the thickness (in native logarithmic scale) of the formed $MoSe_2$ layer increases linearly with the reciprocal selenization temperature. The activation energy of the process was found as $E_a = - 0.7 \pm 0.1$ eV. In the two-zone arrangement the thickness of the formed $MoSe_2$ layer d_L on Mo-foil depends on the selenization duration t linearly and on the Se vapor pressure P_{Se} as a function $d_L \sim P_{Se}^{1/2}$. It was found that the crystal structure and the orientation of the $MoSe_2$ layer change with an increasing substrate temperature. At increasing of the selenization temperature from 470 to 530 °C, the orientation of the formed $MoSe_2$ layers changed from perpendicular to an almost parallel alignment with respect to the Mo substrate plane that could be connected with the diffusion of Na from the glass and formation of Na_2Se_2 that has a peritectic transformation to Na_2Se and liquid Se at around 495 ^oC. The latter can act as a liquid flux for the recrystallization and reorientation of $MoSe_2$ crystals. The optimum selenization temperature of Mo for solar cell back contact was found to be around 530 °C that gave uniform $MoSe_2$ layers without cracks and with the *c*-axis orientation parallel to Mo surface. At higher temperatures, the tension between the layers was found to be remarkable and resulted in cracks and poor adhesion - peeling off $MoSe_2$ either from glass or from $MoSe_2$/Mo interface. The large difference in the molar volume between Mo and $MoSe_2$ is considered to be also one reason for peeling the CISe/($MoSe_2$)/Mo layer off the glass substrate, because it creates significant internal stresses during the selenization processes.

Cu and In layers on Mo were found to impede the growth of $MoSe_2$ in contrast to uncovered Mo samples. The thickness of the $MoSe_2$ layer was higher on the glass/Mo/In samples than on the glass/Mo/Cu samples under the same selenization conditions due to the faster penetration of Se molecules through the formed In_2Se_3 with smaller crystals than with formed compact continuous coverage of CuSe. It was found that the selenization in the two-temperature zone arrangement allows the concentration of oxygen in the $MoSe_2$ layers to be reduced in comparision with the isothermal selenization due to the possibility to condensate the formed SeO_2 (g) to the lower temperature zone as SeO_2 (l, s).

It was found that the selenization of glass/Mo/CuIn samples at 470 and 530 ºC for 1 hour under the selenium pressure of 130 Pa resulted in high-quality dense chalcopyrite CIS films with a preferred orientation of the crystals in the (112) direction. The surface of the films was smooth, providing good starting conditions for their use as absorber layers. At a substrate temperature of 470 and 530 °C and Se evaporation temperature of 365 °C (130 Pa), 0.9 and 1.4 μm thick $MoSe_2$ layers formed in 1 hour.

Electrochemically deposited Cu-Zn-Se precursor layers on Mo were selenized at 450 ÷ 560 °C. It was found that well-crystallized CZTSe material with a crystal size around 1-1.5 μm can be gained at temperatures 530 ÷ 560 °C. XRD and Raman analyses showed a multiphase composition of the films where in addition to CZTSe crystals Cu_xSe, ZnSe, $SnSe_2$ and $MoSe_2$ phases also existed. Thickness of $MoSe_2$ was approximately 1.3 μm, which coincides with the results gained by the selenization of glass/Mo/In and glass/Mo/Cu substrates. Multiphase formation of the composition provides direction for the future research to find the conditions that ensure single phase CZTS absorber layer by electrochemical deposition.

KOKKUVÕTE

Molübdeeni kui päikesepatarei kontaktmaterjali seleniseerimine

Käesolev uurimustöö on keskendunud erinevate saamismeetodite teel kasvatatud Mo-aluste seleniseerimisele, uuring hõlmab ka erinevate katete mõju $MoSe_2$ kihi tekkele seleniseerimisprotsessis. $MoSe_2$ kihi moodustumiseks kasutati järgmisi Mo-aluseid – Mo-leht, tolmustatud Mo/klaas, Mo/ITO/klaas, In/Mo/klaas, Cu/Mo/klaas, tolmustatud Cu-In sulam/Mo/klaas ja elektrokeemiliselt sadestatud Cu-Zn-Sn/Mo/klaas. Ühe- ning kahe- temperatuuritsoonilist seleniseerimismeetodit kasutades uuriti Mo seleniseerimisprotsessi sõltuvust nii ajast kui ka temperatuurist. Moodustunud $MoSe_2$ kihtidel tehti kindlaks koostis, määrati paksus, juhtivustüüp ning uuriti kihi struktuuri ja morfoloogiat kasutades järgnevaid uurimismeetodeid – SEM, EDX, XRD, XPS, Raman ja „kuuma sondi meetod".

P-tüüpi juhtivusega $MoSe_2$ kihid saadi temperatuurvahemikus 375 – 580 °C kuumutamisel seleeni aururõhus. Leiti, et ühetsoonilise katsekorralduse puhul on $MoSe_2$ teke kiirem, võrreldes kahetsoonilise katsekorraldusega, kuna ühetsoonilise meetodi puhul on Mo-aluse lähedal tekkiv seleeni aururõhk kõrge (määratud termotöötluse temperatuuriga). $MoSe_2$ kihtide kasvumäärad (kihtide paksus) on erineva päritoluga Mo- kihtidel erinevad ehk siis Mo seleniseerimisel mängib olulist rolli Mo-kihi saamisviis. Ühetsoonilise katsekorralduse puhul klaas/Mo- alustel tekkinud $MoSe_2$ kihi paksus järgib Arrheniuse võrrandit - moodustunud $MoSe_2$ kihi paksus, (logaritmilises skaalas), kasvab lineaarselt vastavalt seleniseerimise temperatuurile. Leiti, et protsessi aktivatsioonienergia Ea = -0.7 ± 0.1 eV. Kahetsoonilise katsekorralduse käigus Mo-lehe seleniseerimisel tekkinud $MoSe_2$ kihi paksus d_L sõltub lineaarselt seleniseerimise ajast t ning seleeni aururõhust P_{Se} funktsioonina $d_L \sim P_{Se}^{1/2}$.

Leiti, et $MoSe_2$ kihi orientatsioon ja kristallstruktuur muutuvad substraadi temperatuuri tõstes. Ühetsoonilise katsekorralduse puhul - tõstes lõõmutustemperatuuri 470 → 530 °C-ni, muutub moodustunud $MoSe_2$ kihi orientatsioon Mo-aluse suhtes risti olevast paralleelseks. Oletatakse, et nähtus võib olla seotud Na väljadifusiooniga kasutatud klaasalusest Mo- kihti ning seal Na_2Se_2 faasi tekkimisega, mis 495 °C juures laguneb Na_2Se ja Se (l). Viimane käitub sulandajana rekristalliseerumisprotsessis ning $MoSe_2$ kristallide ümberorienteerumisel. Leiti, et Mo kasutamisel päikesepatarei kontaktmaterjalina on optimaalseks Mo seleniseerimise temperatuuriks 530 °C, mis tagab ühtlased pragudeta ning pidevad $MoSe_2$ kihid, mis on orienteeritud Mo–aluskihi suhtes paralleelselt. Kõrgemate temperatuuride juures saadud $MoSe_2$ kihid olid kihtidevaheliste pingete tõttu pragunenud ning sellest tulenevalt ka halva adhesiooniga, mis võib põhjustada kihtide irdumist Mo/$MoSe_2$ või klaas-Mo/$MoSe_2$ piirpindadel.

Cu- ja In- kihid Mo-l mõjutasid $MoSe_2$ kihi kasvu. Samadel seleniseerimistingimustel moodustunud $MoSe_2$ kihi paksus oli klaas/Mo/Cu

puhul väiksem kui klaas/Mo/In aluse puhul, olles tingitud seleeni molekulide kiiremast difusioonist läbi moodustunud In_2Se_3 väikeste kristallide, võrreldes pideva pinda katva CuSe kihiga. Leiti, et kahetsoonilise katsekorralduse puhul on võimalik vähendada hapniku kontsentratsiooni $MoSe_2$ kihis, mis on seotud võimalusega kondenseerida tekkinud gaasiline SeO_2 madalama temperatuuriga tsooni.

Klaas/Mo/CuIn kihtide seleniseerimine Se rõhul 130 Pa 470 ja 530 °C juures ühe tunni vältel andis siledad, (112) suunas orienteeritud kalkopüriitsed $CuInSe_2$ kihid, mis on kasutatavad absorbermaterjalidena päikesepatareides. $CuInSe_2$ ja Mo vahel tekkinud $MoSe_2$ kihtide paksused olid 0.9 ja 1.4 μm, vastavalt 470 ja 530 °C juures seleniseerides.

Elektrokeemiliselt Mo-le sadestatud kihtide seleniseerimisel temperatuurivahemikus 450 kuni 560 °C leiti, et hästi kristallunud CZTSe materjal, kristallisuurusega 1 – 1.5 μm, tekib seleniseerimisel vahemikus 530 – 560 °C. Kasutatud Cu-Zn-Sn kihtide algkoostis andis seleniseerimisel XRD ja Raman analüüside alusel mitmefaasilise materjali, kus lisaks CZTSe faasile esineb ka Cu_xSe, ZnSe, $SnSe_2$ ja $MoSe_2$. Moodustunud $MoSe_2$ vahekihi paksuseks saadi ligikaudu 1.3 μm, mis langeb ligilähedaselt kokku klaas/Mo/In ja klaas/Mo/Cu seleniseerimisel saadud tulemustega. Mitmefaasiline koostise teke annab suuna edaspidisteks uuringuteks sadestusparameetrite muutmise teel leida tingimused ühefaasilise CZTS absorberkihi saamiseks elektrokeemilise sadestuse teel.

REFERENCES

[1] A. E. Becquerel, Mémoires sur les effêts électriques produits sous l'influence des rayons, *Comptes rendus de l'Academie Scientifique* 9 (1839) 561.

[2] W. G. Adams, R. E. Day, The action of light on selenium, Proc. Roy. Soc. London, 25 (1876) 113.

[3] M. D. Archer and R. Hill, 2001, The past and present. In: Clean electricity from photovoltaics, ed., London, *Imperial College Press*, 2001, pp. 1-32.

[4] Wikipedia– online encyclopedia: http//en.wikipedia.org/wiki/Solar_cell#Three_generations_of_solar_cells.

[5] G Suresh Babu, Y B Kishore Kumar, P Uday Bhaskar, Sundara Raja Vanjari, Effect of Cu/(Zn+Sn) ratio on the properties of co-evaporated $Cu_2ZnSnSe_4$ thin films, *Solar Energy Materials & Solar Cells* 94 (2010) 221–226.

[6] R. W. Birkmire, Compound polycrystalline solar cells: Recent progress and Y2K perspective. *Solar Energy Materials& Solar Cells* 65 (2001) 17-28.

[7] http://www.zswbw.de/fileadmin/editor/USER_UPLOAD/Infoportal/Presseinformationen/pi05-2010-ZSW-Worldrecord-TF-CIGS.pdf

[8] R. J. Matson, O. Jamjoum, A. D. Buonaquist, P. E. Russell, L. L. Kazmerski, P. Sheldon, R. K. Ahrenkiel, Metal contacts to $CuInSe_2$, *Solar Cells* 11 (1984) 301.

[9] K. Orgassa, H. W. Schock, J. H. Werner, Alternative back contact materials for thin film $Cu(In,Ga)Se_2$ solar cells, *Thin Solid Films* 431-432 (2003) 387.

[10] P. E. Russell, O. Jamjoun, R. K. Ahrenkiel, L. L. Kazmerski, R. A. Mickelsen, W. S. Chen, Properties of the Mo-$CuInSe_2$ interface, *Appl. Phys. Lett*. 40 (1982) 995.

[11] W. Jaegaerrmann, T. Loher, C. Pettenkofer, *Cryst. Res. Technol*. 31 (1996) 273.

[12] W. N. Shafarman, J. E. Phillips, Direct current-voltage measurements of the Mo/$CuInSe_2$ contact on operating solar cells, in *Conference Record of the 25th IEEE Photovoltaic Specialists Conference, Washington D.C.,* USA, IEEE, Piscataway, New Jersey, 1996, p. 917.

[13] T. Wada, N. Kohara, T. Negami, M. Nishitani, Chemical and structural characterization of $Cu(In,Ga)Se_2$/Mo interface in $Cu(In,Ga)Se_2$ solar cells, *Jpn. J. Appl. Phys*. 35 (1996) L1253.

[14] N. Kohara, S. Nishiwaki, Y. Hashimoto, T. Negami, T. Wada, Electrical properties of the $Cu(In,Ga)Se_2$/ $MoSe_2$/Mo structure, *Solar Energy Materials & Solar Cells* 67 (2001) 209-215.

[15] J. H. Scofield, A. Duda, D. Albin, B. L. Ballard and P. K. Predecki, Sputtered molybdenum bilayer back contact for copper indium diselenide-

based polycrystalline thin-film solar cells, *Thin Solid Films* 260 (1995) 26-31.

[16] S. Asher, D. Albin, J. Tuttle, M. Contreras, D. Niles, R. Reedy, A. Tennant, and R. Noufi, Sodium diffusion, selenization, and microstructural effects associated with various molybdenum back contact layers for CIS-based solar cells, *Proc. of the 24th IEEE Photovoltaic Specialists Conference* (IEEE, New York, 1995), p. 164-167.

[17] L. Brewer and R. H. Lamoreaux, 1980, Atomic Energy Review, Special issue No. 7. Molybdenum: physico-chemical properties of its compounds and alloys, ch. Phase diagrams. *International Atomic Energy Agency, Vienna*, p. 319.

[18] J. E. Dutrizac, Reaction of Se vapour with molybdenum metal, *Canadian Metallurgical Quaterly* 10 (1971) 115.

[19] L. Fister and D. C. Johnson, Controlling solid-state reaction mechanisms using diffusion length in ultra-thin superlattice composites, *J. Am. Chem. Soc*. 114 (1992) 4639.

[20] P. A. Berseth, T. A. Huges, R. Schneidmiller, A. Smalley, D. C. Johnson, Low temperature synthesis using modulated elemental reactants: a new metastable ternary compound, Ni_xMoSe_2, *Solid State Sciences* 4 (2002) 717-722.

[21] H. Tributsch, Hole reactions from d-energy bands of layer type group VI transition metal dichalcogenides: new perspectives for electrochemical solar energy conversion, *J. Electrochem. Soc*. 125 (1978) 1086-1093.

[22] W. Sienicki, Semiconductor properties of molybdenum diselenide intercalated with atoms of the III-A group elements, *Materials Chemistry and Physics* 68 (2001) 119–123.

[23] http://www.webelements.com/compounds/molybdenum/molybdenum_diselenide.html.

[24] Aditya M. Vora, Effect of indium intercalation on various properties of $MoSe_2$ single crystals, *Cryst. Res. Technol*. 42 (2007) 286.

[25] M. P. Deshpande; S. K. Gupta; Ajay Agarwal; M. K. Agarwal, Transport and optical property measurements in indium intercalated molybdenum diselenide single crystals grown by DVT technique, *Synthetic metals* 123 (2001) 73-81.

[26] M. P. Deshpande, Sunil Chaki, Nilesh N. Pandya and Sagar C. Shah, Electrical transport properties of some mixed transition metal dichalcogenides $Mo_XW_{1-X}Se$ (x = 0.3, 0.4, 0.85 & 0.9), *PRAJÑĀ, Journal of Pure and Applied Sciences* 18 (2010) 132 – 135.

[27] P. P. Hankare, P. A. Chate, S. D. Delekar, V. M. Bhuse, M. R. Asabe, B. V. Jadhav and K. M. Garadkar, Structural and opto-electrical properties of molybdenum diselenide thin films deposited by chemical bath method, *Journal of Crystal Growth* Volume 291 (2006) 40-44.

[28] R. Bichsel, F. Lėvy, Electrical and optical properties of $MoSe_2$ films prepared by r.f. magnetron sputtering, *Thin Solid Films* 124 (1985) 75-83.

[29] S. Y. Hu, C. H. Liang, K. K. Tiong, Y. C. Leeand, Y. S. Huang, Preparation and characterization of large niobium-doped $MoSe_2$ single crystals, *Journal of Crystal Growth* 285 (2005) 408-414.

[30] K.-K. Kam, C. –L. Chang, D. W. Lynch, Fundamental absorption edges and indirect band gaps in $W_{1-x}Mo_xSe_2$ ($O \leq x \leq 1$), *J. Phys. C: Solid State Phys.* 17 (1984) 4031-4040.

[31] V. M. Pathak, et al., Improved photoconversion from $MoSe_2$ based PEC solar cells, *Solar Energy Materials & Solar Cells* 73 (2002) 117-123.

[32] S. Y. Hu, C. H. Liang, K. K. Tiong, Y. S. Huang, Effect of Re dopant on the electrical and optical properties of $MoSe_2$ single crystals, *Journal of Alloys and Compounds* 442 (2007) 249-251.

[33] T. Kubart, T. Polcar, L. Kopecký, R. Novák, D. Novákova, Temperature dependence of tribological properties of MoS_2 and $MoSe_2$ coatings, *Surf. Coat. Techn*. 193 (2005) 230.

[34] T. Wada, N. Kohara, S. Nishiwaki, and T. Negami, Characterisation of the Cu(In, Ga)Se_2/Mo interface in CIGS solar cells; *Thin Solid Films*, 387 (2001) 118-122.

[35] J. F. Guillemoles, L. Kronik, D. Cahen, U. Rau, A. Jasenek, and H.- W. Schock, Stability Issues of Cu(In,Ga)Se_2-Based Solar Cells, *J. Phys. Chem. B* 104 (2000) 4849-4862.

[36] H.- W. Schock, and U. Rau, The role of structural properties and defects for the performance of Cu-chalcopyrite-based thin-film solar cells; *Physica B* 308-310 (2001) 1081-1085.

[37] J. F. Guillemoles, P. Cowache, A. Lusson, K. Fezzaa, F. Boisivon, J. Vedel, and D. Lincot, One step electrodeposition of $CuInSe_2$: improved structural, electronic, and photovoltaic properties by annealing under high selenium pressure, *J. Appl. Phys*. 79 (1996) 7293-7302.

[38] R. J. Schwartz, and J. L. Gray, The use of $CuIn_{1-x}Ga_xSe_2$ layers to improve the performance of $CuInSe_2$ cells, *Proc. 21st IEEE Photovolt. Spec. Conf., Kissimmee, FL, USA* (1990) p. 570-574**.**

[39] J. F. Guillemoles, L. Kronik, D. Cahen, U. Rau, A. Jasenek, and H.- W. Schock, Stability Issues of Cu(In,Ga)Se_2-Based Solar Cells, *J. Phys. Chem. B* 104 (2000) 4849-4862.

[40] C. Y. Cummings, G. Zoppi, I. Forbes, P. J. Dale, J. J. Scragg, L. M. Peter, G. Kociok-Köhn, F. Marken, $CuInSe_2$ precursor films electro-deposited directly onto $MoSe_2$, *Journal of Electroanalytical Chemistry* 645 (2010) 16-21.

[41] D. Abou-Ras, D. Mukherji, G. Kostorz, D. Brémaud, M. Kälin, D. Rudmann, M. Döbeli, A. N. Tiwari, 'Dependence of the $MoSe_2$ Formation on the Mo Orientation and the Na Concentration for Cu (In, Ga) Se_2 Thin-film Solar Cells, *MRS Proceedings Volume 865 Symposium Y: Thin-film Compound Semiconductor Photovoltaics*, 865 (F8), 2005, p. 1-6.

[42] D. Abou-Ras, G. Kostorz, D. Brémaud, M. Kälin, F. V. Kurdesau, A. N. Tiwari, M. Döbeli, Formation and characterisation of $MoSe_2$ in $Cu(In,Ga)Se_2$-based solar cells, *Thin Solid Films* 480-481 (2005) 433-438.

[43] S. Nishiwaki, N. Kohara, T. Negami and T. Wada, $MoSe_2$ layer formation at $Cu(In,Ga)Se_2$/Mo Interfaces in High Efficiency $Cu(In_{1-x}Ga_x)Se_2$ Solar Cells, *Jpn. J. Appl. Phys*. 37 (1998) L71-L73.

[44] R. Würz, D. Fuertes Marro´n, A. Meeder, A. Rumberg, S. M. Babu, Th. Schedel-Niedrig, U. Bloeck, P. Schubert-Bischoff, M. Ch. Lux-Steiner, Formation of an interfacial $MoSe_2$ layer in CVD grown $CuGaSe_2$ based thin film solar cells, *Thin Solid Films* 431 –432 (2003) 398–402.

[45] R. Bichsel and F. Lèvy**,** Morphological and compositional properties of $MoSe_2$ films prepared by r.f. magnetron sputtering, *Thin Solid Films* 116 (1984) 367-372.

[46] L. Weinhardt, M. Blum, M. Bär, C. Heske, O. Fuchs, E. Umbach, J.D. Denlinger, K. Ramanathan, R. Noufi, Chemical properties of the $Cu(In,Ga)Se_2$/Mo/glass interfaces in thin film solar cells. *Thin Solid Films* 515 (2007) 6119–6122

[47] R. Latz, K. Michael, M. Scherer, High conducting large area indium tin oxide electrodes for displays prepared by DC magnetron sputtering, *Jpn. J. Appl .Phys*. 30 (1991) L149.

[48] J. S. Kim, M. Granstrom, R. H. Friend, N. Johansson, W. R. Salaneck, R. Daik, W. J. Feast and F. Cacialli, Indium–tin oxide treatments for single- and double-layer polymeric light-emitting diodes: The relation between the anode physical, chemical, and morphological properties and the device performance, *J. Appl. Phys*. 84 (1998) 6859.

[49] P. Topart, P. Houqueble, Infrared switching electroemissive devices based on highly conducting polymers, *Thin Solid Films* 352 (1999) 243.

[50] I. Hamberg, C. O. Granquist, Evaporated Sn‐doped In_2O_3 films: Basic optical properties and applications to energy‐efficient windows, *J. Appl. Phys*. 60 (1986) 123.

[51] H. P. Löbl, M. Huppertz, D. Mergel, ITO films for antireflective and antistatic tube coatings prepared by d.c. magnetron sputtering, *Surf. Coat. Technol*. 82 (1996) 90.

[52] Yalan Hu, Xungang Diao, Cong Wang, Weichang Hao and Tianmin Wang, Effects of heat treatment on properties of ITO films prepared by r.f. magnetron sputtering, *Vacuum* 75 (2004) 183.

[53] Z. Qiao, R. Latz, M. Mergel, Thickness Dependence of In_2O_3:Sn Film Growth, *Thin Solid Films* 466 (2004) 250-258.

[54] F. Nuesch, L. J. Rothberg, E. W. Forsythe, Q. T. Le, Y. L. Gao, A photoelectron spectroscopy study on the indium tin oxide treatment by acids and bases, *Appl.Phys. Lett*. 74 (1999) 880.

[55] R. F. Bianchi, A. J. F. Carvalho, M. A. Pereira-da-Silva, D. T. Balogh, R. M. Faria, Characterization of indium-tin-oxide films treated by different

procedures: effect of treatment time in aqua regia solution, *Materials Science and Engineering* C 24 (2004) 596-599.

[56] M. Altosaar, T. Varema, E. Mellikov, Surface degreasing and activation as important factors for Cu electroplating on ITO substrates, *DAAAM Proceedings, 2nd International Conference,* Tallinn (2000).

[57] A. N. Tiwari, Flexible CIGS Solar Cells and mini-modules (FLEXCIM), Final report, Thin Film Physics Group, Laboratory for Solid State Physics, Swiss, Federal Institute of Technology, 21.08.2007.

[58] B. R. Pamplin. A systematic method of deriving new semiconducting compounds by structural analogy, *J. Phys. Chem. Solids* 25 (1964) 675.

[59] N. Kavcar, M. J. Carter and R. Hill, Characterization of $CuInSe_2$ thin films produced by thermal annealing of stacked elemental layers, *Sol. Energy Mater. Sol. Cells* 27 (1992) 13-23.

[60] J. J. Loferski, Stoichiometric effects on the properties of copper based chalcopyrite I–III–VI_2 semiconductor thin films, *Materials Science and Engineering: B* 13 (1992) 271-277.

[61] A. Feltrin, A. Freundlich, Material considerations for terawatt level deployment of photovoltaics. *Renewable Energy* 33 (2008) 180–185.

[62] W. Thumm, et al., Environmental and health aspects of CIS-module production, use and disposal, *Proc*. *First World Conf. on Photovoltaic*. *Solar Energy Conversion Hawaii* (1994) 262-265.

[63] J. M. Raulot, C. Domain, J. F. Guillemoles, Ab initio investigation of potential indium and gallium free chalcopyrite compounds for photovoltaic application. *Journal of Physics and Chemistry of Solids* 66 (2005) 2019–2023.

[64] K. Ito and T. Nakazawa, Electrical and optical properties of stannite-type quaternary semiconductor thin films, *Jpn. J. Appl. Phys.* 27 (1988) 2094–2097.

[65] H. Matsushita, T. Maeda, A. Katsui, and T. Takizawa, Thermal analysis and synthesis from the melts of Cu-based quaternary compounds Cu–III–IV–VI_4 and Cu_2–II–IV–VI_4 (II=Zn,Cd; III=Ga,In; IV=Ge,Sn; VI=Se). *J. Cryst. Growth* 208 (2000) 416.

[66] T. M. Friedlmeier, H. Dittrich, H. W. Schock, Growth and characterization of Cu_2ZnSnS_4 and $Cu_2ZnSnSe_4$ thin films for photovoltaic applications, *The 11th Conference on Ternary and Multinary Compounds, ICTMC-11, Salford* (1997) 345–348.

[67] H. Katagiri, Cu_2ZnSnS_4 thin film solar cells. *Thin Solid Films* 480–481 (2005) 426- 432.

[68] H. Katagiri, K. Jimbo, Win Shwe Maw, K. Oishi, M. Yamazaki, H. Araki and A. Takeuchi, Development of CZTS-based thin film solar cells. *Resume of L-O5-1, E-MRS Spring Meeting, 27 May, 2008, Strasbourg, France*, http://www.emrs-strasbourg.com.

[69] T. K. Todorov, K. B. Reuter, D. B. Mitzi, High-Efficiency Solar Cell with Earth-Abundant Liquid-Processed Absorber, *Adv. Mater*. 22 (2010) E156–E159.

[70] H. Araki, A. Mikaduki, Y. Kubo, Preparation of Cu_2ZnSnS_4 thin films by sulfurization of stacked metallic layers, *Thin Solid Films* 517 (2008) 1457-1460.

[71] N. Kamoun, H. Bouzouita, B. Rezig. Fabrication and characterization of Cu_2ZnSnS_4 thin films deposited by spray pyrolysis technique, *Thin Solid Films* 515 (2007) 5949-5952.

[72] Y. B. Kumar, G. Suresh Babu, Preparation and characterization of spray-deposited Cu_2ZnSnS_4 thin films, *Solar Energy Materials and Solar Cells* 93 (2009) 1230-1237.

[73] O. Savadogo. Chemically and electrochemically deposited thin films for solar energy materials, *Solar Energy Materials and Solar Cells* 52 (1998) 361-388.

[74] A. Ennaoui, M. Lux-Steiner, A. Weber, Cu_2ZnSnS_4 thin film solar cells from electroplated precursors: Novel low-cost perspective, *Thin Solid Films* 517 (2009) 2511-2514.

[75] J. J. Scragg, P. J. Dale, L. M. Peter, Synthesis and characterization of Cu_2ZnSnS_4 absorber layers by an electrodeposition-annealing route, *Thin Solid Films* 517 (2009) 2481-2484.

[76] N. G. Dhere, Recent developments in Thin-Film Solar Cells, *Thin Solid Films* 193-194 (1990) 757.

[77] G. Sasikala, S. Moorthy Babu and R. Dhanasekaran, Electrocrystallization and Characterization of $CuInSe_2$ Thin Films; *Mater. Chem. Phys*. 42 (1995) 210-213.

[78] L. Zhang, F. D. Jiang, J. Y. Feng, Formation of $CuInSe_2$ and $Cu(In,Ga)Se_2$ films by electrodeposition and vacuum annealing treatment, *Sol. Energy Mater. Sol. Cells* 80 (2003) 483.

[79] J. L. Xu, X. F. Yao, J. Y. Feng, The influence of the vacuum annealing process on electrodeposited $CuInSe_2$ films , *Sol. Energy Mater. Sol. Cells* 73 (2002) 203.

[80] Marc-Roland Kaelin, 2005, Low-cost $Cu(In,Ga)Se_2$ absorbers from nanosized precursor materials for thin- film solar cells, *dissertation for the degree of Doctor of Sciences, Swiss Federal Institute of Technology Zurich*, 2005, 96 pages.

[81] M. Marudachalam, H. Hichri, R. Klenk, R. W. Birkmire, W. N. Shafarman, and J. M. Schultz, Preparation of homogeneous $Cu(InGa)Se_2$ films by selenization of metal precursors in H_2Se atmosphere, *Appl. Phys. Lett*. 67 (1995) 3978-3980.

[82] J. Bekker, V. Alberts, and M. J. Witcomb, Influence of selenization techniques on the reaction kinetics of chalcopyrite thin films, *Thin Solid Films* 387 (2001) 40-43.

[83] R. Caballero, and C. Guillén, Comparative studies between Cu-Ga-Se and Cu-In-Se thin film systems, *Thin Solid Films* 403-404 (2002) 107-111.
[84] C. Guillén, M. A. Martinez, and J. Herrero, $CuInSe_2$ thin films obtained by a novel electrodeposition and sputtering combined method, *Vacuum* 58 (2000) 594-601.
[85] S. Bandyopadhyaya, S. Roy, S. Chaudhuri, and A. K. Pal, $CuIn(S_XSe_{1-X})_2$ films prepared by graphite box annealing of In/Cu stacked elemental layers, *Vacuum* 62 (2001) 61-73.
[86] C. Guillén, and J. Herrero, New approaches to obtain $CuIn_{1-x}Ga_xSe_2$ thin films by combining electrodeposited and evaporated precursors, *Thin Solid Films* 323 (1998) 93-98.
[87] M. Klenk, O. Schenker, V. Alberts, and E. Bucher, Preparation of device quality chalcopyrite thin films by thermal evaporation of compound materials, *Semicond. Sci. Technol*. 17 (2002) 435-439.
[88] M. S. Aida, A. Mosbah, and N. Attaf, Annealing time effect on the properties of $CuInSe_2$ grown by electrodeposition using two electrodes system, *Brazilian Journal of Physics* 39, 2009.
[89] L. Kaupmees, M. Altosaar, O. Volubujeva, E. Mellikov, Study of composition reproducibility of electrochemically co-deposited $CuInSe_2$ films onto ITO. *Thin Solid Films* 15 (2007) 5891 - 5894.
[90] J. J. Scragg, P. J. Dale, L. M. Peter, New routes to sustainable photovoltaics: evaluation of Cu_2ZnSnS_4 as an alternative absorber material, *Physic Status Solid* 245 (2008) 1772-1778.
[91] J. J. Scragg, D. M. Berg, P. J. Dale, A 3.2% efficient Kesterite device from electrodeposited stacked elemental layers, *Journal of Electroanalytical Chemistry* 646 (2010) 52-59.
[92] Olga Volobujeva, SEM Study of Selenization of Different Thin Metallic Films, Thesis on Natural and Exact sciences B77 (2008), Tallinn University of Technology, 111 pages.
[93] J. Seol, S. Lee, J. Lee, H. Nam, K. Kim, Electrical and optical properties of Cu_2ZnSnS_4 thin films prepared by rf magnetron sputtering process, *Solar Energy Materials and Solar Cells* 75 (2003) 155-162.
[94] T. J. Vink, M. A. J. Somers, J. L. C. Daams, and A. G. Dirks, Stress, strain, and microstructure of sputter-deposited Mo thin films, *J. Appl. Phys.* **70** (1991) 4301 - 4308.
[95] P. J. Rostan, J. Mattheis, G. Bilger, U. Rau and J. H. Werner, Formation of Transparent and Ohmic ZnO:Al/$MoSe_2$ Contacts for Bifacial Cu(In,Ga)Se_2 Solar Cells and Tandem Structures, *Thin Solid Films* 480–481 (2005) 67.
[96] N. Barreau and J. C. Bernede, Low-temperature preparation of MoS_2 thin films on glass substrate with NaF additive, *Thin Solid Films* 403-404 (2002) 505–509.
[97] H. A. Al-Thani, F. S Hasoon, M. Young, S. Asher, J. L. Alleman, M. M. Al-Jassim, D. L. Williamson, The effect of Mo back contact on Na out-

diffusion and device performance of Mo/Cu(In,Ga)Se_2/CdS/ZnO solar cells, *IEEE PVSC* 29*,* (2002) p. 720.
[98] M. Bodegard, K. Granath, L. Stolt, A. Rockett, The behaviour of Na implanted into Mo thin films during annealing. *Solar Energy Materials and Solar Cells* 58 (1999) 199.
[99] K. Sakurai, A. Yamada, P. Fons, K. Matsubara, T. Kojima, S. Niki, T. Baba, N. Tsuchimochi, Y. Kimura, H. Nakanishi, Adjusting the sodium diffusion into $CuInGaSe_2$ absorbers by preheating of Mo/SLG substrates, *Journal of Physics and Chemistry of Solids* 64 (2003) 1877-1880
[100] J. Sangster, A. D. Pelton, The Na-Se (Sodium-Selenium) System, *Journal of Phase Equilibria* 18 (1997) 185.
[101] D. Braunger, D. Hariskos, G. Bilger, U. Rau, H. W. Schock, Influence of sodium on the growth of polycrystalline Cu(In,Ga)Se_2 thin films, *Thin Solid Films* 361-363 (2000) 161-166.
[102] A. M. Klimova, V. A. Ananichev, Mohammad Arif, and L. N. Blinov, Investigation of the Saturated Vapor Pressure of Zinc, Selenium, and Zinc Selenide. *Glass Physics and Chemistry* 31 (2005) 760–762.
[103] Ya. I. Gerasimov, A. N. Krestovnikov, S. I. Gorbov, 1974, *Chimicheskaja termodynamica vcvetnoi metallurgii. Izdatelstvo Metallurgija*, Moskva, 23. 101
[104] http://en.wikipedia.org/wiki/Arrhenius_equation.
[105] R. Krishnan, E. A. Payzant, R. Kacnyzki, U. Schoop, J. Brite, R. Noufi and T.J. Anderson, Reaction Kinetics and Pathways of $MoSe_2$, *IEEE Proc PVSC* 35, 2010, p. 1006-1008.
[106] V. M. Glazov, A. S. Pashinkin, and V. A. Fedorov, Phase Equilibria in the Cu-Se System, *Inorganic Materials* 36 (2000) 641-652.
[107] W. Witte, R. Kniese, A. Eicke, M. Powalla, Influence of the Ga content on the Mo/Cu(In,Ga)Se_2 interface formation Proceedings of the 4th IEEE World Conference on Photovoltaic Energy Conversion (WCPEC-4), Waikoloa, USA, May 7–12, 2006, p. 553.
[108] V. Yu. Fominski, R. I. Romanov, A. V. Gusarov, J.-P. Celis, Pulsed laser deposition of antifriction thin-film $MoSe_x$ coatings at the different vacuum conditions, *Surface & Coatings Technology* 201 (2007) 7813–7821.
[109] G. Morell, R. S. Katiyar, S. Z. Weisz, T. Walter, H. W. Schock, I. Balberg, Crystalline Phases at the p- to n-type Transition in Cu-ternary, Semiconducting Films, *Appl. Phys. Lett.* 69 (1996) 987.
[110] G. B. Sakr, I.S. Yahia, M. Fadel, S. S. Fouad, N. Romčević, Optical spectroscopy, optical conductivity, dielectric properties and new methods for determining the gap states of CuSe thin films, *Journal of Alloys and Compounds* 507 (2010) 557–562.
[111] E. Anastassakis; Light scattering in transition metal diselenides $CoSe_2$ and $CuSe_2$, *Solid State Communications* 13 (1973) 1297

[112] J. Weszka, Ph. Daniel, A. Burian, A. M. Burian, A. T. Nguyen, Raman scattering in In_2Se_3 and $InSe_2$ amorphous films, *Journal of Non-Crystalline Solids* 265 (2000) 98-104.
[113] R. Lewandowska, R. Bacewicz, J. Filipowicz, W. Paszkowicz, Raman scattering in α-In_2Se_3 crystals, *Materials Research Bulletin* 36 (2001) 2577–2583.
[114] Spravotchnik chimica II, Chimia, Moskow, 1964 p.201 (In Russian)
[115] M. Ganchev, L. Kaupmees, J. Iliyna, J. Raudoja, O. Volobujeva, H. Dikov, M. Altosaar, E. Mellikov, T. Varema, Formation of $Cu_2ZnSnSe_4$ thin films by selenization of electrodeposited stacked binary alloy layers, *Energy Procedia* 2 (2010) 65–70.
[116] M. Grossberg, J. Krustok, K. Timmo, M. Altosaar, Radiative recombination in $Cu_2ZnSnSe_4$ monograins studied by photoluminescence spectroscopy, *Thin Solid Films* 517 (2009) 2489-2492.
[117] SeJin Ahn, Sunghun Jung, Jihye Gwak, Ara Cho, Keeshik Shin, Kyunghoon Yoon, Doyoung Park, Hyeonsik Cheong, and Jae Ho Yun, Determination of band gap energy (*Eg)* of $Cu_2ZnSnSe_4$ thin films: On the discrepancies of reported band gap values, *Appl. Phys. Lett*. 97 (2010) 021905.
[118] International Center for Diffraction Data: CZTSe – 10708930; $MoSe_2$ – 30653481; SnSe – 10890232; $SnSe_2$ – 10893197; ZnSe – 10715978; CuSe – 10728417; $Cu_{1.8}Se$ – 10882043; Cu_2SnSe_3 – 30654145; Cu_2SnSe_4 – 10780600; Mo – 10714645.

Appendix A

Article I

L. Kaupmees; M. Altosaar; O. Volobujeva; P. Barvinschi, "Study of Mo selenisation process on different Mo substrates". In: Thin-Film Compound Semiconductor Photovoltaics, 2009 MRS Spring Meeting, San Francisco, CA, April 13-17. Warrendale, PA, USA: Materials Research Society. *Materials Research Society Symposium Proceedings* 1165 (2010) 289–294.

Study of Mo selenisation process on different Mo substrates

Journal:	*2009 MRS Spring Meeting*
Manuscript ID:	576917.R1
Symposium:	Symposium M
Date Submitted by the Author:	
Complete List of Authors:	Kaupmees, Liina Altosaar, Mare; Tallinn University of Technology, Materials Science Volobujeva, Olga; Tallinn University of Technology, Materials Science Barvinschi, Paul; West University of Timisoara, Faculty of Physics
Keywords:	Mo, Se, annealing

Study of Mo selenisation process on different Mo substrates

L. Kaupmees[1], M. Altosaar[1], O. Volobujeva[1], P. Barvinschi[2]
[1]Tallinn University of Technology, Department of Materials Science, Ehitajate tee 5, 19086, Tallinn, Estonia
[2]West University of Timisoara, Faculty of Physics, Bvd. V.Parvan 4, 300223, Timisoara, Romania

ABSTRACT

In the present work we studied the influence of selenisation temperature, Se vapour pressure and duration of the process on the properties of $MoSe_2$ layer formed on Mo-foil and on sputtered Mo layers on soda lime and Mo-on-ITO glasses. We found that $MoSe_2$ layer thickness (d_L) on Mo-foil depended linearly on selenisation time. The thickness of $MoSe_2$ layer on Mo-foil (d_L) depended on Se vapour pressure as a function $d_L \sim P_{Se}^{\ n}$, where $n \approx 0.5$. The same dependence was also found for sputtered Mo layers in low Se vapour pressure region of 13 – 133 Pa. $MoSe_2$ layer thickness depended on the origin of Mo layer which is related with the density of Mo layer: $MoSe_2$ on Mo foil was thicker than on sputtered Mo. All the $MoSe_2$ layers were full of cracks if Se vapour pressure was higher than 1333 Pa. All tested $MoSe_2$ layers showed *p-type* conductivity.

INTRODUCTION

Mo is widely used as a back contact material in thin film solar cells. The main requirements for the back contact are low series resistance and ohmic behaviour in contact with the absorber layer. Matson et. al. [1] and Jaegermann et. al. [2] reported that Schottky barrier was formed. Several groups [2-5] have recognized a very thin $MoSe_2$ layer between $CuInGaSe_2$ absorber layer and Mo back contact layer that improved the back contact quality. $MoSe_2$ grown perpendicularly to the surface of Mo (c-axis parallel to the Mo surface) contributes to the improvement of adhesion at the CIGS/Mo interface and the hetero-contact is found to be ohmic one (*p-type* $MoSe_2$) [3,4]. Even ZnO:Al ohmic back contacts for CIGS solar cells have been achieved by using a thin Mo interlayer on the ZnO:Al together with additional NaF precursor, that catalysed the redox selenisation of the opaque Mo to transparent $MoSe_2$ during the $CuInGaSe_2$ evaporation process and transformed the rectifying ZnO:Al/CIGS interface into an ohmic contact [6]. $MoSe_2$ formation process has been investigated in many previous works [5, 7-10]. Jäger-Waldau et. al. [7] have studied the composition and morphology of $MoSe_2$ thin films. They found that the basal plane of the crystallites was oriented either perpendicular or nominally parallel to the Mo substrate surface depending on the used selenium partial pressure. Mallouky et. al. [8] claimed that the c-axis orientation depended strongly on the absorber thin film composition before annealing. They also found that stoichiometric $MoSe_2$ thin films were obtained after appropriate annealing for any kind of Mo substrate and that thin films of $MoSe_2$ crystallize in the hexagonal structure [9]. Abou-Ras et. al. [10], using dc-magnetron sputtered Mo layers on Si substrates and studying the reaction kinetics of the $MoSe_2$ formation, found that the $MoSe_2$ layer thickness selenised at 723 K for 10 to 60 min. was nearly constant (about 10 nm) and started to increase at temperatures higher than 823 K. They interpreted the phenomenon with the c-axis orientation of the hexagonal layered structure of $MoSe_2$ perpendicular to the Mo

substrate that hindered the $MoSe_2$ growth rate due to low diffusion rates of Se through the $MoSe_2$ at 723 K. The c-axis of $MoSe_2$ layer that was formed at 853 K was parallel to the Mo substrate [10]. From the other hand, it is also known, that the properties of Mo layers depend on the deposition process. Assmann et. al [5] showed that the suitability of Mo films depended strongly on the target substrate distance and the argon pressure during rf. sputtering deposition.

As it can be seen, the formation and properties of $MoSe_2$ layers between absorber and Mo depend on many factors of processing. The important question that needs to be clarified is the following: what parameters of the preparation process determine the growth and structural properties of the $MoSe_2$ layer. In the present paper, we have described the evolution of $MoSe_2$ layers on dc. and rf. sputtered Mo layers on soda-lime glass substrates and on Mo foil. $MoSe_2$ layers were obtained by direct selenisation of Mo with selenium vapour in a two-zone vacuum ampoules where Se vapour pressure is determined by the temperature of Se source.

EXPERIMENTAL DETAILS

Cleaning procedure of Mo surfaces. All Mo samples used in the selenisation tests were cleaned by plasma etching in argon (100 W, 40 Pa, 5 min.) before the thermal annealing in Se vapour. Dry plasma etching was found to be preferable to wet chemical procedures. Before plasma etching the Mo-foils were also treated with concentrated H_2SO_4 to degrease the substrate surface.
Thermal selenisation. The quartz ampoules (1 cm in diameter and 35 cm in length) were etched with mixture of concentrated HF+ HNO_3 (1:1), rinsed with DI water and heated in the flame of $C_3H_8 + O_2$ gas. The ampoules with Mo samples in the one end and Se pellets in the other end were evacuated down to $13 \cdot 10^{-3}$ Pa and sealed. The sealed ampoules were transferred into the preheated two-zone tubular furnace where temperatures of both zones were independently heated and controlled (Figure 1). The molybdenum substrates (0.75 x 2.5 cm^2) were placed into the higher temperature zone. Selenium in the other end of ampoules was heated at lower temperatures to produce reactive Se vapour atmosphere. In such arrangement, after the achievement of the equilibrium, the vapour pressure of Se in ampoules is determined by the temperature of inexhaustible Se source.

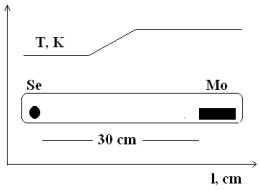

Figure 1. Temperature profile in two-zone tubular furnace.

With the aim to understand the formation kinetics of $MoSe_2$, Mo samples were selenised at 743 K and 803 K for different periods. Temperature of the selenium zone was fixed at 573, 638, 723 and 773 K that corresponds to Se vapour pressures of 13, 133, 1333 and 4399 Pa respectively. The selenisation process was stopped so that the ampoules were pulled out from the hot furnace and cooled down on a ceramic plate at room temperature.
Characterisation. Films were studied by XRD and SEM using a Bruker D8 Advance diffractometer and high resolution scanning electron microscopes LEO SUPRA 35 and Zeiss

Ultra 55 SEM. Composition was determined by EDX method using a Röntec EDX XFlash 3001 detector and the Thermo Noran Maxray ER Parallel Beam spectrometer. For thickness measurements polished (Mo foil) and broken Mo-on-glass samples were used in cross-sectional SEM studies. $MoSe_2$ conductivity type was determined by hot probe method.
Mo substrates. The investigations were based on four types of Mo samples of different origin (Figure 2): 1) Mo-foil (99.95%, 250 µm thick) from Strem Chemicals Inc.; 2) 1 mm thick sodalime glass substrates covered with 1µm thick Mo^1 layer, rf. sputtered (Mo target 99.997%, short step: high power deposition for 30 sec, 3 kW, 200 Pa Ar and long step: low power deposition for 5 minutes, 0.7 kW, 500 Pa Ar) in ETH Zurich (Eidgenössische Technische Hochschule Zürich), 3) 1 mm thick glass substrates covered with 1 µm thick Mo^2 layer, dc. sputtered in ZSW (Zentrum für Sonnenenergie- und Wasserstoff-Forschung, Stuttgart), (unknown processing); 4) 1 mm thick glass substrates covered with 500 nm ITO with 70 nm Mo layers on it, dc. sputtered in ZSW (unknown processing).

RESULTS AND DISCUSSION

Morphology. The $MoSe_2$ layers were full of cracks if Se vapour pressure was higher than 1333 K, probably due to tensions in thick $MoSe_2$ layers. Annealing Mo under low Se vapour pressures (lower temperatures of Se source) resulted in smooth $MoSe_2$ surfaces and uniform dense layers. The cross-sectional micrographs of selenised Mo samples (Figure 2 (a)-(d)) show that polycrystalline $MoSe_2$ grains have columnar structure. The *p-type* of nature of the films was confirmed by the hot-probe method in all cases.

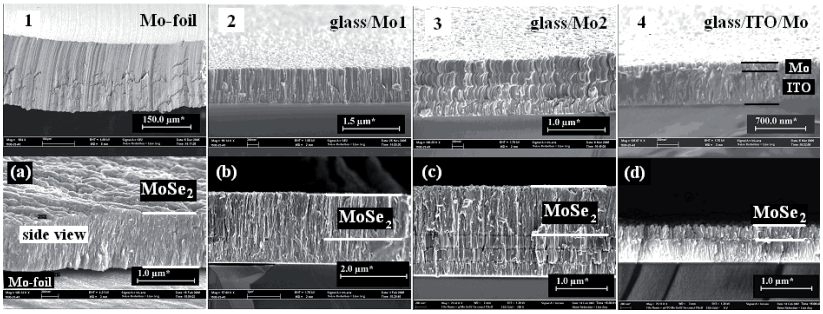

Figure 2. Side view and cross-sectional SEM images of Mo samples before and after the selenisation process (T_{Mo}= 803 K; T_{Se}= 638 K, t = 20 minutes): 1(a) 250 µm thick Mo-foil; 2(b) 1 µm Mo^1/glass; 3(c) 1 µm Mo^2/glass; 4(d) 70 nm Mo/500 nm ITO/glass.

Identification of the Mo-Se phase. Both XRD and EDX measurements suggest that the Mo-Se compound can be identified as $MoSe_2$. The composition of Mo-Se films on metallic Mo substrates analysed by EDX method was found to be Mo:Se = 1:2, corresponding to $MoSe_2$ (see Table I). XRD patterns of selenised Mo-foil, glass/Mo and glass/ITO/Mo samples are shown in Figure 3. There are only two peaks corresponding to the $MoSe_2$ phase in the XRD patterns [JCPDS cards for the hexagonal phases of this compound are 29-0914; 77-1715 and 87-2419], that indicate a strong preferred orientation of $MoSe_2$ with respect to the Mo substrate: the

average orientation of the *c*-axis is parallel to the Mo surface (in other words, the $MoSe_2$ layers are perpendicular to the Mo surface) [10].

Table I. Elemental composition of selenised Mo-films: T_{Mo}= 803 K; t = 20 minutes; selenium vapour pressures 133 and 4399 Pa correspond to 638 K and 773 K for the Se side of ampoule.

Substrate	$\mathbf{p_{Se}}$, Pa	**Mo**, at. %	**Se**, at. %
Mo-foil	133	35.25	64.75
Mo-foil	4399	34.14	65.86
glass/Mo[1]	133	35.11	64.89
glass/Mo[1]	4399	32.87	67.13
glass/Mo[2]	133	35.41	64.59

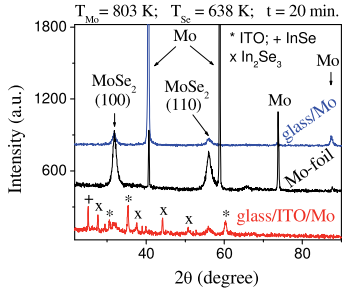

Figure 3. X-ray diffraction patterns of selenised glass/ITO/Mo, Mo-foil and glass/Mo[1,2] films at T_{Se} = 638 K (133 Pa), T_{Mo} = 803 K for 20 minutes.

Despite of the fact that the orientation of Mo grains in Mo-foil was random compared with oriented sputtered Mo grains on glass, the $MoSe_2$ phase on both substrates was grown in the same crystallographic direction (this is seen from the presence of only two reflections (100) and (110) in XRD patterns of the samples discussed here). The analysis of XRD patterns of the selenised glass/ITO/Mo substrates revealed that we have several phases: $MoSe_2$, ITO and also In_2Se_3 and InSe phases have been obtained by selenisation of indium oxide layers.

Growth rate. $MoSe_2$ layer thickness on substrates selenised at 743 K compared with the ones selenised at 803 K was much lower, but it increased with increasing temperature. On glass/ITO/Mo samples, even for short period of selenisation, all the thin molybdenum layers were fully selenised. The dependences of Mo-Se layer thickness on selenisation time and vapour pressure are presented in Figure 4. The growth rates of $MoSe_2$ films on Mo layers of various origin are different. Figure 4 (a) shows that the thickness of $MoSe_2$ layer on Mo-foil selenised at 803 K in Se vapour of 4399 Pa increases linearly with time. The growth rate of the thickness is about 0.7 µm per minute in this case. The $MoSe_2$ film thickness of sputtered glass/Mo samples of various origin (ETH Zurich and ZSW Stuttgart), was different under the same conditions. For example, after annealing for 20 minutes at 803 K under the selenium pressure of 133 Pa, the thickness of $MoSe_2$ on the glass/Mo[1] samples was about 1.5 times higher than that one on the glass/Mo[2] substrates being about 1.3 µm (65 nm/min.) and 0.9 µm (45 nm/min.) respectively (Figure 4 (b)). The growth rate is a lot higher than the one found in the work [10] (3 nm/min.) for dc. sputtered Mo on Si substrates, also selenised in two-zone arrangement at 850 K, but in a carrier gas stream where the process rate was suppressed by the inflow of Se. The authors of the work [10] explained the growth of $MoSe_2$ layer thickness as a process limited by the diffusion of Se atoms through the grown $MoSe_2$ layer and they fitted the experimental data and estimated the value of diffusion coefficient from the dependence $D=x^2/2t$, where x means the thickness of $MoSe_2$ layer (d_L in the present paper) and t is selenisation time, from where $x=\sqrt{2Dt}$. It means that thickness should increase on time as square root function dependance. This fitting does not coinside with experimental data very well. If to take account all their experimental data the linear

fitting would match better. In our tests (also in the work of [10], Fig. 6) $MoSe_2$ layer thickness increased linearly with time in all cases.

The dependences of the $MoSe_2$ layer thickness on selenium vapour pressure both for Mo-foil and for sputtered Mo/glass samples are presented in Figure 4 (c).

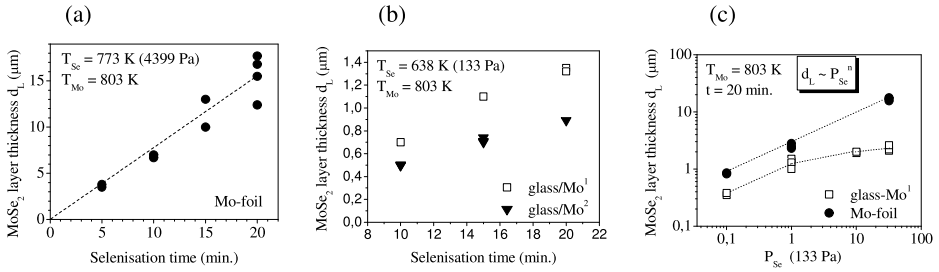

Figure 4. $MoSe_2$ layer thickness depending on: a) and b) selenisation time; c) Se vapour pressure.

The growth of $MoSe_2$ layer thickness d_L on Mo-foil depending on Se vapour pressure can be described as a power function: $d_L \sim P_{Se}^{1/2}$. If we consider that vapor phase of selenium at temperatures used in the present work consists of molecules given in Table II, from where it can be seen that Se_2 and Se_5 molecules (weight average around 4 atoms) prevail there, the formation process of $MoSe_2$ at constant temperature can be written as follows:

$$Mo + 1/2Se_{4\ (\text{weight average})} \rightarrow MoSe_2. \quad (1)$$

On the basis of reaction (1) the d_L can be described as:

$$d_L \sim k\, P_{Se}^{1/2}, \quad (2)$$

where k is the velocity constant of reaction (1). On this basis we can conclude that diffusion of Se does not inhibit the growth rate of $MoSe_2$ on Mo foil and is limited by selenium availability on the Mo surface.

Table II. Partial pressure (atm.) of different Se molecules in vapour phase of Se [11]

T / K	**T/** deg.C	$\sum$**P$_{Se}$** /atm.	**Se_2**	**Se_3**	**Se_5**	**Se_6**	**Se_7**	**Se_8**
650	**377**	2.46×10^{-3}	5.54×10^{-4}	1.32×10^{-5}	1.32×10^{-3}	3.89×10^{-4}	1.55×10^{-4}	2.75×10^{-5}
Partial load (%)		100	22.5	0.54	53.66	15.8	6.3	1.1

The selenisation process of sputtered Mo layer differs from the one of Mo-foil. The similar, $d_L \sim P_{Se}^{1/2}$, behavior is visible only in the low Se vapour pressure region. The growth of $MoSe_2$ layer proceeds due to the diffusion of selenium atoms or molecules through layered structure of $MoSe_2$ followed by their subsequent interaction with molybdenum atoms at the Mo-$MoSe_2$ interface. The straggling Mo grains in Mo-foil compared with dense sputtered Mo on glass could enable faster diffusion of Se atoms through the grown layer. As ΔG of the reaction $Mo + Se_2 \rightarrow MoSe_2$ is negative at 803 K: $\Delta G = -126 \cdot 10^3$ J, we can conclude that difference in the

density of Mo in substrates of various origin could be the reason for different packing density of columnar structure of $MoSe_2$ as well, and this is the reason of different growth rates under the same processing conditions.

CONCLUSIONS

The formation of $MoSe_2$ of *p-type* conductivity on different Mo substrates at 743 and 803 K in dependence of selenium vapour pressure and annealing duration was studied. Annealing Mo under low Se vapour pressures resulted in smooth $MoSe_2$ surfaces and dense $MoSe_2$ layers with $MoSe_2$ grains of columnar structure. Selenisation under higher selenium vapour pressures resulted in $MoSe_2$ layers with cracks. The growth rate of $MoSe_2$ on Mo-foil was much higher than the one on sputtered Mo layers. We found that the thickness of $MoSe_2$ layer on Mo-foil depended linearly on selenisation time and on Se vapour pressure as a function $d_L \sim P_{Se}^{1/2}$. We conclude that difference in the density of Mo in substrates of various origin could be the reason of different packing density of columnar structure of $MoSe_2$ as well, and this is the reason of different growth rates under the same processing conditions.

ACKNOWLEDGMENTS

The financial support of the European Union Energy Programme and European Social Fund Fund's Doctoral Studies and Internationalisation Programme DoRa and the Estonian Science Foundation under contacts № 6160 and 6179 are gratefully acknowledged.

REFERENCES

1. R. J. Matson, O. Jamjoum, A. D. Buonaquisti, P. E. Russell, L. L. Kazmerski, P. Sheldon and R. K. Ahrenkiel, Solar Cells 11, 301-305 (1984).
2. W. Jaegermann, T. Löher and C. Pettenkofer, Cryst. Res. Technol. 31, 273 (1996).
3. T. Wada, N. Kohara, S. Nishiwaki, T. Negami, Thin Solid Films 387, 118-122 (2001).
4. R. Würz, D. Fuertes Marron, A. Meeder, A. Rumberg, S. M. Babu, Th.S. Niedrig, U. Bloeck, P.Schubert-Bischoff, M.Ch. Lux-Steiner, Thin Solid Films 431–432, 398 (2003).
5. L. Assmann. J. C. Bernède, A. Drici, C. Amory, E. Halgand, M. Morsli, Appl. Surface Science 246, 159-166 (2005).
6. P. J. Rostan, J. Mattheis, G. Bilger, U. Rau, J. H. Werner, Thin Solid Films 480-481, 67-70 (2005).
7. A. Jäger-Waldau, M. Lux-Steiner, R. Jäger-Waldau, R. Burkhardt and E. Bucher, Thin Solid Films 189, 339-345 (1990).
8. A. Mallouky and J. C. Bernede, Thin Solid Films 158, 285-298 (1988).
9. J. C. Bernede, A. Mallouky and J. Pouzet, Materials Chemistry and Physics 20, 201-214 (1988); J.C. Bernede, J. Pouzet and Z. K. Alaoui, Appl. Phys. A 51, 155-159 (1990).
10. D. Abou-Ras, G. Kostorz, D. Bremaud, M. Kälin, F. V. Kurdesau, A. N. Tiwari, M. Döbeli, Thin Solid Films 480-481, 433-438 (2005).
11. Ya. I Gerasimov, A. N. Krestovnikov, S. I. Gorbov, Chimicheskaja termodynamica v cvetnoi metallurgii. Izdatelstvo Metallurgija, Moskva, (1974) p. 23.

Appendix A

Article II

L. Kaupmees, M. Altosaar, O. Volobujeva, T. Raadik, M. Grossberg, E Mellikov, M. Danilson, P. Barvinschi, ”Isothermal and two-temperature-zone selenization of Mo layers”. *Advances in Material Science and Engineering,* Accepted 6 October 2011, MS no. 345762, (see online: Articles in Press).

Isothermal and two-temperature-zone selenization of Mo layers

L. Kaupmees[1], M. Altosaar[1], O. Volobujeva[1], T. Raadik[1], M. Grossberg[1], M. Danilson[1], E Mellikov[1], P. Barvinschi[2]
[1]Tallinn University of Technology, Department of Materials Science, Ehitajate tee 5, 19086, Tallinn, Estonia
[2]West University of Timisoara, Faculty of Physics, Bvd. V.Parvan 4, 300223, Timisoara, Romania
liina3112@staff.ttu.ee

Abstract
Glass/Mo, Mo foil, glass/Mo/In and glass/Mo/Cu stacked layers were selenized in closed vacuum tubes by isothermal and/or two-temperature zone annealing in Se vapors. The selenization process was studied in dependence of Se vapor pressure, temperature and time. Samples were selenized from 375 to 580 ºC for 30 and 60 minutes. The applied Se pressure was varied between 130 and $4.4 \cdot 10^3$ Pa. The increase of $MoSe_2$ film thickness was found to depend on the origin of Mo. $MoSe_2$ thickness d_L on Mo-foil was much higher than on sputtered Mo layers and it depended linearly on time and as a power function $d_L \sim P_{Se}^{1/2}$ on Se vapor pressure. The residual oxygen content in the formed $MoSe_2$ layers was much lower in the two-zone selenization process. If Mo was covered with Cu or In before selenization these were found to diffuse into formed $MoSe_2$ layer. All the $MoSe_2$ layers showed *p*-type conductivity.

Keywords: Mo selenization, indium, copper, molybdenum diselenide

1. Introduction

Mo is widely used as a back contact material in thin film solar cells. In $CuInSe_2$ based solar cell production Mo reacts with Se forming a thin layer of $MoSe_2$. $MoSe_2$ has been extensively studied as a consequence of having both interesting physical properties (superconductivity, charge density waves, magnetism, etc.) and the ability to prepare many metastable derivates of these compounds via intercalation reactions [1]. $MoSe_2$ has been reported as an efficient compound for photoelectrochemical conversion of solar energy [2]. $MoSe_2$ in the form of a polycrystalline thin film has become an attractive semiconductor compound for electronics [3]. $MoSe_2$ belongs to a class of compounds called layered transition metal dichalcogenides [1]. Hexagonal $MoSe_2$ consists of planes of Mo covalently bonded to Se atoms, but these planes are weakly bonded to each other by Van der Waal forces. It has been suggested that the orientation of $MoSe_2$ planes with respect to the Mo substrate plays an important role in adhesion and electrical properties. Good adhesion between Mo and $MoSe_2$ is observed when $MoSe_2$ layers are oriented perpendicular to the Mo substrate (it means $MoSe_2$ with *c*-axis parallel to Mo surface) since a strong covalent bond can form at the interface between Se and the underlying Mo. So, it is important for the practical use of Mo substrates in solar cell production to determine the

growth orientation of $MoSe_2$ with respect to the surface and the rate of selenization. Bernede et al. found that it is necessary to anneal a Mo layer at temperatures higher than 377 °C to obtain reproducibly $MoSe_2$ layers without any other phase [4]. There is till limited information on mechanism of selenization of Mo and no quantitative model describing $MoSe_2$ formation. Up to now only Krishnan et al. has discussed on the reaction pathways during selenization of Mo [5].

In this paper we present the results of selenization of Mo and of $MoSe_2$ formation in isothermal and two-temperature-zone selenization processes.

2. Experimental details

2.1. Sample preparation

Different Mo substrates were used, like Mo-foil, glass/Mo, glass/Mo/In and glass/Mo/Cu. Molybdenum substrates, cleaned by dry etching in Ar plasma for 5 minutes, together with Se pellets were sealed into quartz vacuum ampoules after pumping down to $13 \cdot 10^{-3}$ Pa. The quartz ampoules (1 cm in diameter and 7 cm (isothermal selenization) or 35 cm (2-zone selenization) in length) were etched with a mixture of concentrated HF + HNO_3 (1:1), rinsed with DI water and heated in the flame of $C_3H_8 + O_2$ gas prior using.

The filled ampoules were inserted into a pre-heated horizontal tube furnace and heated for different periods (up to 1 hour). Mo substrates were selenized by two different methods: (1) isothermal (one-zone) selenization – the Mo samples (0.75 x 2.5 cm^2) and elemental selenium were heated in the same temperature zone where the pressure of Se vapor is determined by the used annealing temperature (375, 470, 530 and 580 ºC); (2) two-zone selenization - samples were annealed in a two-temperature-zone quartz tubular vacuum reactor where temperatures of the Se source and the reaction zone were controlled and regulated independently. Mo substrates were heated in the higher temperature zone for at 470, 530 and 580 ºC while the inexhaustible selenium source (Se pellets) was heated in the lower temperature zone to produce controlled reactive Se vapor atmosphere between 130 and $4.4 \cdot 10^3$ Pa. After annealing, in both cases, the ampoules were taken out of the furnace and cooled down on a ceramic plate at room temperature.

2.2. Characterization techniques

Produced films have been studied by X-ray diffraction (XRD) method on a Bruker D8 Advance diffractometer, by energy dispersive X-ray spectroscopy (EDX) method using a Röntec EDX XFlash 3001 detector and by RT Raman spectroscopy using a Horiba`s LabRam high resolution spectrometer equipped with a multichannel detection system in the backscattering configuration. The conductivity type of selenized samples was determined by the hot probe

method. The surface morphology and thickness of selenized layers were studied and determined by a high resolution scanning electron microscope Zeiss Ultra 55 SEM. X-ray photoelectron spectroscopy (XPS), AXIS Ultra ^{DLD}, was used to characterize the surface chemical composition of formed layers.

3. Results and discussion

3.1. Characterization of isothermally selenized glass/Mo films

3.1.1. Morphological and structural study of $MoSe_2$ by SEM and XRD

1 mm thick glass substrates covered with 1 μm thick Mo layer (marked as glass/Mo[2]), dc. sputtered in ZSW (Zentrum für Sonnenenergie- und Wasserstoff-Forschung, Stuttgart) were used. XRD and EDX - measurements suggest that the Mo-Se compound formed by selenization can be identified as $MoSe_2$. The composition of Mo-Se films on metallic Mo substrates analysed by EDX method was found to be Mo:Se = 1:2. XRD patterns of selenized glass/Mo samples (see Fig.1 and Fig.4(c)) show peaks corresponding to the hexagonal $MoSe_2$ phase [JCPDS cards 29-0914; 77-1715 and 87-2419]. All the synthesized $MoSe_2$ layers had *p*-type conductivity.

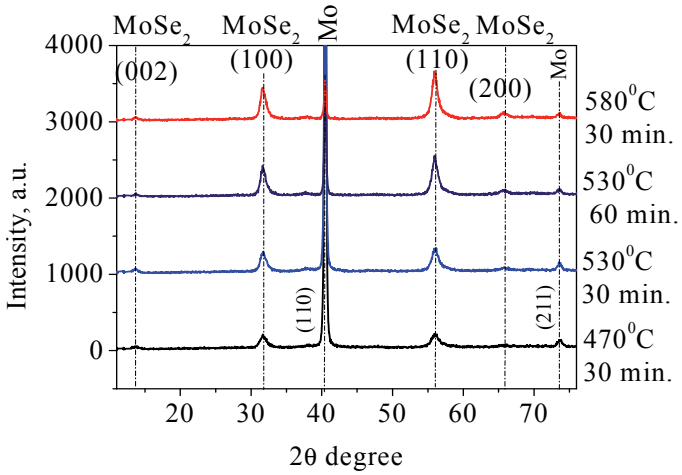

Figure 1. XRD patterns of Mo/$MoSe_2$ samples annealed in the isothermal conditions at 470, 530 and 580 °C for 30 and 60 minutes. Two upper patterns belong to samples selenized under Ar over-pressure.

Analyzing samples which were selenized for 30 minutes at different temperatures under isothermal conditions the following features can be drawn.

1) $MoSe_2$ grown at 375 °C was non-orientated; the surface was not smooth nor dense and porous. The total thickness of the Mo/$MoSe_2$ layers was about 1.3 μm, wherefrom the $MoSe_2$ layer thickness was determined to be approximately 250 nm.
2) Annealing at 470 °C resulted in $MoSe_2$, composed of two layers, the top layer was similar to the previously described 375 °C layer and the next layer under the top layer (following the initial layered structure of as deposited Mo) was orientated with the *c*-axis parallel to the Mo surface. The total thickness of the formed $MoSe_2$ was around 1.5 μm, with thicknesses of the two layers described above being 700 and 800 nm, respectively. According to SEM analysis, thickness of the upper non-orientated layer of $MoSe_2$ diminished with increasing the selenization temperature.
3) The selenization at 530 °C was found to be a breaking point from where (at higher temperatures) mainly $MoSe_2$ with *c*-axis parallel to Mo surface grows. Although 30 minutes selenization resulted a mixture of $MoSe_2$ with *c*-axis parallel and perpendicular to the Mo layer. The surface layer was quite thin, about 330 nm, which is expected to disappear with prolonged process.

With increasing selenization temperature from 470 to 530 °C, the orientation of the $MoSe_2$ layers changes from perpendicular to an almost parallel alignment with respect to the Mo substrate plane, as it was also found in the work [4]. In the work [6] the authors connected the change in MoS_2 orientation with the formation of an intermediate solid solution Na_2S_x-MoS_2 (x=1–6≠5) at temperatures higher than 550 °C. Similar behavior can be proposed in the case of $MoSe_2$ because of the close values of electronic affinities of Se and S (2.4 and 2.5 respectively). The only sodium source in our case can be the used glass substrates. Na out-diffusion from SLG substrate plays an important role also in the fabrication of CIGS based solar cells enabling the growth of the crystals of the absorber material [7]. As it is known that sputtered Mo layers contain molybdenum oxides in Mo grain boundaries [6, 8] that create efficient channels for Na diffusion [8]. From Na-Se phase diagram [9] it is seen that at around 495 ^oC there occurs peritectic transformation of Na_2Se_2 to Na_2Se and liquid Se forms. The latter can act as liquid flux for recrystallisation of both - the CIGS absorber material and $MoSe_2$ crystals. At low Se partial pressure the formation of Na_2Se_x (x=1) dominates and no Se is available. This was used to explain the lowered selenization of Mo in the presence of Na at low Se partial pressure [10]. At high Se partial pressures the formation of Na_2Se_x (x>1) dominates and Se is available for Mo selenization at higher than 495 °C. The reason for the evolution of the described upper layer of $MoSe_2$ in the isothermal selenization process, where the Se source and the Mo sample are placed into the close vicinity of each other, could be the rapid selenium flow from the Se source to the Mo sample surface in the initial period of the process when occurs the temperature difference between the colder sample and the hotter ampoule wall. Jäger-Waldau et al. studied $MoSe_2$ film composition and morphology and they

also found that the $MoSe_2$ orientation depended on selenium partial pressure [11].

XRD patterns (Fig.1) of the Mo-Se films prepared in the isothermal selenization conditions at 470, 530 and 580 °C show peaks related to $MoSe_2$ [JCPDS cards 29-0914; 77-1715 and 87-2419] and indicate to the preferential growth of hexagonal $MoSe_2$ in the (100) and (110) direction. Similar results were found in the work [4]. The preferential orientation of $MoSe_2$ with respect to the Mo substrate facilitates the diffusion of Se through the already formed $MoSe_2$, thus leading to the growth of thicker $MoSe_2$ layers. The preferred orientation in (100) and (110) direction, i.e. the average orientation of the *c*-axis of the $MoSe_2$ layer parallel to the Mo surface, becomes more pronounced for $MoSe_2$ layers grown at 530 and 580 °C for 60 and 30 minutes, respectively. XRD patterns indicate also to un-reacted Mo in each sample with preferred orientation in the (110) direction [JCPDS card 42-1120].

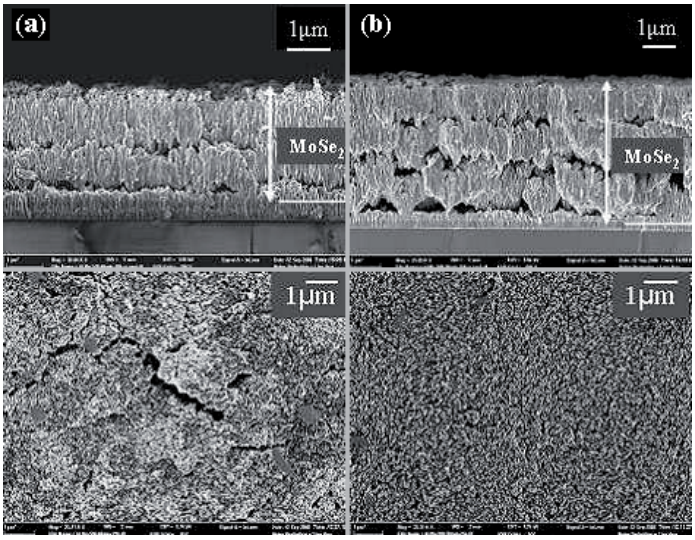

Figure 2. SEM cross-sectional and surface images of $Mo/MoSe_2$ samples annealed under Ar over-pressure in the isothermal conditions at 530 °C for 60 minutes (a) and at 580 °C for 30 minutes (b).

Using argon environment during the selenization, we can balance the processes taking place, to hold back the reaction and condensation of selenium on the surfaces of the samples.

Selenization in the isothermal process arrangement at higher temperatures (530 and 580 °C) causes intense selenization of Mo corresponding to a quite high selenium pressures determined by the used temperatures. SEM cross-sectional images of $Mo/MoSe_2$ samples annealed in the isothermal conditions at 530 °C for 60 minutes and at 580 ^{o}C for 30 minutes under Ar over-pressure are presented in Fig.2 and indicate that all the layers are full of cracks.

3.1.2. Growth rate of $MoSe_2$ layer in isothermal selenization process

The thickness of $MoSe_2$ on glass/Mo samples follows the Arrhenius equation - the thickness (in native logarithmic scale) of the formed $MoSe_2$ layer increases linearly with the reciprocal selenization temperature (see Fig.3).

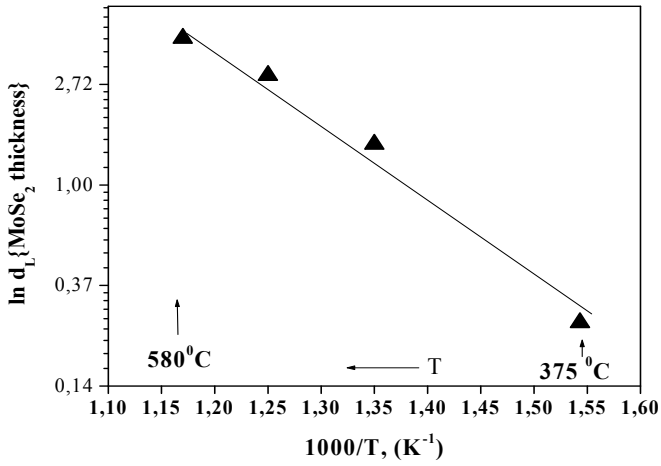

Figure 3. Thickness of $MoSe_2$ on glass/Mo in dependence of reciprocal selenization temperature. Straight line remarks the linear fitting of test points.

From the Arrhenius plot the activation energy of the layer growth process was found to be - E_a = - 0.7 ± 0.1 eV that is close to the activation energy found in the work [5].

3.2. Two-zone selenization of Mo substrates

Selenization of glass/Mo^2 substrates for 60 minutes at 530 and 580 °C under selenium vapor pressure of $4.4 \cdot 10^3$ Pa (T_{Se}= 500 °C**)** resulted in dense and thick layers of $MoSe_2$ (see Fig.4(a, b)).

The comparision of the corresponding XRD patterns (see Fig.4(c)) show that $MoSe_2$ layers selenized at 580 °C have better crystallinity compared with 530 °C (peaks are narrower and higher in the difractogram) but the Mo layer is thoroughly selenized at 580 °C - Mo peak had disappeared in XRD pattern.

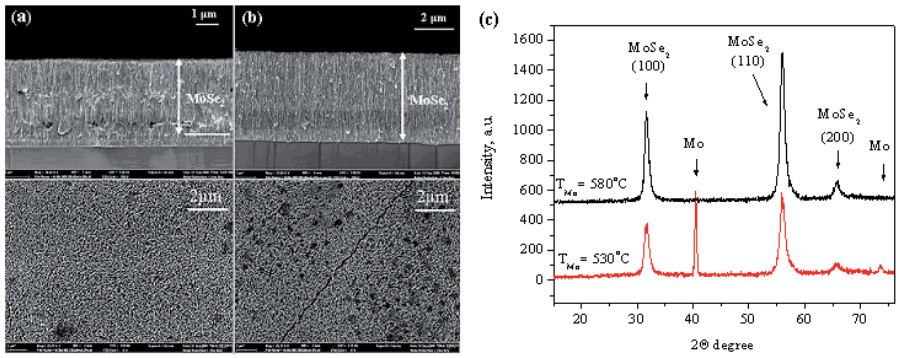

Figure 4. (a, b) SEM cross- sectional and surface images of glass/Mo[2] samples selenized for 1 h at 530 °C (a) and 580 °C (b) in two-zone ampoules under selenium vapor pressure of $4.4 \cdot 10^3$ Pa (T_{Se}= 500 °C); (c) XRD patterns of selenized samples.

3.2.1 Growth rate of $MoSe_2$

Two type of sputtered glass/Mo substrates - 1) rf sputtered (Mo[1]) and 2) dc sputtered (Mo[2]) and Mo-foil were used in two-zone selenization to find out the dependences of Mo-Se layer thickness on selenization time and on Se vapor pressure. Graphs are presented in Fig.5(a) and Fig.5(b), more detailed information is given in work [12].

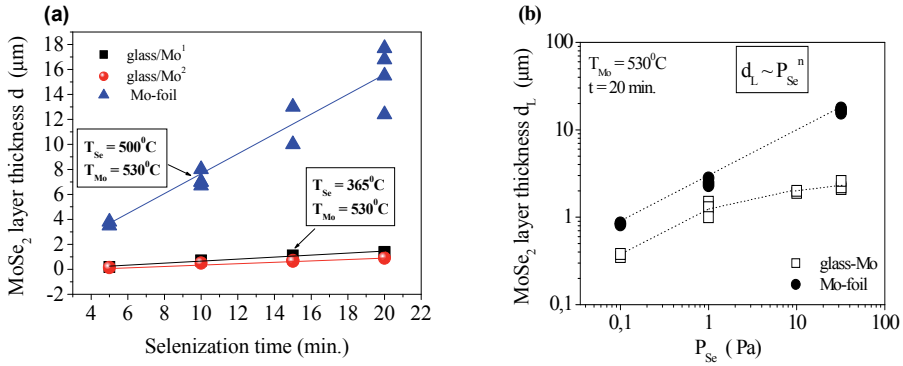

Figure 5. Thickness of $MoSe_2$ layer in dependence on selenization time (a) and on Se vapor pressure (b).

respectively (Fig.5(a) and work [12]). The growth rate of $MoSe_2$ layer in Fig.5(a) shows that the thickness of $MoSe_2$ layer on Mo selenized at 530 °C in constant Se vapor pressure increases linearly with the increase of selenization duration. The thickness of the $MoSe_2$ layer on Mo-foil increases with the rate of about 0.7 μm per minute at 530 °C and P_{Se}= $4.4 \cdot 10^3$ Pa (T_{Se} = 500 °C). The thickness of $MoSe_2$ film on sputtered glass/Mo samples depends from the origin

of initial Mo layer and technology of its production. For example, the thickness of $MoSe_2$ on the glass/Mo[1] samples after annealing for 20 minutes at 530 °C under the selenium pressure of 130 Pa (T_{Se} = 365 °C) was about 1.5 times bigger than the one on the glass/Mo[2] substrates (1.3 and 0.9 μm respectively) resulting in growth rates of about 65 nm/min. and 45 nm/min. our experiments is much higher than the growth rate found in the work [13] (3 nm/min.) for dc sputtered Mo on Si substrates, where the selenization was also performed in the two-zone arrangement at 577 °C, but in a carrier gas stream where the process rate was regulated and suppressed by the inflow of Se. The authors of the work [13] explained the growth of $MoSe_2$ layer thickness as a process limited by the diffusion of Se atoms through the as-grown $MoSe_2$ layer and they fitted the experimental data and estimated the value of diffusion coefficient of Se in $MoSe_2$ from the dependence $D=x^2/2t$, where x means the thickness of $MoSe_2$ layer (in the present study d_L) and t is selenization duration. From the above-given equation x is equal to $x=\sqrt{2Dt}$. It means that thickness has to increase with time in square root function dependence (see the dashed curve in Fig.6).

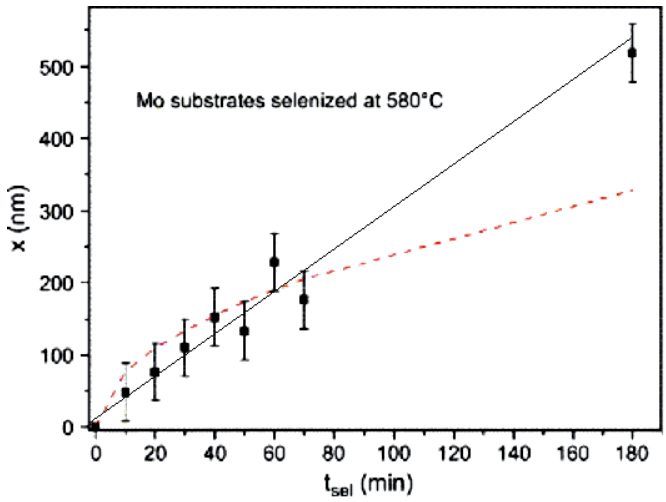

Figure 6. The thickness x of $MoSe_2$ layer versus the selenization duration t_{sel}, $Ts_{substrate}$ = 580 °C; the dashed curve gives the $x(t_{sel})$ square root dependence with $D=5\times10^{-14}$ cm^2/s. [13]. The solid line marks the linear fit.

The used in [13] fitting does not coincide even well with all the experimental data of the work. Linear dependence fits match much better for all the experimental data of work [13] (straight line in Fig.6). It means that our results and results by [13] are pointing out the similar dependence: the linear increase of $MoSe_2$ layer thickness with duration of selenization.

The dependences of the $MoSe_2$ layer thickness on selenium vapor pressure both for Mo-foil and for sputtered Mo/glass samples are presented in Fig.5(b). The growth of $MoSe_2$ layer thickness d_L on Mo-foil depending on Se vapor pressure could be described as a power function: $d_L \sim P_{Se}^{1/2}$. If to consider that the vapor phase of selenium at temperatures used in the present work consists of molecules given in Table 1, from where it can be seen that Se_2 and Se_5 molecules (weight average around 4 atoms) prevail in the used temperature range, the formation process of $MoSe_2$ at constant temperature can be written as follows:

$$\mathbf{Mo + 1/2Se_{4\ (weight\ average)} \rightarrow MoSe_2.} \quad (1)$$

On the basis of the reaction (1) the thickness of $MoSe_2$ layer d_L in dependence on Se vapor pressure can be described as:

$$\boldsymbol{d_L \sim k\, P_{Se}^{1/2}}, \quad (2)$$

where k is the velocity constant of reaction (1).

Table 1. Partial pressure (atm.) of different Se molecules in vapor phase of Se [14].

T, K	T, °C	∑Pse, atm.	Se_2	Se_3	Se_5	Se_6	Se_7	Se_8
650	377	2.46 x10^{-3}	5.54 x10^{-4}	1.32 x10^{-5}	1.32 x10^{-3}	3.89 x10^{-4}	1.55 x10^{-4}	2.75 x10^{-5}
Partial pressure (%)		100	22.5	0.54	53.66	15.8	6.3	1.1
800	527	9.2 x10^{-2}	2,35 x10^{-2}	1.26 x10^{-4}	5.76 x10^{-2}	6.92 x10^{-3}	3.23 x10^{-3}	5.88 x10^{-4}
Partial pressure (%)		100	25.54	0.14	62.61	7.52	3.51	0.64

This result could be explained by the straggling Mo grains in Mo-foil that enable fast diffusion of Se atoms through the grown $MoSe_2$ layer. This dependence is confirmation that selenization of Mo foil is limited by selenium availability on the interface and not by the diffusion of Se through $MoSe_2$. The regularities of selenization of dense sputtered Mo layers differ from the regularities of selenization of Mo-foil. The similar, $d_L \sim P_{Se}^{1/2}$, behavior is visible only in the low Se vapor pressure region (see Fig.5(b)). The growth of $MoSe_2$ layer proceeds due to the diffusion of selenium atoms or molecules through dense layered structure of $MoSe_2$ followed by their subsequent interaction with molybdenum atoms at the Mo-$MoSe_2$ interface. As ΔG of the reaction $Mo+Se_2 \rightarrow MoSe_2$ is negative at 530 °C: ΔG = - 145 kJ, we can conclude the difference in the density of Mo in substrates of various origin could be the reason for different packing density of columnar structure of $MoSe_2$ as well, and this is the reason of different growth rates under the same processing conditions.

3.3. Comparison of isothermal and two-zone arrangements of the selenization process of Mo

In the isothermal arrangement, the selenium source and the Mo sample are situated in close vicinity to each other in the same temperature zone. Rapid formation of a relatively high vapor pressure of Se in the vicinity of the Mo sample (determined by the heat treatment temperature) allows faster start of the $MoSe_2$ formation reaction in comparison with two-temperature zone arrangement where the Se source is at a distance of about 30 cm from the reaction zone. In the isothermal arrangement the extent of selenization of Mo could be tailored by the amount of Se in the reaction ampoule. For example: heating for one hour at 530 °C resulted in thoroughly consumed Se and partly selenized Mo layers with the final thickness of $Mo/MoSe_2$ layer of about 3 μm (possible maximum thickness being 4.4 μm). XRD analysis confirmed the existence of both, un-reacted Mo and $MoSe_2$ phases. SEM investigations of surface morphology did not show any cracks in layers. However, after the 30 minutes selenization at 580 °C, nearly the same thickness of $MoSe_2$ layer was gained with the same amount of Se. This means that the amount of Se was limiting the process of selenization in the isothermal arrangement. We can conclude that the selenization process in isothermal arrangement can be controlled by the annealing time or the process can be limited by the added amount of elemental Se.

Experiments showed that the optimum selenization temperature of Mo layers is 530 °C. At higher temperatures, the tension between the layers is remarkable and as a result thermal stresses resulted in cracks. If the layer is growing too fast, or the Mo layer is thoroughly selenized to $MoSe_2$ there could occur adhesion problems - peeling off either from glass or $MoSe_2$/Mo interface.

3.4. Characterization of isothermally selenized Mo films covered with Cu and In layers

The influence of In and Cu coverage on molybdenum to the selenization process of Mo was investigated. The structural evolution of layers is illustrated in Fig.7.

In the case of In coverage (see left side photos in Fig.7) at 300 ^{o}C Mo is covered with a polycrystalline core of formed In-Se compounds. At higher temperatures little crystals of In-Se are sparsely standing in the layer giving a possibility to Se molecules to penetrate the layer easily. Cu on Mo (see right side photos in Fig.7) forms a compact continuous layer with big sintered crystals at lower temperatures. At higher temperatures the crystals in the layer grow larger and, at the highest temperatures, gather into large single aggregates. It is visible that the Cu and In layers on Mo impede the growth of $MoSe_2$ compared with uncovered Mo samples (see Fig.10), while the samples with indium gave thicker $MoSe_2$ layers than the samples with copper. The former is understandable when considering that CuSe forms on Mo a compact continuous coverage seen in Fig. 7 that inhibits the access of Se molecules to Mo.

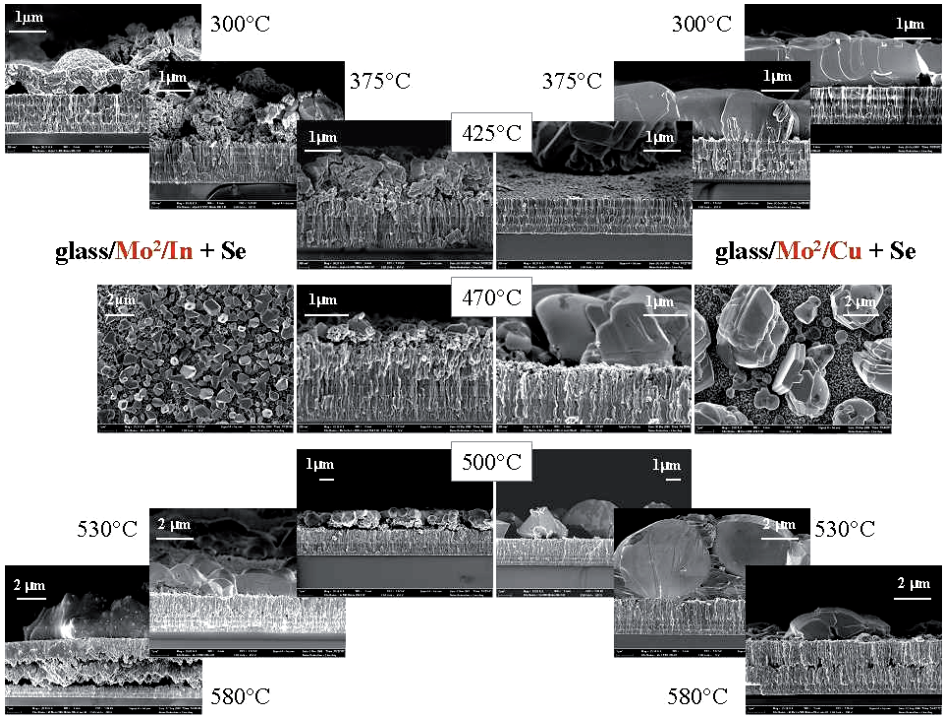

Figure 7. SEM micrographs of selenized glass/Mo/In and glass/Mo/Cu substrates, the structural evolution of layers selenized at different temperatures.

SEM micrographs of Mo samples covered with Cu and In and selenized at 530 °C are presented in Fig.8. The formed $MoSe_2$ interlayer is clearly seen on the SEM images (Fig.7 and Fig.8) and its existence was confirmed by the EDS line scanning profiles (Fig.9), results of XRD (Fig.11) and Raman analysis (Fig.12).

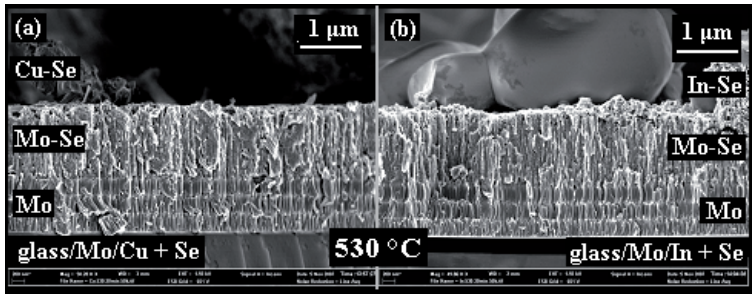

Figure 8. SEM micrographs of Mo/Cu (a) and Mo/In (b) layers selenized at 530 °C.

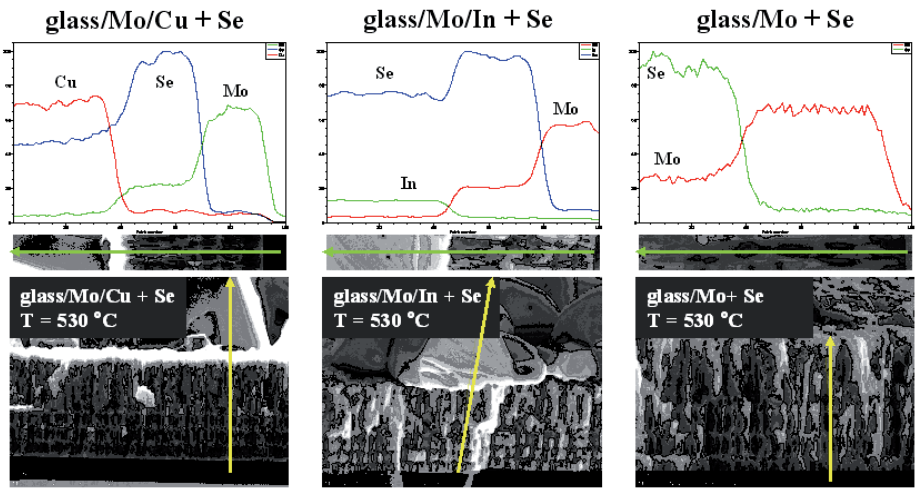

Figure 9. EDS line scanning profile of the cross-section of glass/Mo, glass/Mo/In and glass/Mo/Cu layers selenized at 530 °C for 30 minutes.

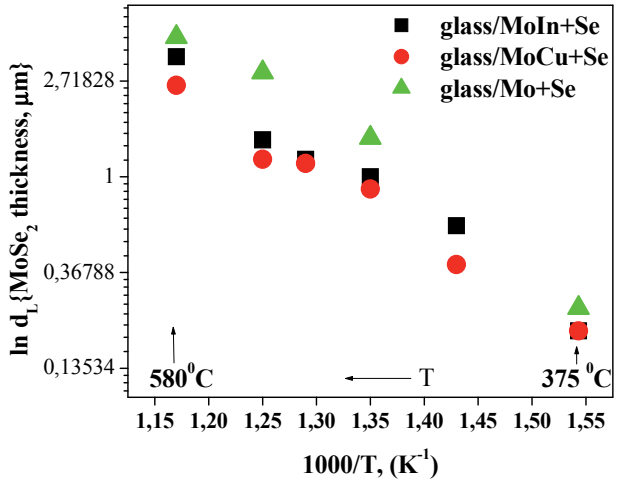

Figure 10. Thickness of $MoSe_2$ on glass/Mo, glass/Mo/In and glass/Mo/Cu in dependence of reciprocal selenization temperature.

The XRD analyses confirm that in addition to the hexagonal $MoSe_2$ (JCDPS card 29-0914) phase, large CuSe crystals (JCDPS card 34-0171, 20-1020) and In_2Se_3 as agglomerated rounded crystals on the surface (Fig.7 and Fig.8). (JCDPS card 40-1407) are present in selenized $MoSe_2$ films. The formation of CuSe only is understandable if to consider that in closed ampoules the applied Se overpressure avoids the thermal decomposition of CuSe to Cu_2Se and Se that is presumptive by Cu-Se phase diagram [15]. The native logarithmic

dependences of the thicknesses of the $MoSe_2$ films as a function of reciprocal temperature are shown in Fig.10. The thickness of $MoSe_2$ on uncovered Mo follows the Arrhenius equation (see Fig.3). It is visible that the Cu and In layers on Mo impede the growth of $MoSe_2$ in comparison with uncovered Mo samples (see Fig.10), while the influence of indium coverage to the rate of selenization process is less pronounced than the influence of copper coverage.

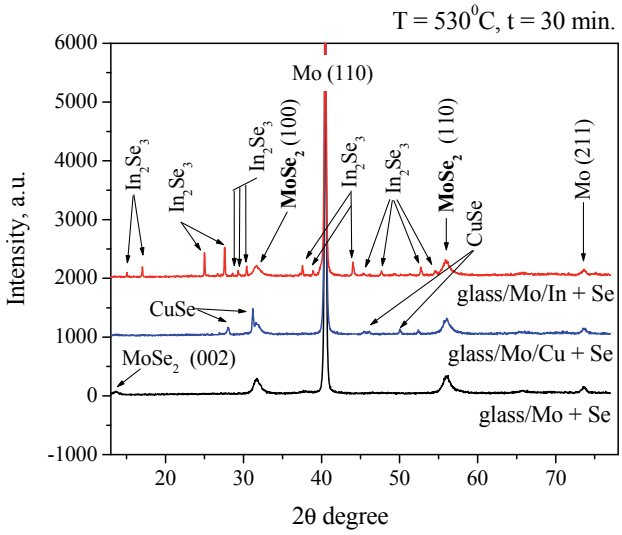

Figure 11. XRD patterns of glass/Mo, glass/Mo/In and glass/Mo/Cu layers selenized isothermally at 530 °C for 30 minutes.

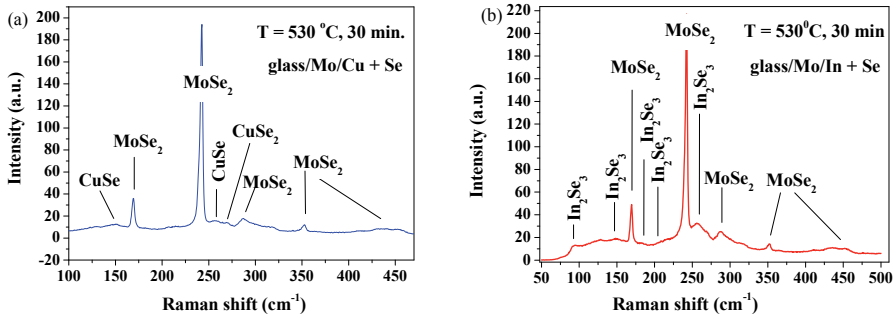

Figure 12. Raman spectra of (a) glass/Mo/Cu layers and of (b) glass/Mo/In layers selenized at 530 °C for 30 minutes.

Micro-Raman spectra in Fig.12(a) and Fig.12(b) of selenized Mo-In and Mo-Cu samples show the peaks at 169, 240, 280 and 350 cm^{-1} characteristic to

$MoSe_2$ [16, 17]. Analysis of the Raman spectrum (Fig.12(a)) of the glass/Mo/Cu layer selenized at 530 °C for 30 minutes shows the additional existence of different Cu-Se phases - Raman peaks at 147 and 260 cm^{-1} belong to CuSe [18, 19] and a peak at 270 cm^{-1}can be associated with Cu_2Se or $CuSe_2$ [20]. Analysis of the Raman spectrum of the glass/Mo/In layer selenized at 530 °C for 30 minutes (Fig.12(b)) reveals beside $MoSe_2$ the existence of In containing phase – In_2Se_3 (Raman peaks at 91, 148, 182, 204 and 256 cm^{-1} [21, 22].

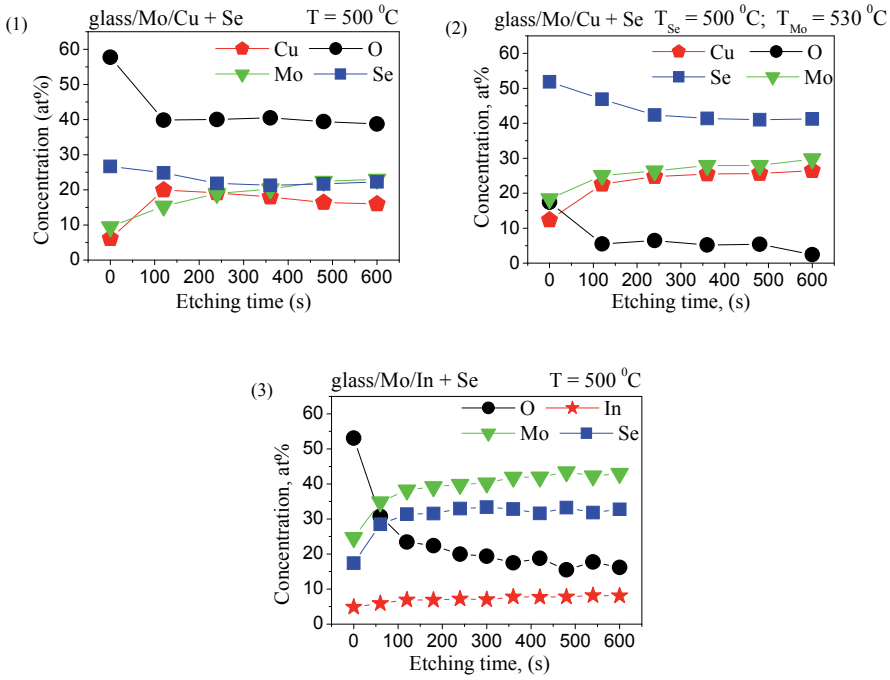

Figure 13. XPS depth profiles of glass/Mo/Cu substrates selenized under (1) isothermal and (2) two-temperature zone arrangement, (3) XPS depth profile of glass/Mo/In substrates selenized under isothermal arrangement.

The XPS depth profiles of selenized glass/Mo/In and glass/Mo/Cu layers are presented in Fig.13. It is seen that all the Mo-Se layers contain oxygen and that some Cu and In from surface have diffused into Mo-Se layer.

It is known that as deposited Mo films sputtered without intentional substrate heating contain significant amount of oxygen bound as MoO_2 and MoO_3 [6, 8]. In the work [8] the oxygen content of rf sputtered Mo films was 8 at% as determined by RBS. It is important to point out that in the case of two-temperature zone arrangement the concentration of oxygen in the layers is diminished in comparison with the isothermal selenization. This can be explained by SeO_2 formation that has remarkable vapor pressure at the applied temperatures and the two-temperature arrangement enables SeO_2 to condensate

into the lower temperature zone (melting point of solid SeO_2 is 340-350 ^oC [23]).

CONCLUSIONS

The formation of $MoSe_2$ of *p*-type conductivity on Mo substrates at temperatures from 375 to 580 °C in dependence of selenium vapor pressure and annealing duration was studied. We found that the thickness of $MoSe_2$ layer on Mo-foil depends on the selenization duration linearly and on the Se vapor pressure as a function $d_L \sim P_{Se}^{1/2}$. According to XPS analysis, Cu and In have been diffused into Mo-Se layer. It is important finding that the residual oxygen content in the formed $MoSe_2$ layers was much lower in the case of two-temperature zone arrangement. In the case of isothermal arrangement, quick formation of a relatively high vapor pressure of Se in the vicinity of the Mo sample (determined by the heat treatment temperature) allows a faster start of the $MoSe_2$ formation in comparison with two-temperature zone arrangement. We can conclude that the selenization process in isothermal arrangement can be controlled by the annealing duration and temperature if added amount of elemental Se is unlimited or by the limited amount of Se. The thickness of $MoSe_2$ on glass/Mo samples follows the Arrhenius equation - the thickness (in native logarithmic scale) of the formed $MoSe_2$ layer increases linearly with the reciprocal selenization temperature. From the Arrhenius plot the activation energy of the process was determined as E_a = - 0.7±0.1 eV. The optimum selenization temperature was 530 °C which resulted in uniform $MoSe_2$ layers without cracks and with the *c*-axis orientation parallel to Mo surface. At higher temperatures, the tension between the layers was found to be remarkable and resulted in cracks and bad adhesion - peeling off $MoSe_2$ either from glass or from $MoSe_2$/Mo interface. Cu and In layers on Mo impede the growth of $MoSe_2$ compared with uncovered Mo samples. Due to the smaller crystal size of formed In_2Se_3 compared to compact continuous coverage of CuSe, the penetration of Se molecules is faster through In_2Se_3 crystals and the thickness of $MoSe_2$ layer is thicker on the glass/Mo/In samples than on glass/Mo/Cu samples under the same selenization conditions.

Acknowledgements

Financial support of the Estonian Ministry of Science and Higher Education under by the contract T099 and of Estonian Science Foundation under contracts № 6160, 6179, 8147 and 8964 is gratefully acknowledged.

References

[1] P. A. Berseth, T. A. Huges, R. Schneidmiller, A. Smalley, D. C. Johnson, Low temperature synthesis using modulated elemental reactants: a new metastable ternary compound, NixMoSe$_2$, *Solid State Sciences,* vol. 4, pp. 717-722, 2002.

[2] H. Tributsch, Hole Reactions from d-Energy Bands of Layer Type Group VI Transition Metal Dichalcogenides: New Perspectives for Electrochemical Solar Energy Conversion, *J. Electrochem. Soc*., vol. 125, pp. 1086-1093, 1978.
[3] W. Sienicki, Semiconductor properties of molybdenum diselenide intercalated with atoms of the III-A group elements, *Materials Chemistry and Physics,* vol. 68, pp. 119 – 123, 2001.
[4] J. C. Bernède, J. Pouzet, Z. K. Alaoui, Preparation and Characterization of Molybdenum Diselenide Thin Films, *Applied Physics A* 51, pp. 155-159, 1990.
[5] R. Krishnan, E. A. Payzant, R. Kacnyzki, U. Schoop, J. Brite, R. Noufi and T.J. Anderson, Reaction Kinetics and Pathways of $MoSe_2$, *IEEE Proc PVSC* 35, pp. 1006-1008, 2010.
[6] N. Barreau and J. C. Bernede, Low-temperature preparation of MoS_2 thin films on glass substrate with NaF additive, *Thin Solid Films,* vol. 403-404, pp. 505 – 509, 2002.
[7] H. A. Al-Thani, F. S Hasoon, M. Young, S. Asher, J. L. Alleman, M. M. Al-Jassim, D. L. Williamson, The effect of Mo back contact on Na out-diffusion and device performance of Mo/Cu(In,Ga)Se_2/CdS/ZnO solar cells, *IEEE PVSC* 29*,* pp. 720, 2002.
[8] M. Bodegard, K. Granath, L. Stolt, A. Rockett, The Behavior of Na Implanted Into Mo Thin Films During Annealing, *Solar Energy Materials and Solar Cells,* vol. 58, pp. 199, 1999.
[9] J. Sangster, A. D. Pelton, The Na-Se (Sodium-Selenium) System, *Journal of Phase Equilibria*, vol. 18, pp. 185, 1997.
[10] D. Braunger, D. Hariskos, G. Bilger, U. Rau, H. W. Schock, Influence of sodium on the growth of polycrystalline Cu(In,Ga)Se_2 thin films, *Thin Solid Films,* vol. 361-362, pp. 161 – 166, 2000.
[11] A. Jäger-Waldau, M. Lux-Steiner, R. Jäger-Waldau, R. Burkhardt, E. Bucher, *Thin Solid Films* 189, pp. 339-345, 1990.
[12] L. Kaupmees, M. Altosaar, O. Volobujeva, P. Barvinschi, Study of Mo selenisation process on different Mo substrates, MRS spring meeting, San Francisco, CA, April 13-17. USA: *Materials Research Society Proceedings*; vol. 1165, M08-01, 2009.
[13] D. Abou-Ras, G. Kostorz, D. Brémaud, M. Kälin, F. V. Kurdesau, A. N. Tiwari, M. Döbeli, Formation and characterisation of $MoSe_2$ for Cu(In,Ga)Se_2 based solar cells, *Thin Solid Films*, vol. 480-481, pp. 433-438, 2005.
[14] Ya. I. Gerasimov, A. N. Krestovnikov, S. I. Gorbov, *Chimicheskaya thermodynamica v cvetnoi metallurgii. Izdatelstvo Metallurgija*, Moskva 23, pp. 101, 1974.
[15] V. M. Glazov, A. S. Pashinkin, and V. A. Fedorov, Phase Equillibria in the Cu-Se System, *Inorganic Materials,* vol. 36, pp. 641-652, 2000.

[16] W. Witte, R. Kniese, A. Eicke, M. Powalla, Influence of the Ga content on the Mo/Cu(In,Ga)Se_2 interface formation, *Proceedings of the fourth IEEE World Conference on Photovoltaic Energy Conversion (WCPEC-4)*, Waikoloa, USA, May 7–12, pp. 553, 2006.

[17] V. Yu. Fominski, R. I. Romanov, A. V. Gusarov, J.-P. Celis, Pulsed laser deposition of antifriction thin-film $MoSe_x$ coatings at the different vacuum conditions, *Surface & Coatings Technology,* vol. 201, pp. 7813–7821, 2007.

[18] G. Morell, R. S. Katiyar, S. Z. Weisz, T. Walter, H. W. Schock, I. Balberg, Crystalline Phases at the p- to n-type Transition in Cu-ternary, Semiconducting Films, *Appl. Phys. Lett.* vol. 69, pp. 987, 1996.

[19] G. B. Sakr, I.S. Yahia, M. Fadel, S. S. Fouad, N. Romčević, Optical spectroscopy, optical conductivity, dielectric properties and new methods for determining the gap states of CuSe thin films, *Journal of Alloys and Compounds,* vol. 507, pp. 557–562, 2010.

[20] E. Anastassakis; Light scattering in transition metal diselenides $CoSe_2$ and $CuSe_2$, *Solid State Communications,* vol. 13, pp. 1297 - 1301, 1973.

[21] J. Weszka, Ph. Daniel, A. Burian, A. M. Burian, A. T. Nguyen, Raman scattering in In_2Se_3 and $InSe_2$ amorphous films, *Journal of Non-Crystalline Solids,* vol. 265, pp. 98-104, 2000.

[22] R. Lewandowska, R. Bacewicz, J. Filipowicz, W. Paszkowicz , Raman scattering in α-In_2Se_3 crystals, *Materials Research Bulletin* , vol. 36, pp. 2577–2583, 2001.

[23] Spravotchnik chimica II, Chimia, Moscow (In Russian), pp. 201, 1964.

Appendix A

Article III

O. Volobujeva, M. Altosaar, J. Raudoja, E. Mellikov, M. Grossberg, **L. Kaupmees**, P. Barvinsch, „SEM analysis and selenization of Cu–In alloy films produced by co-sputtering of metals". *Solar Energy Materials and Solar Cells* 93 (2009) 11 - 14.

Available online at www.sciencedirect.com
ScienceDirect
Solar Energy Materials & Solar Cells 93 (2009) 11–14
Solar Energy Materials and Solar Cells
www.elsevier.com/locate/solmat

SEM analysis and selenization of Cu–In alloy films produced by co-sputtering of metals

O. Volobujeva[a,*], M. Altosaar[a], J. Raudoja[a], E. Mellikov[a], M. Grossberg[a], L. Kaupmees[a], P. Barvinschi[b]

[a]*Tallinn University of Technology, Ehitajate tee 5, Tallinn 19086, Estonia*
[b]*West University of Timisoara, Bvd. V.Parvan 4, 300223 Timisoara, Romania*

Received 28 August 2007; received in revised form 7 January 2008; accepted 12 January 2008
Available online 21 February 2008

Abstract

Co-sputtered copper–indium (Cu–In) alloy layers were investigated as precursors for $CuInSe_2$ (CIS) formation. Results of scanning electron microscopy (SEM), EDS and X-ray diffraction (XRD) studies reveal the inhomogeneity of the films composition. The films have a rough surface structure with well-defined islands crystallized within the film matrix. The elemental composition of the island-type crystals corresponds to the compound $CuIn_2$ and the composition of the matrix area corresponds to the $Cu11In_9$ phase. The influence of heating temperature, time and Se pressure on the morphology and composition of films is studied using SEM, XRD and Raman spectroscopies. Thereby optimal technological parameters for the production of single-phase CIS layers are determined.

Keywords: Cu–In alloy; Selenization; $CuInSe_2$; Thin films; Scanning electron microscopy

1. Introduction

Chalcopyrite polycrystalline semiconductors have been extensively studied due to their importance in optoelectronic applications. $CuInSe_2$ (CIS) thin films are characterized by a suitable band gap, a high absorption coefficient that exceeds $10^5\,cm^{-1}$ and good stability [1].

Several techniques have been used for the growth of CIS films such as metalorganic vapor phase [2] and molecular beam epitaxy [3], flash evaporation [4], coevaporation [5,6] and electrodeposition [7]. The two-stage process of the selenization of metallic precursor layers has shown a promise of low-cost and large-scale production of films with quality acceptable for photovoltaic applications [8–10]. A major problem is the low homogeneity of selenized films due to the inhomogeneity of copper–indium (Cu–In) alloy. Co-sputtering has several advantages such as the promotion of a complete mixture of the elemental species and the precise control of the fluxes of the sputtered elements which enables the formation of uniform and well-defined Cu–In alloy composition. The weak point of the two-stage process is the use of highly toxic H_2Se for the selenization. Thus, great effort has been taken during the past few years to develop elemental Se vapor selenization as an alternative [11,12].

2. Experimental

Cu–In alloy films were formed at ambient temperature on molybdenum covered soda-lime glass substrates by magnetron sputtering of Cu/In alloy targets. High purity (99.998%) argon plasma was used during the co-sputtering process. The thickness of the Cu/In films of 1 μm was adjusted by the sputtering time. The Cu/In ratio of sputtered films was controlled by composition of Cu/In alloy targets ([Cu]/[In] = 0.88). Two different experimental set-ups were used for selenization: (a) selenization in isothermal sealed quartz ampoules, in which the Se pressure was controlled by the temperature of the selenization; (b) selenization in two temperature-zone sealed quartz ampoules, in which the Se pressure was determined by the lower temperature zone of the ampoule.

*Corresponding author. Tel.: +372 620 3368.
E-mail address: v.olga@staff.ttu.ee (O. Volobujeva).

0927-0248/$ - see front matter © 2008 Elsevier B.V. All rights reserved.
doi:10.1016/j.solmat.2008.01.007

The temperature of selenization was varied from 300 to 550 °C and the duration of the selenization was between 0.25 and 2 h. The Se pressure was varied between 0.1 and 25 Torr.

Evolution of the surface morphology and the crystalline structure of the co-sputtered precursor Cu–In and the selenized films was analyzed by a high-resolution scanning electron microscope (HR-SEM) Zeiss ULTRA 55 equipped with an In-Lens SE detector for topographic imaging and energy and angle selective backscattered (EsB) detector for compositional contrast. The chemical composition of films was determined using an energy dispersive X-ray (EDX) analysis (Röntec EDX XFlash 3001) detector. Bulk structure and phase compositions were studied using X-ray diffraction (XRD) and Raman spectroscopy. A Bruker D8 ADVANCE diffractometer was used to identify the phases of the films. CuKα was used as an X-ray source (40 kV, 40 mA) in a Bragg–Brentano geometry. The room temperature micro-Raman spectra were recorded by using a Horiba LabRam HR spectrometer. The incident laser light with a wavelength of 532 nm was focused on samples within a spot 1 μm in diameter and the spectral resolution of the spectrometer was about 0.5 cm^{-1}.

3. Results and discussion

3.1. Investigation of co-sputtered precursor Cu–In alloy layers

Precursor Cu–In alloy films exhibit a rough bilayer structure of the surface in which island-type crystals were formed in a "small-crystalline" matrix layer (Fig. 1). The cross-sectional SEM image of a Cu– In alloy film (Fig. 1a) indicates that island-type crystals extend through the matrix layer down to the Mo layer. EDS analysis show that the matrix area of co-sputtered Cu–In alloy layers is Cu rich (Cu/In = 1.48) while island shape crystals are In rich (Cu/In = 0.68). The literature data let us assume that the matrix area consists of $Cu_{11}In_9$ and that the island-type crystals consist of $CuIn_2$ [13]. The existence of a $CuIn_2$ phase in sputtered Cu–In alloy films at low temperatures was postulated by different authors [14–18]. The observed discrepancy of the results obtained by EDS analysis can be explained with small sizes of the island crystals and the matrix areas between them, that is smaller than the lateral sensitivity of the EDS analysis. The results of the XRD analysis (Fig. 2) indicate the existence of $Cu_{11}In_9$ and $CuIn_2$ phases and thereby confirm the assumption of a multiphase composition of the films. The presence of $CuIn_2$ in the form of island-type crystals could be attributed to the high $CuIn_2/Cu_{11}In_9$ interfacial energy [19].

3.2. Investigation of selenized Cu–In alloy layers

3.2.1. Cu–In layers selenized at 300 °C.

The films, selenized at 300 °C (Fig. 3a), show rough surface structures. The surface is characterized by relatively big crystals (1) with sizes of up to 1 μm and with rounded grains that are located in the small-crystalline matrix layer (2) (with crystal sizes between 20 and 50 nm). In contrast to the alloy films here, these big crystals do not extend down to the substrate Mo layer being located only on the surface

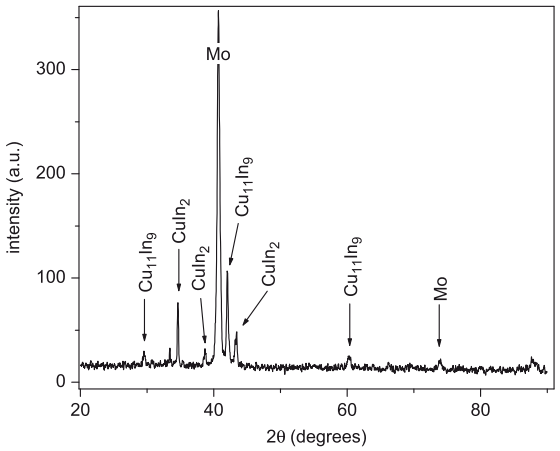

Fig. 2. XRD pattern of the co-sputtered Cu–In alloy film. The peaks of $CuIn_2$ and $Cu_{11}In_9$ are revealed.

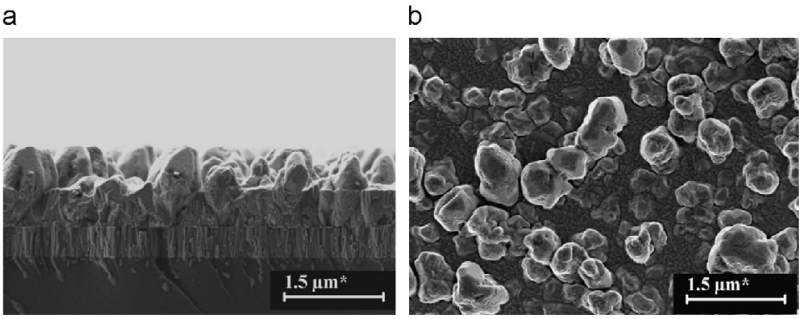

Fig. 1. SEM images of the surface and cross-section of the Cu–In alloy film (Cu/In = 0.88). A rough bilayer structure of the surface is well seen.

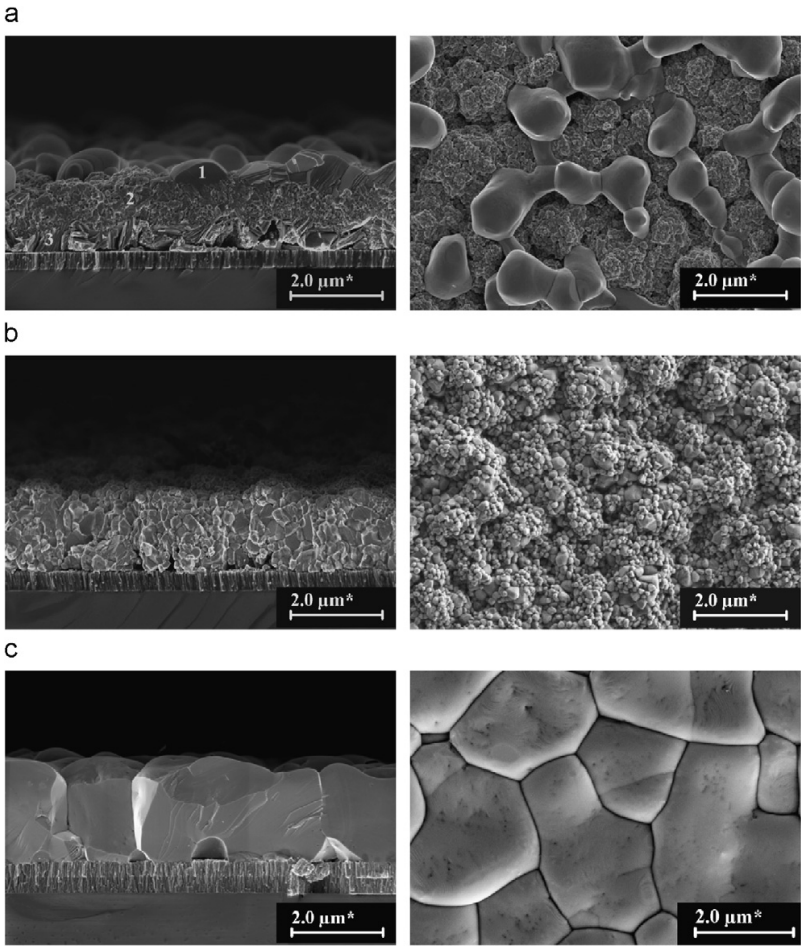

Fig. 3. The structural evolution of films with the selenization temperature. Surface and cross-sectional images of selenized Cu–In alloy layers: (a) selenization temperature 300 °C, 1 h, $p_{se} = 0.15$ mm Hg; (b) selenization temperature 375 °C, 1 h, $p_{se} = 22$ mm Hg; (c) selenization temperature 470 °C, 1 h, $p_{se} = 25$ mm Hg.

of the films. The lower part of the selenized layers close to the Mo-covered substrate consists of needle-type crystals (3) that are very different from the crystals in the matrix layer. Such a difference in the morphology of the surface and the inner structure of the layers suggests that the layers exhibit a multiphase composition. Raman spectra (Fig. 4) give additional confirmation of the multiphase structure of the layers. A weak peak at 174 cm^{-1} is generally linked to the A_1 mode of CIS [20]. An additional peak at 262 cm^{-1} has been generally attributed to binary copper selenides (CuSe, $Cu_{2-x}Se$) [21]. The peaks at 114 and 226 cm^{-1} indicate the presence of InSe [22]. Results of the EDS analysis at points 1, 2, 3 (Fig. 3a) confirm that the formations on the surface of the layers consist of a "pure" CuSe phase ([Cu] = 50.9%, ([Se] = 49.1%), that the small-crystalline matrix is the CIS phase with nearly stoichiometric composition, and that the needle-like crystals at the bottom represent InSe ([In] = 50.5%, ([Se] = 49.5%).

3.2.2. *Cu–In layers selenized at 375 °C*

The surface and cross-sectional SEM images (Fig. 3b) indicate that the structure of the layers selenized at 375 °C is different from that of the precursor layers and of the layers selenized at 300 °C. The layers consist of densely packed crystals with sizes varying from 50 to 200 nm. The surface of the layers is characterized by relatively big, but shallow, holes and hills that could be the origin of island-like structures in the precursor layers. The compositional sensitive EBS detector indicates a single-phase composition of layers selenized at 375 °C and Cu/In ratio is close to the initial ratio in the precursor layer. Results of XRD and Raman spectroscopy (Fig. 4) investigations confirm the single phase (CIS) composition of the layers.

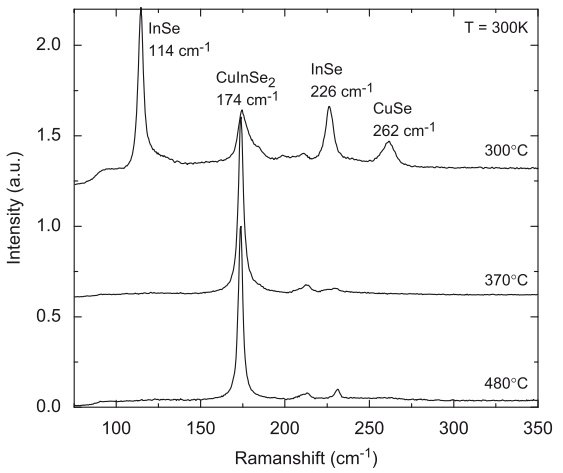

Fig. 4. Compositional evolution (Raman spectra) of selenized alloy films with selenization temperature.

3.2.3. *Cu–In layers selenized at 480 °C*

The surface and the cross-sectional SEM images (Fig. 3c) of layers selenized at 480 °C exhibit uniform, large and densely packed crystals with sizes of about 2–3 μm. The surface of the films is relatively smooth providing good starting conditions for their use as absorber layers. The results of XRD analysis confirm that the layers selenized at 480 °C were nearly single phased. Micro-Raman studies revealed the existence of an InSe separate phase of very low concentration that was lower than the sensitivity of EDS and XRD analyses. The results of EDS analysis indicate that the layers selenized at 480 °C were homogeneous in composition, Se rich and with Cu/In ratio near that of the Cu/In ratio of the sputtering target. Preferred (1 1 2) orientation of crystals was observed for all films annealed above 400 °C. The thickness of well-grown CIS films is about three times larger than that of precursor layers. The formation of $MoSe_2$ was detected only in completely selenized films, where no intermediate binary compounds were monitored by XRD. The results confirm the assumptions [11] that the formation of CIS proceeds through three different processes. At lower temperatures the dominating processes are Se incorporation and Cu out-diffusion and the formation of different copper and indium selenides (Figs. 3a and 4). This is followed by the reaction between the binary selenides with excess Se vapor and results in the formation of CIS (Figs. 3b and 4). The final stage is the growth of CIS crystals leading to well-formed films with crystals of large sizes (Figs. 3c and 4).

4. Conclusions

Co-sputtering of Cu–In layers leads to the formation of rough layers with a bilayer structure of the surface in which island-type crystals were formed in a small crystalline matrix layer. The elemental composition of the island-type crystals corresponds to the compound $CuIn_2$ and the matrix (area) consists of copper-rich $Cu_{11}In_9$ phase. The pathway to form the CIS phase under pressure of elemental Se is kinetically controlled and the phase composition of selenized films depends on the temperature of selenization. The important role of Cu out-diffusion in CIS formation mechanism and kinetics is confirmed. It is shown that the selenization of co-sputtered Cu–In alloy films at high temperatures in evacuated quartz ampoules results in high-quality dense chalcopyrite CIS films with crystals of about 2 μm and with a preferred orientation of the crystals in the (1 1 2) direction.

Acknowledgments

Financial support of the European Union by Energy program and Estonian Science Foundation under Contract nos. 6160 and 6179 is gratefully acknowledged.

References

[1] A. Luque, S. Hegedus (Eds.), Handbook of Photovoltaic Science and Engineering, Wiley, New York, 2006.
[2] N. Rega, S. Siebentritt, I. Beckers, J. Beckmann, J. Alberts, M. Lux-Steiner, Thin Solid Films 431–432 (2003) 186.
[3] S. Niki, A. Yamada, R. Hunger, P.J. Fons, K. Iwata, K. Matsubara, A. Nishio, H. Nakanishi, J. Cryst. Growth 237–239 (2002) 1993.
[4] A.A.S. Akl, A. Ashour, A.A. Ramadan, K. Abd El-Hady, Vacuum 61 (2001) 75.
[5] M. Bodegard, O. Lundberg, J. Lu, L. Stolt, Thin Solid Films 431–432 (2003) 26.
[6] G. Hanna, J. Mattheis, V. Laptev, Y. Yamamoto, U. Rau, H.W. Schock, Thin Solid Films 431-432 (2003) 31.
[7] D. Lincot, Thin Solid Films 487 (2005) 40.
[8] J. Bekker, V. Alberts, A.W.R. Leitch, J.R. Botha, Thin Solid Films 431–432 (2003) 116.
[9] K. Ellmer, J. Hinze, J. Klaer, Thin Solid Films 413 (2002) 92.
[10] R. Caballero, C. Guillén, Sol. Energy Mater. Sol. Cells 8 (2005) 1.
[11] F.D. Jiang, J.Y. Feng, Thin Solid Films 515 (2006) 1950.
[12] S. Merdes, L. Bechiri, Z. Hadjoub, M. Sano, S. Ando, Phys. Stat. Sol. C 8 (2006) 2535.
[13] F.O. Adurodija, J. Song, K.H. Yoon, S.K. Kim, S.D. Kim, S.H. Kwon, B.T. Ahn, J. Mater. Sci. 9 (1998) 361.
[14] M. Gossla, H. Metzner, H.-E. Mahnke, J. Appl. Phys. 86 (1999) 3624.
[15] T. Nakano, S. Sato, S. Baba, Vacuum 74 (2004) 591.
[16] E. Rudigier, J. Djordjevic, C. von Klopmann, B. Barcones, A. Perez-Rodrıguez, R. Scheer, J. Phys. Chem. Solids 66 (2005) 1954.
[17] T. Nakano, H. Mizuhshi, S. Baba, Jpn. J. Appl. Phys. 44 (2005) 1932.
[18] A. Brummer, V. Honkimäki, P. Berwian, V. Probst, J. Palm, R. Hock, Thin Solid Films 437 (2003) 297.
[19] C.H. Chung, S.D. Kim, H.J. Kim, F.O. Adurodija, K.H. Yoon, J. Song, Solid State Commun. 126 (2003) 185.
[20] D. Papadimitriou, N. Esser, C. Xue, Stat. Sol. (b) 242 (2005) 2633.
[21] G. Morell, R.S. Katiyar, S.Z. Weisz, T. Walter, H.W. Schock, I. Balberg, Appl. Phys. Lett. 69 (1996) 987.
[22] O.A. Balitskii, V.P. Savchyn, V.O. Yukhymchuk, Semicond. Sci. Technol. 17 (2002) L1.

Appendix A

Article IV

M. Ganchev; **L. Kaupmees**; J. Iliyna; J. Raudoja; M. Altosaar; O. Volobujeva; E. Mellikov; T. Varema; H. Dikov, "Formation of $Cu_2ZnSnSe_4$ thin films by selenization of electrodeposited stacked binary alloy layers". Proceedings of EMRS, Strasbourg, June 2009, *Energy Procedia* 2 (2010) 65–70.

Available online at www.sciencedirect.com
ScienceDirect
Energy Procedia 2 (2010) 65–70
Energy Procedia
www.elsevier.com/locate/procedia

E-MRS Spring Meeting 2009, Symposium B

Formation of $Cu_2ZnSnSe_4$ thin films by selenization of electrodeposited stacked binary alloy layers

M.Ganchev[a]*, L.Kaupmees[a], J.Iliyna[a], J.Raudoja[a], O. Volobujeva[a], H. Dikov[b], M.Altosaar[a], E.Mellikov[a], T.Varema[a]

[a]*Materials Science Institute, Tallinn University of Technology, Ehitajate tee 5, 19086 Tallinn, Estonia*
[b]*Central Laboratory of Solar Energy-Bulgarian Academy of Sciences, 72 Tzarigradsko shaussee, 1784 Sofia, Bulgaria*

Received 1 June 2009; received in revised form 1 December 2009; accepted 20 December 2009

Abstract

Brass-Bronze thin-stacked layers electrodeposited in Potentiostatic conditions were selenized in an iso-thermal quartz tubular reactor. The ratio of metal components in selenized films was adjusted through appropriate choice of composition and thickness of the constituent layers. Focus is on the influence of annealing conditions on crystalline structure, phase composition, surface morphology and optical properties of the obtained $Cu_2ZnSnSe_4$ (CZTSe) thin films and pecularities of formation CZTSe thin films.

Electrodeposition, Precursor selenisation, $Cu_2ZnSnSe_4$

1. Introduction

Future development of thin film photovoltaics depends on the deployment of low cost and easily up scalable deposition methods for abundant and non-toxic compounds [1]. Ternary chalcopyrites $CuInS_2$ (CIS) and $Cu(In,Ga)Se_2$ were a promising solution but increasing prices of the rare metals In and Ga have affected the cost-efficiency ratio. Replacement of III group metals with cheap and widespread Zinc and Tin serve as another opportunity for diversification and industrialization of compound thin film photovoltaics [2]. $Cu_2ZnSnSe_4$ (CZTSe) is a structure analog of CIS where III group (Indium or Gallium) atoms are exchanged with Zinc and Tin. CZTSe is a prospective material with a direct band gap near 1.44 eV, close to the optimum for the solar irradiation spectra and a high absorption coefficient ranging to 10^4 cm^{-1} [3].

* Corresponding author. Tel.: +37 25 637 9736; fax: +37 26 203 367.
E-mail address: mganchev@abv.bg.

1876-6102 © 2010 Published by Elsevier Ltd
doi:10.1016/j.egypro.2010.07.012

There are numerous investigations on the sulfur compound Cu_2ZnSnS_4 developed by atom beam sputtering [4], thermal evaporations [5] and electron beam evaporated precursors processed in H2Satmosphere [6]. Later, electrodeposition routes [7,8] for the formation of substrate metallic precursors subjected subsequently to sulfurization were explored. Abou-Ras et al. [7] studied Electrodeposition route developed specifically by the formation of metallic alloy Cu-Zn-Sn precursor layers [9] to build solar cells.
The Selenium compound CZTSe thin layer absorbers were grown by pulsed laser ablation [10], one step RF magnetron sputtering [11] or with sequential selenization [12] as well as synthesis from melts [13]. The monograin thin film $Cu_2ZnSnSe_4$ solar cell recently developed has given Voc = 422 mV, J= 21.3 mA/cm^2 and FF 44 % with an overall efficiency of 2.16% [14].
This article focuses on the formation of $Cu_2ZnSnSe_4$ absorber layers by sequential electrodeposition of the Cu-Zn alloy and Cu-Sn stacked precursors, followed by reactive annealing in the atmosphere of selenium vapors.

2. Experimental details

Electrodeposition of precursor layers was performed in a potentiostatic condition with Wenking Bank PGstat 3440 in a three-electrode configuration at room temperature (20^{o}C). Reference was a Saturated Silver Chloride electrode (Ag/AgCl: 3M KCl) and Platinum gauze with much higher active surface than the cathode served as a counter electrode. The working electrodes were molybdenum covered (near 1 μm thick) soda-lime glass substrates sized approximately 1 X 2.5 cm^2 or molybdenum foils with the same dimensions. Solutions for deposition Cu-Zn and Cu-Sn layers contained 0.6M Potassium Pyrophosphate and salts of Cu^{2+}, Zn^{2+} and Sn^{2+} following formulations in [15]. Due to the oxidizing ability of Sn^{2+} on the anode or by the oxygen from air, the electrolytic cell for the deposition of Bronze layers was divided and the anode compartment was isolated ?through an Ion (Na^+) selective membrane. Anolyte was 0.2M Na_2CO_3 and to keep constant cation equilibrium concentrations for the membrane the catolyte contained 0.2M $Na_4P_2O_7$ and 0.4M $K_4P_2O_7$ as well as 0.1M Hydroquinone as an antioxidant.
Substrate layers Cu-Zn/Cu-Sn were selenized under isothermal conditions in evacuated 5-cm long quartz ampoules at 530^{o}C – 560^{o}C during 15 minutes at a 1.5-m thermal tubular reactor. In order to perform the thermal annealing samples with ampoules were placed in a preliminary preheated quartz holder pipe with wall thickness of 2mm, length of 60 cm and with inner diameter of 2.5 cm. After that the pipe with the ampoule inside was comparatively slowly moved out for cooling down to near 50 ^{o}C for another 20 minutes. Estimated annealing temperature profile is shown schematically in Fig.1. Other annealing experiments were performed for 1 h at 400^{o}C preliminary preheating in a vacuum of 150 Torr for metal alloy sublayer homogenization and reactive selenization for 1 h at 560^{o}C. Some singles, high temperature experiments, were performed at 750^{o}C for 2 hours with alloy substrate samples deposited onto molybdenum foil.

Fig.1. Scheme of time-temperature profile for fast annealing experiments

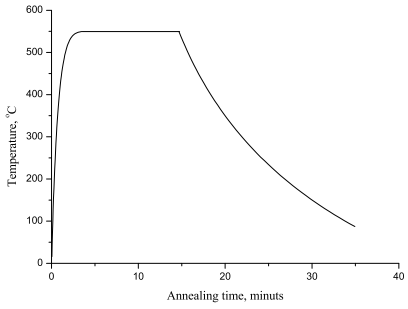

Fig.1. Thermal profile for selenization of thin alloy Brass – Bronze layers

Scanning electron microscopy investigations and EDX composition measurements were performed on Hitachi TT1000 unit supplied with X-ray source and detector equipment with accelerating voltage 15.0 kV and acquisition time 90 sec. High resolution micrograms and fine impurities composition measurements were done on Zeiss

ULTRA 55 at accelerating voltage 1.74 kV through an In lens. The room temperature (RT) micro – Raman spectra were recorded by Horiba LabRam 800 high-resolution spectrometer equipped with a multichannel detection system on backscattering configuration. The spectrometer operated by Green 532 nm wavelength laser focused within a 1 μm spot diameter providing the incident light with a spectral resolution of 0.5 cm^{-1}.
X – ray diffraction analysis (XRD) was performed on Rigaku Ultima IV with Cu - Kα radiation (λ=1.5418Å) and 4 kV accelerating voltage. The diffracted beam was scanned in steps by 0.01° for 2 sec in an angular range from 10 to 80 degrees in 2Θ. A comparison with JCDPS file cards [16] was made to assign the observed peaks. Phases manifested at least with three reflexes are taken into considerations. Optical investigations for determining the type and width of the band gap were carried out on UV-VIS-NIR spectrophotometer JASCO V-670 in the range of 200 to 2500 nm.

3. Results and discussion

Metal substrate layers were formed by two-step electrodepositing of alloys Brass (Cu-Zn) and Bronze (Cu-Sn) films, respectively. Final total film composition depends on the ratio of metals in the pair sublayers and its relative thickness. Total metal film thickness is defined by the sum of the thickness of the partial layers. The sequence of depositing Cu-Sn onto Cu-Zn was followed but an opposite order is possible as well. A 40-minute electrodeposition of Brass layer was followed by a 3-minute electrodeposition of Bronze layer to ensure formation of 1.5 – 2 μm thick CZTSe layer after selenization.

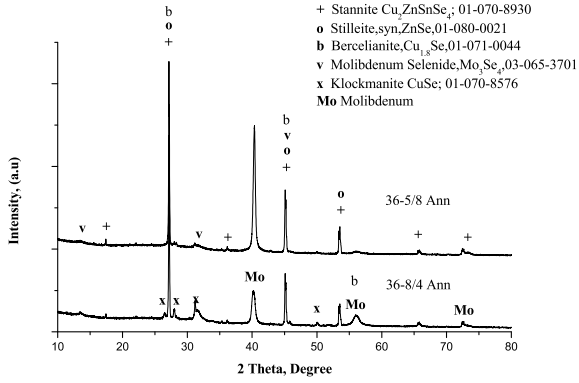

Fig.2. X-Ray diffraction patterns of thin layer $Cu_2ZnSeSe_4$ annealed in different regimes: Sample 36-5/8 – selenization of 15 minutes at 530 °C and 20 minutes slow cooling down; 36-8/4 – 1 hour annealing in vacuum and 1 hour selenization at 560°C

Fig.2 presents XRD patterns of samples 36-8/4 and 36-5/8. The first one had passed preliminary homogenization annealing in vacuum for 1 hour at 400°C, followed by reactive isothermal annealing in Selenium vapors for 1 hour at 560°C. The other sample had been treated for a short time (15 minutes) at 530°C and slow cooling down, following the procedure described by Fig.1. In both cases typical main reflexes of CZTSe at 45.1°, 27.16° and 53.52° in scale 2Θ as well as minorities at 17.44°, 36.25°, 65.98° and 72.65° can be seen. Signals are strong and sharp indicating a well-crystallized Stannite – JCDPS 01-070-8930. Well-defined reflexes from the Molybdenum substrate layer at 40.18°, 56.03° and 72.45° in units 2Θ were detected. There are other peaks, which could be attributed to the Molybdenum substrate as well - reflexes at 11.54° and 31.66°. If we assume the tall peak at 45.1° as a compound caused not only by the Stannite, there is obviously Mo_3Se_4 (JCDPS 03-06503701) - a product of selenization of the substrate. Detailed structural analysis has revealed non-monophase thin film materials in both cases. There are minor but well distinguished reflexes at 26.58°, 28°, 31.2° and 50.02° obviously related to CuSe (Klockmanite – 01-070-8576). Further, following the thesis for a compound character of the XRD pattern, another issue should be

mentioned. Probably it is possible that a thin film material consists of a cubic ZnSe (Stilleite – JCDPS 01-080-0021) the pattern of which coincides with the Stannite one at 27.16°, 45.1° and 53.52° in 2Θ scale. In addition, a scrupulous analysis supposes the existence of another phase – $Cu_{1.8}Se$ (Bercelianite – JCDPS 01-071-0044) with reflexes at 27.16°, 45.1° and 56.03°.

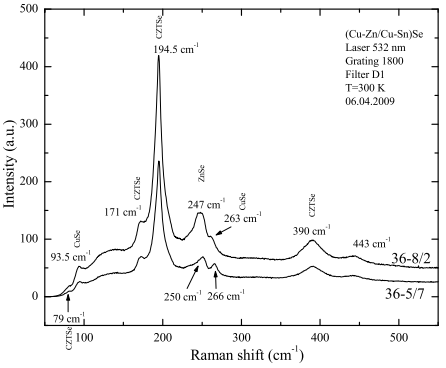

Fig.3. Room temperature Raman spectra of Cu2ZnSnSe4 thin layers

Fig.3 shows the RT Raman spectra of samples 36-8/2 and 36-5/7 deposited and annealed in the same conditions as sample 36-5/8 in Fig.2. The patterns present defined spectra for the well-formed Stannite by almost all important vibrations at 79 cm^{-1}, 173 cm^{-1}, 196 cm^{-1}, 231 cm^{-1} and 390 cm^{-1}, respectively. There are two peaks that could be attributed to CuSe – at 94 cm^{-1} and near 263 cm^{-1}. Another signal at 247 cm^{-1} was registered, which may be due to the cubic ZnSe. The weak vibration at 443 cm^{-1} could be attributed to the bond Si-O-Si from the substrate [17]. As the samples are similar in composition and are annealed in the same conditions, the differences in signal intensities in the spectra should be related to the differences in layer thickness.

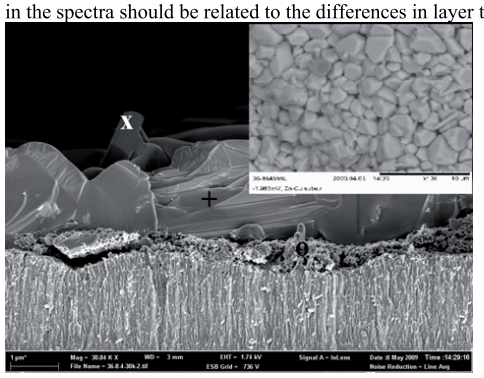

Fig.4. SEM cross section microgram of the CZTSe thin film, annealed in vacuum for 1 hour, followed by a selenization at 560°C for 1 hour. Insertion presents the surface morphology image of the same film.

Fig.4 presents a SEM microgram of sample 36-8/4 preliminarily annealed in vacuum for 1 hour at 400°C and selenized at 560°C for 1 hour. As we could take insights from the XRD and Raman spectra, the CZTSe thin layer was found to consist of large grains sized more than 1μm. More detailed observations revealed fine grains situated

mainly on the large grain boundaries at the bottom of the layer and flat hexagonal well-formed crystals situated mainly on the surface of the layer. High definition EDX allowed us to determine the composition peculiarities of the described objects. Large grain composition (measured at point +) indicates to slightly Tin rich CZTSe (23.77 at% Cu- 11.30 at% Zn- 13.67 at% Sn – 51.25 at% Se) thin film material. Fine powder crystallites on the interface Mo - CZTSe indicated as **o** shows a composition of 52.65 at% Zn – 47.35 at% Se that corresponds to the Stilleite phase presented in Fig.2. Flat plate crystal grains on the surface – indicated as **x** were defined to correspond to the Klockmanite (Fig.2), giving 47.48 at% Cu – 52.52 at% Se.

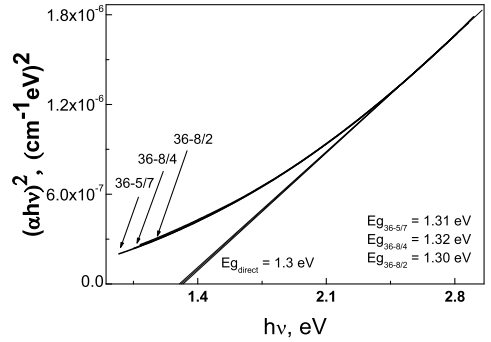

Fig.5. Plot for determining the band gap of $Cu_2ZnSnSe_4$ films selenized in different conditions: 36-8/4 -1 hour at 400°C in vacuum +1 hour at 560°C and 36-8/2&36-5/7 for 10 minutes at 530 °C. The analysis is based on the assumption that CZTSe is a direct band gap material.

Fig.5 shows the dependence of the curves of $(\alpha h\nu)^2$ on the dropping optical light energy hν for layers CZTSe deposited in similar conditions but annealed both by fast (10 minutes selenization at 530°C -36-8/2&36-5/7) or through preliminary metal alloy homogenization at 400°C for 1 hour and 1 hour selenization at 560°C – sample 36-8/4. The direct optical band gap was approximated by plotting $(\alpha h\nu)^2$ versus the energy in eV and extrapolating the linear part of the spectrum $(\alpha h\nu)^2 = f(h\nu)$ to zero. Thus, the band gap of the CZTSe thin films was estimated to be 1.31 eV ± 0.01 eV. This value is much lower than those reported earlier [3,5] 1.44 eV and 1.56 eV. It seems closer to those close to 1 eV proposed recently in the investigations of monograin materials [18]
Comparison of the data in Fig.2 enables to conclude that a longer annealing time acts favourably to the formation of well-crystallized Stannite $Cu_2ZnSeSe_4$ and different binaries (Klockmanite - CuSe and Stilleite - ZnSe) as well as those for thicker under-layer of Mo_3Se_4.

4. Conclusions

Electrodeposition of alloys Brass and Bronze substrate layers followed by selenization results in successful formation of well-crystallized Stannite thin film structures. Shorter annealing time may lead to favorable formation of Stannite thin films but the system is still not a perfect mono phase. All thin layer materials showed similar optical properties and a band gap near 1.31 eV.

5. Acknowledgements

European Researcher's Mobility Program of Estonian Science Foundation under Contract JD 98 is gratefully acknowledged.

6. References

1. A Vision for Photovoltaic Technology for 2030 and Beyond, European Commission, 2004.
2. Feltrin, A. Freindlich, Material considerations for terawatt level deployment of photovoltaics, Renew. Energy 33 (2008) 180–185.
3. H.Matsushita, T.Maeda, A.Katsui and T.Takadzawa, J.Cryst.Growth 208, 416 (2000).
4. K. Ito, T. Nakazawa, Jpn. J. Appl. Phys. 27 (1988) 2094
5. Th. M. Friedlmeier, N. Wieser, T. Walter, H. Dittrich, H.-W. Schock, Proceedings of the 14th European Conference of Photovoltaic Solar Energy Conference and Exhibition, Belford, 1997, p. 1242.
6. H. Katagiri, K. Jimbo, K. Moriya, K. Tsuchida, Proceedings of the 3rd World Conference on Photovoltaic Solar Energy Conversion, Osaka, 2003, p. 2874.
7. Ennaoui A., Lux-Steiner M., Weber A., Abou-Ras D., Kotschau I., Schock H.-W., Schur R., Holzing A., Jost S., Hock R., Voss T., Schulze J., Kirbs A., Thin Solid Films, xxx (2008) xxx-xxx
8. Scragg J., Dale P., Peter L., Electrochemistry Communications 10 (2008) 639-642
9. H. Kühnlein, J. Schulze, T. Voß, Metal plating composition and method for the deposition of copper–zinc–tin suitable for manufacturing thin film solar cell, Patent WO2007134843, Nov. 29, 2007.
10. R.A.Wibowo, E.S.Lee, B.Munir, K.H.Kim, Pulsed laser deposition of quaternaryCu2ZnSnSe4 thin films, Phys. Status Solidi (a)204(2007) 3373–3379.
11. R.A.Wibowo,W.S.Kim,E.S.Lee,B.Munir,K.H.Kim,Single step preparation of quaternary Cu2ZnSnSe4 thin films by RF magnetron sputtering from binary chalcogenide targets, J.Phys.Chem.Solids68(2007)1908–1913
12. O.Volobijeva, J.Raudoja, E.Mellikov, M.Grossberg, S. Bereznev, R.Traksmaa, Cu2ZnSnSe4 films by selenization of Sn-Zn-Cu sequential films, Journal of Physics and Chemistry of Solids, 2009
13. M.Altosaar, J.Raudoja, K.Timmo, M.Danilson, M.Grossberg, J.Krustok, E. Mellikov, Cu2Zn1_x Cdx Sn(Se1_y Sy)4 solid solutions as absorber materials for solar cells, Phys. Status Solidi (a)205(2008)167–170.
14. Mellikov E., Meissner D., Varema T., Altosaar M., Kauk M., Volobujeva O., Raudoja J., Timmo K., Danilson M., Monograin materials for solar cells, Sol. Energy Mater.Sol.Cells, 93,1(2009), 65-68
15. Ямпольский А.М., Ильин В.А., Краткий Справочник Гальванотехника, Ленинград “Машиностроение”, 1981
16. Powder Diffraction File, Joint Committee on Powder Diffraction Standards, American Society for Testing and Materials, Philadelphia, Pa, 1967, PDF 40-1487.
17. Instrument Engineers' Handbook: Process measurement and analysis, Béla G. Lipták,Edition: Published by CRC Press, 2003; ISBN 0849310830, 9780849310836.
18. Grossberg M., Krustok J., Timmo K., Altosaar M., Radiative recombination in Cu2ZnSnSe4 monograins studied by photoluminescence spectroscopy, Thin Solid Films 517, 7 (2009), 2489-2492

Appendix A

Article V

M. Ganchev, J. Iljina, **L. Kaupmees**, T. Raadik, O. Volobujeva, A. Mere, M. Altosaar, J. Raudoja, E. Mellikov, "Phase composition of selenized $Cu_2ZnSnSe_4$ thin flms determined by X-ray diffraction and Raman spectroscopy", *Thin Solid Films* 519 (2011) 7394–7398.

Thin Solid Films 519 (2011) 7394–7398

Contents lists available at ScienceDirect

Thin Solid Films

journal homepage: www.elsevier.com/locate/tsf

Phase composition of selenized $Cu_2ZnSnSe_4$ thin films determined by X-ray diffraction and Raman spectroscopy

M. Ganchev *, J. Iljina, L. Kaupmees, T. Raadik, O. Volobujeva, A. Mere, M. Altosaar, J. Raudoja, E. Mellikov

Department of Materials Science, Tallinn University of Technology, Ehitajate tee 5, 19086 Tallinn, Estonia

ARTICLE INFO

Available online 4 March 2011

Keywords:
$Cu_2ZnSnSe_4$
Stannite
Thin films

ABSTRACT

Thin layers of Sn onto Cu–Zn alloy with different component ratios were processed at different temperatures. Scrupulous comparative analyses were performed by room temperature Raman spectroscopy and X-ray-diffractometry. An excess of tin on the surface results in isothermal selenization at 450 °C in the hexagonal residuals of unstable $SnSe_2$ in the well-crystallized Stannite — $Cu_2ZnSnSe_4$. In similar selenization conditions, copper-rich layers as precursors result in the Stannite phase with micro-immersions of CuSe. Low-temperature photoluminescence spectra of selenized films indicated to two Gaussian shaped bands at 0.81 and 1.16 eV.

1. Introduction

Thin film chalcopyrites and in particular the compounds based on abundant elements of Cu, Zn and Sn have strengthened their position in photovoltaics [1]. Solar cells on mixed sulfur–selenium $Cu_2ZnSn(S,Se)_4$ layers have been reported to show a record efficiency of 9.66% [2], confirming their potential to play a serious role in photovoltaics through the cost–efficiency ratio in material diversification. The first thin film CZTSe device grown by evaporation has shown a 2% efficiency [3].Thin $Cu_2ZnSnSe_4$ (CZTSe) layers have been formed also by pulsed laser ablation [4], selenization of one-step RF sputtered [5] or sequentially deposited substrates [6] as well as by synthesis from melts [7]. CZTSe single crystals were first formed by [8] and compound materials have been shown to crystallize in the Stannite structure with direct band gap near 1.44 eV and a high absorption coefficient tending to 10^4 cm^{-1} [9].

This study analyzes in detail the phase composition of CZTSe layers with different metals ratios selenized under gradual temperature conditions.

2. Experimental details

Substrate layers were deposited electrochemically in potentiostatic conditions using the classic three-electrode cell configuration. Working electrodes were 2×1 cm^2 sized molybdenum covered soda lime glasses positioned against platinum gauze and a saturated mercury sulfate (MSE) reference electrode (0.6151 V vs. SHE). Electrolytes for electrodeposition of Cu–Zn alloy and Sn layers were aqueous pyrophosphate solutions of the sulfate salts of Cu^{2+}, Zn^{2+} and Sn^{2+}. Selenization was performed in isothermal conditions at sealed quartz ampoules placed into the tubular furnace. A cooling-down process procedure was followed, that ensure extra selenium vapors to be condensed in the external empty part of the ampoule far away of the samples. Configurations and regimes were the same as described elsewhere [10].

Routine scanning electron microscopy and energy dispersive X-ray analysis (EDAX) was performed on Hitachi TM 1000 unit supplied with an X-ray source and detector equipment with an accelerating voltage of 15.0 kV and acquisition time of 90 s. Film morphology was examined by Zeiss ULTRA 55 at an accelerating voltage 1.74 kV.

In the X-ray diffraction (XRD) analysis a Rigaku Ultima IV diffractometer with Cu–Kα radiation ($\lambda = 1.5418$ Å) at 40 kV accelerating voltage was used. The diffracted beam was scanned in steps by 0.01° for 2 s in an angular range from 10 to 80° 2Θ.

Qualitative phase analysis was performed on PDXL Rigaku's ICDD PDF2 phase research platform [11]. The room temperature (RT) micro Raman spectra was recorded on Horiba LabRam 800 high-resolution spectrometer equipped with a multichannel detector on backscattering regime. Light source was a green laser with a 532 nm wavelength focused at least on 10 μm spot diameter, providing a spectral resolution of 0.5 cm^{-1}. Photoluminescence measurements were carried out in a closed-cycle He cryostat at 15 K. The PL excitation was done by 441 nm He–Cd laser line and registered with a SPM2 Carl Zeiss Jena monochromator and InGaAs detector.

3. Results and discussion

The influence of the initial composition of the films was studied for Cu-rich, stoichiometric and Cu-poor layers selenized at 450 °C. Temperature dependence experiments were conducted at temperatures

* Corresponding author. Tel.: +372 6203374; fax: +372 6203367.
E-mail address: mganchev@abv.bg (M. Ganchev).

0040-6090/$ – see front matter © 2011 Elsevier B.V. All rights reserved.
doi:10.1016/j.tsf.2011.01.388

Table 1
Temperature of annealing, elemental composition and components ratio of thin CZTSe films, formed by isothermal selenization of sequential Cu + Zn and Sn layers.

N	T, °C	Cu, a%	Zn, a%	Sn, a%	Se, a%	Cu/(Zn + Sn)	Zn/Sn	Me/CZTSe
Samp1	450	22.7	16.7	10.9	49.7	0.8	1.5	0.5
Samp2	450	20.9	17.4	11.9	49.8	0.7	1.5	0.5
Samp3	450	26.4	12.9	11.8	48.9	1.1	1.1	0.5
Samp4	450	28.6	10.7	12.1	48.6	1.2	0.9	0.5
Samp5	490	15.4	25.0	10.8	48.8	0.4	2.3	0.5
Samp6	530	19.9	17.5	13.4	49.2	0.5	1.3	0.5
Samp7	560	13.5	20.7	9.1	56.7	0.5	2.2	0.4

450 °C, 490 °C, 530 °C and 560 °C only for copper-poor samples. XRD analysis was also carried out in addition to the Raman backscattering analysis for comparative investigations of the phase composition of the CZTSe layers.

All samples were Sn-poor ([Zn]/[Sn]>1) after selenization with the exception of the samples prepared using Cu-rich precursors only. The composition of the layers and selenization parameters for all the samples used are summarized in Table 1.

The XRD patterns of CZTSe samples with different [Cu]/{[Zn] + [Sn]} ratios are shown in Fig. 1. Phase composition of the samples as determined by XRD analysis is presented in Table 2. The stannite — $Cu_2ZnSnSe_4$ [11] is recognizable by the main reflections at 27.16°, 45.1° and 53.52° and other minor peaks which are marked in Fig. 1 with s. In addition there are reflections of Mo [11] at 40.2° and 73.5° and three other peaks at 11.5°, 31.6° and 56.0° attributable to $MoSe_2$ [11] (d) — the phase formed by the selenization. Detailed analysis confirmed the existence of $Cu_{1.8}Se$ [11] (marked as b) — with reflections at 27.2°, 45.1° and 56.1°. Also a possible phase is ZnSe [11] — (z) the main peaks of which coincide or lie very close to those of Stannite at 27.16°, 45.1° and 53.5°. The XRD pattern for the Cu-poor sample presents (0,0,1), (0,0,2), (0,0,3) and (0,0,4) reflections of the $SnSe_2$ phase [11] — (T)at angles of 14.44°, 29.09°, 44.25° and 60.29, respectively, resulting in a dominant growth in the polar c-plane orientation. Increased copper concentration provokes a preferable growth of CuSe [11], marked with k, indicated by minor peaks at 26.6°, 28.1°, 31.2° and 50°. In addition the detailed analysis revealed several other phases. The layers Samp3 and Samp4 were shown also to contain ternaries Cu_2SnSe_3 [11] (cts) and Cu_2SnSe_4 [11] (dctts); in addition, Samp3 contain of SnSe (t) [11].

Fig. 2 shows the XRD patterns of layers formed by annealing of Cu–Zn/Sn films in selenium vapors at different temperatures — Samp1 – at 450 °C, Samp5 – 490 °C, Samp6 – 530 °C and Samp7 – at 560 °C, respectively. All samples were Cu-poor, with phase content as shown in Table 2. At the initial temperature, the representative pattern is the same as in the previous description for the Cu-poor case (Samp1). As the temperature rises the main dominant phases are again $Cu_2ZnSnSe_4$, $Cu_{1.8}Se$ and ZnSe. Minor presence of CuSe was registered also but their intensity decreases sharply with the temperature increasing. Respective phases are denoted in Fig. 2 with the same codes s, b, z and k. The most intense peaks are at angles 2Θ — 27.2°, 45.1° and 53.3°. As it was mentioned, the reflections are composite (attributable to many phases: CZTSe, $Cu_{1.8}Se$, ZnSe) with no indication to qualitative distribution. In addition, the phases of $SnSe_2$ and SnSe are also noticeable. The group of ternary Cu_2SnSe_3 is seen

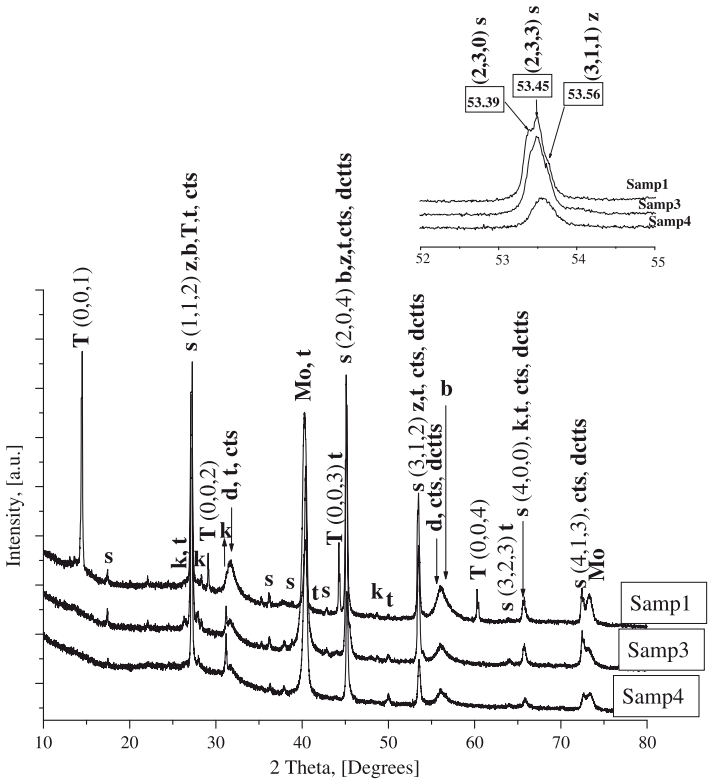

Fig. 1. XRD patterns of Cu-poor (Samp1), Stoichiometric — Cu = (Zn + Sn) (Samp3) and Cu-rich (Samp4) CZTSe thin films, obtained by isothermal selenization at 450 °C of metal Cu–Zn/Sn layers onto Mo covered soda lime glass substrates. Phase symbols: s—$Cu_2ZnSnSe_4$; z—ZnSe; b—$Cu_{1.8}Se$; k—CuSe; t—SnSe; T—$SnSe_2$; d—$MoSe_2$; cts—Cu_2SnSe_3; dctts—Cu_2SnSe_4; Mo—Molybdenum. Inset present the pattern in interval 52°–55° for distinct of CZTSe and ZnSe.

Table 2
Phases, detected by XRD in the samples CZTSe, selenized in isothermal condition according to Table 1: * – existing phase; o – not detected phase.

N	T,	$Cu_2ZnSnSe_4$	Cu_2SnSe_3	Cu_2SnSe_4	$SnSe_2$	$Cu_{1.8}Se$	CuSe	ZnSe	SnSe
	°C	s	cts	dctts	T	b	k	z	t
Samp1	450	*	o	*	*	*	*	*	o
Samp2	450	*	o	*	o	*	*	*	*
Samp3	450	*	*	*	o	*	*	*	*
Samp4	450	*	*	*	o	*	*	*	o
Samp5	490	*	*	*	*	*	*	*	o
Samp6	530	*	*	*	o	*	*	*	o
Samp7	560	*	*	*	*	*	*	*	o

accompanied with Cu_2SnSe_4. When the temperature increases, the signal of the substrate fades and reflections from the layer becomes dominant. CZTSe and ZnSe phases can be distinguished in the vicinity of 53°–54°[12]. Here CZTSe presents twins at 53.39° (2,3,0) and 53.45° (2,3,3) whereas ZnSe presents (3,1,1) peak at 53.56°. As can be seen at the inset of Fig. 2, at lower and higher temperatures (Samp4 and Samp7) ZnSe exists as a minor compound and its crystallinity improves at 530 °C. The same trend can be seen in the crystallization of the phase $Cu_2ZnSnSe_4$. It is also interesting to follow the dependence of CZTSe–ZnSe peaks ratio through the Cu compositional gradient. As can be seen from the inset of Fig. 1, twin peak corresponding to CZTSe dominates and ZnSe is present as a trace in the layers.

Fig. 3 shows the Raman spectra of samples selenized at 450 °C with different Cu concentrations — Cu-poor, stoichiometric CZTSe ($Cu_2ZnSnSe_4$) and Cu-rich CZTSe (Samp2, Samp3 and Samp4, respectively) and samples annealed at different temperatures — Samp5@490 °C; Samp6@530 °C and Samp7@560 °C (in accordance with Table 1). In all samples CZTSe is the dominant phase presenting main vibrations at 79 cm^{-1}, 171 cm^{-1}, 194 cm^{-1}, 231 cm^{-1} and 390 cm^{-1}. For the Cu-rich and stoichiometric samples resonance at 262 cm^{-1} was recorded and taken together with those at 91 cm^{-1} assigned to CuSe (k). In the spectra for Samp2 a signal near 250 cm^{-1} was detected. We attributed it to the phase ZnSe, in accordance with the phase distribution, evidenced in Fig. 1. When the temperature rose from 450 °C to 560 °C, a dominating signal had arisen at the same wave number (250 cm^{-1}), indicating preferential crystallization of ZnSe.

Fig. 4 exhibits the morphology of the quaternary CZTSe films. The micrographs present the surface image of Samp6 (Table 1) annealed at 530 °C (image a) and its cross-section view (image b). The layer is uniform, dense and well crystallized with grain size near 1 μm. On the border of the grains small hexagonal crystals of impurity phases (marked in circles) are seen.

Amongst recognized phases here, CuSe and $SnSe_2$ are hexagonal. As is shown elsewhere [10], ZnSe sets usually on the bottom whereas preferable distribution of copper selenides is on the surface and

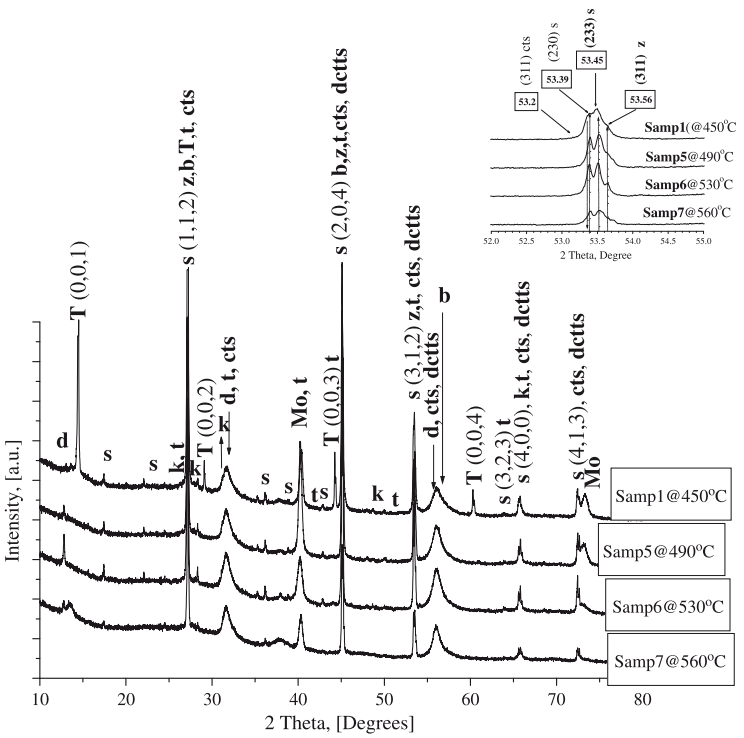

Fig. 2. XRD pattern of CZTSe samples formed by isothermal reactive annealing in Se vapors of Cu–Zn/Sn metal layers at different temperatures: Samp1 — 450 °C; Samp5 — 490 °C; Samp6 — 530 °C and Samp7 — 560 °C. The layers are Cu-poor. For phase symbols refer Fig. 1. Inset presents the pattern in 2Θ interval 52°–55° to gain distinction of CZTS and ZnSe.

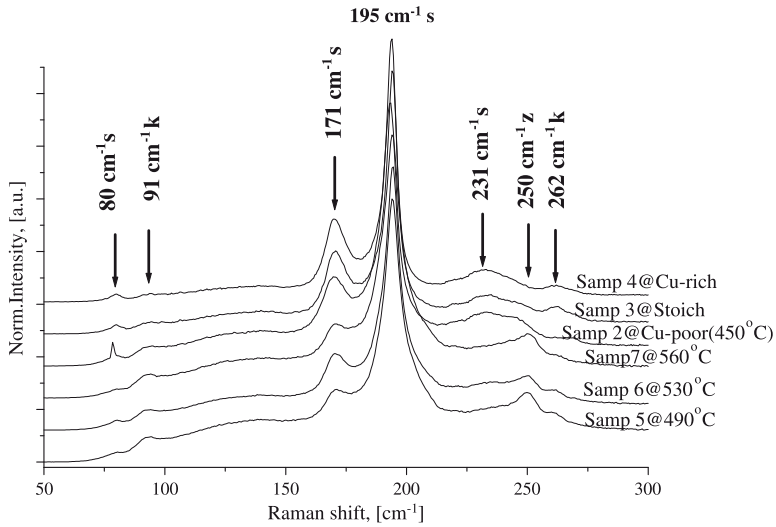

Fig. 3. Raman spectra for thin CZTSe layers: with different Cu concentration annealed at different temperatures. For phase symbols refer Fig. 1. (See also Table 1 and text).

among grain borders of the layer. It was shown above that even copper-poor layers contain separate copper selenide phases.

The low-temperature (T = 15 K) photoluminescence spectra of the annealed CZTSe (Samp1) film are presented in Fig. 5. The PL spectrum of that sample consists of two Gaussian-shaped PL bands at 0.81 and 1.16 eV, respectively. The first one has been recognized already in the monophase CZTSe [13], where temperature and excitation power dependences defined it as a BI-emission. The second band is caused obviously by CuSe contaminants. Previous investigations [10] have shown similar dominating PL emission in the presence of CuSe.

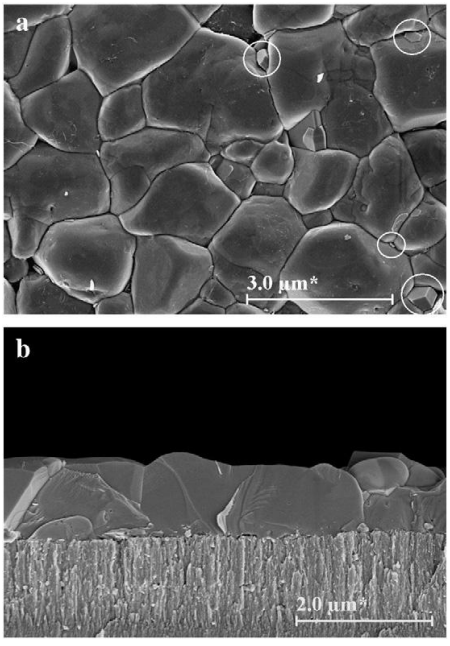

Fig. 4. High resolution SEM micrograph of thin layer CZTSe (Samp6) (a), selenized at 530 °C for 30 min in closed isothermal conditions and (b) — cross section of the film. With circles are marked surface hexagonal impurities on the grain borders.

To complete the overview on the reaction pathway, the inferences made in ref. 12 should be taken into considerations. Results show that at temperatures 200 °C the synthesis of binaries (Cu_2Se, CuSe, SnSe, and ZnSe) takes place. When the temperature rises up to 450 °C, the binary forms the ternary Cu_2SnSe_3, which adsorb ZnSe and form the quaternary $Cu_2ZnSnSe_4$.

$$Sn + 2Se \rightarrow SnSe_2 \quad (1)$$

$$Cu + 2Se \rightarrow Cu_2Se \quad (2)$$

$$Cu + Se \rightarrow CuSe \quad (3)$$

$$Zn + Se \rightarrow ZnSe \quad (4)$$

$$Cu_2Se + SnSe_2 \rightarrow Cu_2SnSe_3 \quad (5)$$

$$Cu_2SnSe_3 + ZnSe \rightarrow Cu_2ZnSnSe_4 \quad (6)$$

$$Cu_2Se + 2SnSe_2 \rightarrow Cu_2SnSe_4 + SnSe \quad (7)$$

$$SnSe_2 \leftrightarrow SnSe + Se \quad (8)$$

Sequence of Reactions 1, 2, 4, 5 and 6 on analogy with [14] gives an interaction chains to form the quaternary CZTSe compound. Obviously Reactions 5 and 6 do not pass up to the last and together with Reaction 3 give an idea of how to explain the phase composition, revealed by XRD and partially by Raman backscattering analyses. The phase of Cu_2SnSe_4 could be formed at higher concentrations of $SnSe_2$, e.g. by Reaction 7. This interaction could give an insight into the SnSe assumed by XRD.

Reaction 7 gives an idea of SnSe in the films but SnSe could come from another interaction, which should be taken into consideration. Equilibrium of tin compounds with selenium depends on the temperature and respectively on the pressure of the selenium vapors by equilibrium 8.

As it follows from equilibrium 8 according to the Le Chatelier–Braun principle, at high temperatures selenium vapor pressure is high and reaction equilibrium is moved on the left, keeping tin in the high

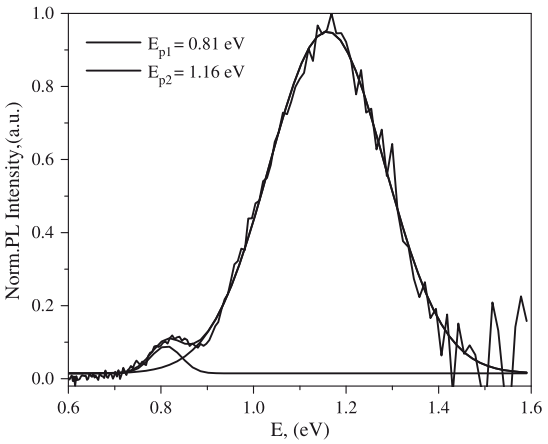

Fig. 5. Low temperature (15 K) photoluminescence spectra of thin CZTSe film (Samp1), annealed in closed isothermal conditions.

valence form. Samples in the ampoule are cooled down to ensure selenium to be moved to condensate preferably away from the sample. The samples should be held in a comparatively warmer part of the ampoule, in fact, to stimulate the decay of $SnSe_2$ in the layers.

Precise phase research analysis, performed by the PDXL software platform and the appropriate methodology for the experiments provides also an insight into the relative phase distribution and copper fraction in the grown films. For example, the composite reflection in Fig. 1 at 27.2° could be consistent with Stannite(s), Zinc Selenide (z), $Cu_{1.8}Se$ (b), $SnSe_2$ (T), SnSe — (t) and Cu_2SnSe_3 — (cts). About ZnSe an inset is added, which can provide an imagination of its part. $SnSe_2$ disposes individual reflections at 14.4°, 29.4°, 44.4° and 60.4° and the set of diffractograms shows that it consists only at the lower temperature 450 °C for copper poor sample (Samp1). The low valent form SnSe has individual reflections at 42° and 50.1° beside those at 26.4°, 31.6°, 40.3°, 45.5°, 48.6°, 53.5°, 64° and 65.7°. The set of curves presents an increase in the reflection height at 50.1°, its role being additionally described with the set of proposed formation reactions. Berzellianite ($Cu_{1.8}Se$ — b) disposes individually at 56.8° near the reflection of Drysdallite — ($MoSe_2$ — d) at 56.0°. The set of diffractograms shows that it appears at the copper-rich sample as a little shoulder, which could be recognized as an indication of presence in traces only at copper rich samples. Cu_2SnSe_3 disposes reflections at 27.16°, 31.6°, 45.1°, 53.5°, 56°, 65.7° and 72.5°, corresponding to the planes (1,1,1), (2,0,0), (2,2,0), (3,1,1), (2,2,2), (4,0,0) and (3,3,1) respectively. Cu_2SnSe_4(dctts) [11] presents at 45.2°, 53.4°, 55.95°, 65.8° and 72.5° from the respective planes (2,2,0), (3,1,1), (2,2,2), (4,0,0) and (3,3,1). Cu_2SnSe_3 appears together with SnSe, $Cu_2ZnSnSe_4$ and ZnSe at 31.6° close to the large reflection of $MoSe_2$ at 31.8° and after the reflection of the CuSe (k) at 31.2°. The lack of another visible shoulder besides the reflection of CuSe on the large reflection of $MoSe_2$ (keeping in mind the considerations for SnSe) would suggest a presence of Cu_2SnSe_3 as very small part. The same considerations could be made for reflections at 45.1° and 53.5°, respectively and to conclude that the main phase is Stannite ($Cu_2ZnSnSe_4$) and all other phases present as minorities or traces.

4. Conclusions

The study adds insights into the thermal interactions of metals Cu, Zn and Sn with Se at the temperature interval of 450 °C–560 °C for samples with a deficiency of Cu against stoichiometry of $Cu_2ZnSnSe_4$. Features of the phase composition depending on the relative Cu concentration at 450 °C were revealed for quaternary compound samples $Cu_2ZnSnSe_4$.

Acknowledgments

Authors would like to thank Dr J. Krustok and K. Timmo for discussions on PL and XRD. Estonian National Science Foundation under Contract JD 98, grants G-8147 and G-6954 and HTM (Estonia) under the project No. SF0140099s08 are gratefully acknowledged.

References

[1] H. Katagiri, K. Jimbo, W.S. Maw, K. Oishi, M. Yamazaki, H. Araki, A.Takeuchi, Thin Solid Films 517 (2009) 2455–2460.
[2] T. Todorov, K. Reuter, D. Mitzi, Adv. Mater. 22 (2010) 1.
[3] T.M. Friedlmeier, H. Dittrich, H.W. Schock, Inst. Phys. Conference Ser. No. 152, Proc. 11th ICTMC (Salford) P 345, 1997.
[4] R.A. Wibowo, E.S. Lee, B. Munir, K.H. Kim, Phys. Status Solidi A 204 (2007) 3373.
[5] R.A. Wibowo, W.S. Kim, E.S. Lee, B. Munir, K.H. Kim, J. Phys. Chem. Solids 68 (2007) 1908.
[6] O. Volobujeva, J. Raudoja, E. Mellikov, M. Grossberg, S. Bereznev, R. Traksmaa, J. Phys. Chem. Solids 70 (2009) 567.
[7] M. Altosaar, J. Raudoja, K. Timmo, M. Danilson, M. Grossberg, J. Krustok, E. Mellikov, Phys. Status Solidi A 205 (2008) 167.
[8] H. Hahn, H. Schulze, Naturwissenshaften 52 (1965) 426.
[9] L. Guen, W.S. Glaunsinger, A. Wold, Mater. Res. Bull. 14 (1979) 463.
[10] M. Ganchev, L. Kaupmees, J. Iliyna, J. Raudoja, O. Volobujeva, H. Dikov, M. Altosaar, E. Mellikov, T. Varema, Physics Procedia 2 (2010) 65.
[11] International Center for Diffraction Data: CZTSe – 10708930; MoSe2 – 30653481; SnSe – 10890232; SnSe2 – 10893197; ZnSe – 10715978; CuSe – 10728417; Cu1.8Se – 10882043; Cu2SnSe3 – 30654145; Cu2SnSe4 – 10780600; Mo – 10714645.
[12] P.M.P. Salomé, P.A. Fernandez, A.F. da Cunha, Thin Solid Films 517 (2009) 2531.
[13] J. Krustok, K. Timmo, M. Altosaar, Thin Solid Films 517 (2009) 2489.
[14] R. Schurr, A. Hölzing, S. Jost, R. Hock, T. Voß, J. Schulze, A. Kirbs, A. Ennaoui, M. Lux-Steiner, A. Weber, I. Kotschau, H.-W. Schock, Thin Solid Films 517 (2009) 2465.

Appendix B

Curriculum Vitae

Appendix B

ELULOOKIRJELDUS

Ees- ja perekonnanimi:	Liina Kaupmees
Sünniaeg ja –koht:	31.12.1976, Tallinn
E-posti aadress:	liina3112@staff.ttu.ee
Hariduskäik	2004 – Tallinna Tehnikaülikool, Keemia- ja Materjalitehnoloogia teaduskond, doktorantuur 2004 - Tallinna Tehnikaülikool, Keemia- ja Materjalitehnoloogia teaduskond, loodusteaduste magistrikraad 2001 - Tallinna Tehnikaülikool, Keemia- ja Materjalitehnoloogia teaduskond, loodusteaduste bakalaureusekraad 1995 – Tallinna Tehnikagümnaasium, keskharidus
Teenistuskäik	2005 - Tallinna Tehnikaülikool, Materjaliteaduse Instituut, teadur 2001-2004 - Tallinna Tehnikaülikool, Materjaliteaduse Instituut, insener
Kaitstud lõputööd	„Elektrokeemiliselt sadestatud $CuInSe_2$ kilede koostise ja morfoloogia uurimine“, magistritöö, juhendaja vanemteadur Mare Altosaar „I-III-VI_2 tüüpi ühendite elektrokeemiline süntees“, bakalaureusetöö, juhendaja vanemteadur Mare Altosaar
Täiendusõpe	nov. 2006, veeb., mai 2007 West University of Timisoara, Rumeenia, külalisteadur veeb. 25 – 27, 2006 Chemistry and physics of photovoltaics, European Union Centre of Excellence in PV materials and Devices, Tallinn, Eesti aug. 21 – 25, 2006 European Union Centre of Excellence in PV materials and Devices, „YSSS – 2006 on PV“, Pärnu, Eesti juuni – aug. 2000, Outokumpu Research OY, Pori, Soome, praktikant

Appendix B

CURRICULUM VITAE

Name:	Liina Kaupmees
Date and place of birth:	31.12.1976, Tallinn
E-mail:	liina3112@staff.ttu.ee
Education	2004 – Tallinn University of Technology, Faculty of Chemical and Materials Technology, doctoral study 2004 - Tallinn University of Technology, Faculty of Chemical and Materials Technology, Master of Science in Natural Sciences 2001 - Tallinn University of Technology, Faculty of Chemical and Materials Technology, Bachelor of Science in Natural Sciences 1995 – Tallinn Technical Secondary School
Professional Employment	2005 - Tallinn University of Technology , Faculty of Chemical and Materials Technology; Department of Materials Science, Chair of Semiconductor Materials Technology, Researcher 2001 – 2004 Tallinn University of Technology, Faculty of Chemical and Materials Technology; Department of Materials Science, Chair of Semiconductor Materials Technology, Engineer
Defended theses	"Study of morphology and composition of electrochemically deposited $CuInSe_2$ thin films", Master thesis, supervisor Senior Research Scientist Mare Altosaar "Electrochemical synthesis of I-III-VI_2 type compounds", Bachelor thesis, supervisor Senior Research Scientist Mare Altosaar
Training Courses	Nov. 2006, Feb., May 2007, West University of Timisoara, Faculty of Physics, Romania, guest researcher 21.08.2006 – 25.08.2006, European Union Centre of Excellence in PV Materials and Devices, Estonia, "YSSS – 2006 on PV" 25.02.2006 – 27.02.2006, Chemistry and physics of photovoltaics, European Union

Centre of Excellence in PV Materials and Devices, Estonia
June – Aug. 2000, Outokumpu Research OY, Pori, Finland, trainee.

List of publications

1. Volobujeva, O.; Altosaar, M.; Raudoja, J.; Mellikov, E.; Grossberg, M.; **Kaupmees**, L.; Barvinsch, P. (2009). „SEM analysis and selenization of Cu–In alloy films produced by co-sputtering of metals". *Solar Energy Materials and Solar Cells* 93 (2009) 11 - 14.
2. **Kaupmees**, L.; Altosaar, M.; Volobujeva, O.; Barvinschi, P. (2010). "Study of Mo selenisation process on different Mo substrates". In: Thin-Film Compound Semiconductor Photovoltaics — 2009: 2009 MRS spring meeting, San Francisco, CA, April 13-17, Warrendale, PA, USA: Materials Research Society, 1165 (2009) M08-01. *Materials Research Society Symposium Proceedings* 1165 (2010) 289–294.
3. Ganchev, M.; **Kaupmees**, L.; Iliyna, J.; Raudoja, J.; Altosaar, M.; Volobujeva, O.; Mellikov, E.; Varema, T.; Dikov, H. (2010). Formation of $Cu_2ZnSnSe_4$ thin films by selenization of electrodeposited stacked binary alloy layers. Proceedigs of EMRS, Stasbourg, June 2009, *Energy Procedia* 2 (2010) 65–70.
4. Mellikov, E.; Altosaar, M.; Krunks, M.; Krustok, J.; Varema, T.; Volobujeva, O.; Grossberg, M.; **Kaupmees**, L.; Dedova, T.; Timmo, K.; Ernits, K.; Kois, J.; Oja Acik, I.; Danilson, M.; Bereznev, S. (2008). "Research in solar cell technologies at Tallinn University of Technology". *Thin Solid Films* 516 (2008) 7125 - 7134.
5. **Kaupmees**, L.; Altosaar, M.; Volubujeva, O.; Mellikov, E. (2007). "Study of composition reproducibility of electrochemically co-deposited $CuInSe_2$ films onto ITO". *Thin Solid Films* 15 (2007) 5891 - 5894.
6. Ganchev, M.; Iljina, J.; **Kaupmees,** L.; Raadik, T.; Volobujeva, O.; Mere, A.; Altosaar, M.; Raudoja, J.; Mellikov, E. (2011). "Phase composition of selenized $Cu_2ZnSnSe_4$ thin films determined by X-ray diffraction and Raman spectroscopy", *Thin Solid Films* 519 (2011) 7394–7398.
7. **Kaupmees, L.**; Altosaar, M.; Volobujeva, O.; Grossberg, M.; Raadik, T.; Danilson, M.; Mellikov, E.; Barvinschi, P. (2011). „Isothermal and two-temperature-zone selenization of molybdenum layers". Advances in Material Science and Engineering. Accepted 6 October 2011, MS no. 345762, (see online: Articles in Press).

Appendix B

Tables

Table 8. Composition of electrodeposited precursor films and selenized films as determined by EDX

Scheme of precursor film deposition	Sample	Concentration of elements in precursor film, [at%]			Concentration of elements in selenized film, [at%]				Selenization conditions	
		Cu	Zn	Sn	Cu	Zn	Sn	Se	t, min.	T, °C
Cu-Sn is deposited on Cu-Zn layer	36-5/7	43.7	8.4	47.9	21.2	16.0	13.4	49.4	10	530
	36-5/8	43.6	16.2	40.2	20.3	21.5	9.0	49.2	15	530
	36-8/2	34.0	16.6	49.2	16.0	23.3	10.7	50.0	20	530
	36-8/4	35.6	17.2	47.2	24.0	17.0	11.0	48.0	60	560
Sn is deposited on Cu-Zn layer	S-3s1	15.0	8.2	76.8	22.7	16.7	11	49	30	450
	S-3s4	40.9	17.3	41.8	24.4	12.9	11.9	50.9	30	450
	S-4s3	56.0	12.7	31.3	28.5	10.7	12.1	48.6	30	450
	S-6s3	28.4	21.6	49.9	13	20	9	56	30	560
	S-6s5	26.6	20.7	52.7	15	25	10	50	30	490
	S-6s6	35.7	18.0	46.2	22	14	15.8	47.9	30	530

Table 9. Temperature of annealing, elemental composition, component ratios and detected phases of thin CZTS films formed by isothermal selenization of sequential Cu+Zn and Sn layers on Mo substrates. "*" marks phases which exist in every sample - $Cu_2ZnSnSe_4$, Cu_2SnSe_4, $Cu_{1.8}Se$, CuSe, ZnSe, $MoSe_2$ and Mo [118].

Sample	**T, °C**	**Cu** [at%]	**Zn** [at%]	**Sn** [at%]	**Se** [at%]	**Cu/(Zn+Sn)**	**Zn/Sn**	**Metals/Se**	**Formed phases ***
S- S3s1	450	22.69	16.72	10.90	49.68	0.82	1.5	1.01	$SnSe_2$
S- S4s4	450	20.87	17.42	11.90	49.80	0.71	1.5	1.01	SnSe
S- S3s4	450	26.45	12.86	11.80	48.89	1.07	1.1	1.05	Cu_2SnSe_3 SnSe
S- S4s3	450	28.57	10.73	12.14	48.56	1.25	0.9	1.06	Cu_2SnSe_3
S- S6s5	490	15.36	25.01	10.84	48.78	0.43	2.3	1.05	Cu_2SnSe_3 $SnSe_2$
S- S6s6	530	19.97	17.48	13.41	49.12	0.65	1.3	1.04	Cu_2SnSe_3
S- S6s3	560	13.45	20.68	9.16	56.69	0.45	2.2	0.76	Cu_2SnSe_3 $SnSe_2$

DISSERTATIONS DEFENDED AT TALLINN UNIVERSITY OF TECHNOLOGY ON *NATURAL AND EXACT SCIENCES*

1. **Olav Kongas**. Nonlinear Dynamics in Modeling Cardiac Arrhytmias. 1998.

2. **Kalju Vanatalu**. Optimization of Processes of Microbial Biosynthesis of Isotopically Labeled Biomolecules and Their Complexes. 1999.

3. **Ahto Buldas**. An Algebraic Approach to the Structure of Graphs. 1999.

4. **Monika Drews**. A Metabolic Study of Insect Cells in Batch and Continuous Culture: Application of Chemostat and Turbidostat to the Production of Recombinant Proteins. 1999.

5. **Eola Valdre**. Endothelial-Specific Regulation of Vessel Formation: Role of Receptor Tyrosine Kinases. 2000.

6. **Kalju Lott**. Doping and Defect Thermodynamic Equilibrium in ZnS. 2000.

7. **Reet Koljak**. Novel Fatty Acid Dioxygenases from the Corals *Plexaura homomalla* and *Gersemia fruticosa.* 2001.

8. **Anne Paju**. Asymmetric oxidation of Prochiral and Racemic Ketones by Using Sharpless Catalyst. 2001.

9. **Marko Vendelin**. Cardiac Mechanoenergetics *in silico*. 2001.

10. **Pearu Peterson**. Multi-Soliton Interactions and the Inverse Problem of Wave Crest. 2001.

11. **Anne Menert**. Microcalorimetry of Anaerobic Digestion. 2001.

12. **Toomas Tiivel**. The Role of the Mitochondrial Outer Membrane in *in vivo* Regulation of Respiration in Normal Heart and Skeletal Muscle Cell. 2002.

13. **Olle Hints**. Ordovician Scolecodonts of Estonia and Neighbouring Areas: Taxonomy, Distribution, Palaeoecology, and Application. 2002.

14. **Jaak Nõlvak**. Chitinozoan Biostratigrapy in the Ordovician of Baltoscandia. 2002.

15. **Liivi Kluge**. On Algebraic Structure of Pre-Operad. 2002.

16. **Jaanus Lass**. Biosignal Interpretation: Study of Cardiac Arrhytmias and Electromagnetic Field Effects on Human Nervous System. 2002.

17. **Janek Peterson**. Synthesis, Structural Characterization and Modification of PAMAM Dendrimers. 2002.

18. **Merike Vaher**. Room Temperature Ionic Liquids as Background Electrolyte Additives in Capillary Electrophoresis. 2002.

19. **Valdek Mikli**. Electron Microscopy and Image Analysis Study of Powdered Hardmetal Materials and Optoelectronic Thin Films. 2003.

20. **Mart Viljus**. The Microstructure and Properties of Fine-Grained Cermets. 2003.

21. **Signe Kask**. Identification and Characterization of Dairy-Related *Lactobacillus*. 2003

22. **Tiiu-Mai Laht**. Influence of Microstructure of the Curd on Enzymatic and Microbiological Processes in Swiss-Type Cheese. 2003.

23. **Anne Kuusksalu**. 2–5A Synthetase in the Marine Sponge *Geodia cydonium*. 2003.

24. **Sergei Bereznev**. Solar Cells Based on Polycristalline Copper-Indium Chalcogenides and Conductive Polymers. 2003.

25. **Kadri Kriis**. Asymmetric Synthesis of C_2-Symmetric Bimorpholines and Their Application as Chiral Ligands in the Transfer Hydrogenation of Aromatic Ketones. 2004.

26. **Jekaterina Reut**. Polypyrrole Coatings on Conducting and Insulating Substracts. 2004.

27. **Sven Nõmm**. Realization and Identification of Discrete-Time Nonlinear Systems. 2004.

28. **Olga Kijatkina**. Deposition of Copper Indium Disulphide Films by Chemical Spray Pyrolysis. 2004.

29. **Gert Tamberg**. On Sampling Operators Defined by Rogosinski, Hann and Blackman Windows. 2004.

30. **Monika Übner**. Interaction of Humic Substances with Metal Cations. 2004.

31. **Kaarel Adamberg**. Growth Characteristics of Non-Starter Lactic Acid Bacteria from Cheese. 2004.

32. **Imre Vallikivi**. Lipase-Catalysed Reactions of Prostaglandins. 2004.

33. **Merike Peld**. Substituted Apatites as Sorbents for Heavy Metals. 2005.

34. **Vitali Syritski**. Study of Synthesis and Redox Switching of Polypyrrole and Poly(3,4-ethylenedioxythiophene) by Using *in-situ* Techniques. 2004.

35. **Lee Põllumaa**. Evaluation of Ecotoxicological Effects Related to Oil Shale Industry. 2004.

36. **Riina Aav**. Synthesis of 9,11-Secosterols Intermediates. 2005.

37. **Andres Braunbrück**. Wave Interaction in Weakly Inhomogeneous Materials. 2005.

38. **Robert Kitt**. Generalised Scale-Invariance in Financial Time Series. 2005.

39. **Juss Pavelson**. Mesoscale Physical Processes and the Related Impact on the Summer Nutrient Fields and Phytoplankton Blooms in the Western Gulf of Finland. 2005.

40. **Olari Ilison**. Solitons and Solitary Waves in Media with Higher Order Dispersive and Nonlinear Effects. 2005.

41. **Maksim Säkki**. Intermittency and Long-Range Structurization of Heart Rate. 2005.

42. **Enli Kiipli**. Modelling Seawater Chemistry of the East Baltic Basin in the Late Ordovician–Early Silurian. 2005.

43. **Igor Golovtsov**. Modification of Conductive Properties and Processability of Polyparaphenylene, Polypyrrole and polyaniline. 2005.

44. **Katrin Laos**. Interaction Between Furcellaran and the Globular Proteins (Bovine Serum Albumin β-Lactoglobulin). 2005.

45. **Arvo Mere**. Structural and Electrical Properties of Spray Deposited Copper Indium Disulphide Films for Solar Cells. 2006.

46. **Sille Ehala**. Development and Application of Various On- and Off-Line Analytical Methods for the Analysis of Bioactive Compounds. 2006.

47. **Maria Kulp**. Capillary Electrophoretic Monitoring of Biochemical Reaction Kinetics. 2006.

48. **Anu Aaspõllu.** Proteinases from *Vipera lebetina* Snake Venom Affecting Hemostasis. 2006.

49. **Lyudmila Chekulayeva**. Photosensitized Inactivation of Tumor Cells by Porphyrins and Chlorins. 2006.

50. **Merle Uudsemaa**. Quantum-Chemical Modeling of Solvated First Row Transition Metal Ions. 2006.

51. **Tagli Pitsi**. Nutrition Situation of Pre-School Children in Estonia from 1995 to 2004. 2006.

52. **Angela Ivask**. Luminescent Recombinant Sensor Bacteria for the Analysis of Bioavailable Heavy Metals. 2006.

53. **Tiina Lõugas**. Study on Physico-Chemical Properties and Some Bioactive Compounds of Sea Buckthorn (*Hippophae rhamnoides* L.). 2006.

54. **Kaja Kasemets**. Effect of Changing Environmental Conditions on the Fermentative Growth of *Saccharomyces cerevisae* S288C: Auxo-accelerostat Study. 2006.

55. **Ildar Nisamedtinov**. Application of ^{13}C and Fluorescence Labeling in Metabolic Studies of *Saccharomyces* spp. 2006.

56. **Alar Leibak**. On Additive Generalisation of Voronoï's Theory of Perfect Forms over Algebraic Number Fields. 2006.

57. **Andri Jagomägi**. Photoluminescence of Chalcopyrite Tellurides. 2006.

58. **Tõnu Martma**. Application of Carbon Isotopes to the Study of the Ordovician and Silurian of the Baltic. 2006.

59. **Marit Kauk**. Chemical Composition of $CuInSe_2$ Monograin Powders for Solar Cell Application. 2006.

60. **Julia Kois**. Electrochemical Deposition of $CuInSe_2$ Thin Films for Photovoltaic Applications. 2006.

61. **Ilona Oja Açik**. Sol-Gel Deposition of Titanium Dioxide Films. 2007.

62. **Tiia Anmann**. Integrated and Organized Cellular Bioenergetic Systems in Heart and Brain. 2007.

63. **Katrin Trummal**. Purification, Characterization and Specificity Studies of Metalloproteinases from *Vipera lebetina* Snake Venom. 2007.

64. **Gennadi Lessin**. Biochemical Definition of Coastal Zone Using Numerical Modeling and Measurement Data. 2007.

65. **Enno Pais**. Inverse problems to determine non-homogeneous degenerate memory kernels in heat flow. 2007.

66. **Maria Borissova**. Capillary Electrophoresis on Alkylimidazolium Salts. 2007.

67. **Karin Valmsen**. Prostaglandin Synthesis in the Coral *Plexaura homomalla*: Control of Prostaglandin Stereochemistry at Carbon 15 by Cyclooxygenases. 2007.

68. **Kristjan Piirimäe**. Long-Term Changes of Nutrient Fluxes in the Drainage Basin of the Gulf of Finland – Application of the PolFlow Model. 2007.

69. **Tatjana Dedova**. Chemical Spray Pyrolysis Deposition of Zinc Sulfide Thin Films and Zinc Oxide Nanostructured Layers. 2007.

70. **Katrin Tomson**. Production of Labelled Recombinant Proteins in Fed-Batch Systems in *Escherichia coli*. 2007.

71. **Cecilia Sarmiento**. Suppressors of RNA Silencing in Plants. 2008.

72. **Vilja Mardla**. Inhibition of Platelet Aggregation with Combination of Antiplatelet Agents. 2008.

73. **Maie Bachmann**. Effect of Modulated Microwave Radiation on Human Resting Electroencephalographic Signal. 2008.

74. **Dan Hüvonen**. Terahertz Spectroscopy of Low-Dimensional Spin Systems. 2008.

75. **Ly Villo**. Stereoselective Chemoenzymatic Synthesis of Deoxy Sugar Esters Involving *Candida antarctica* Lipase B. 2008.

76. **Johan Anton**. Technology of Integrated Photoelasticity for Residual Stress Measurement in Glass Articles of Axisymmetric Shape. 2008.

77. **Olga Volobujeva**. SEM Study of Selenization of Different Thin Metallic Films. 2008.

78. **Artur Jõgi**. Synthesis of 4'-Substituted 2,3'-dideoxynucleoside Analogues. 2008.

79. **Mario Kadastik**. Doubly Charged Higgs Boson Decays and Implications on Neutrino Physics. 2008.

80. **Fernando Pérez-Caballero**. Carbon Aerogels from 5-Methylresorcinol-Formaldehyde Gels. 2008.

81. **Sirje Vaask**. The Comparability, Reproducibility and Validity of Estonian Food Consumption Surveys. 2008.

82. **Anna Menaker**. Electrosynthesized Conducting Polymers, Polypyrrole and Poly(3,4-ethylenedioxythiophene), for Molecular Imprinting. 2009.

83. **Lauri Ilison**. Solitons and Solitary Waves in Hierarchical Korteweg-de Vries Type Systems. 2009.

84. **Kaia Ernits**. Study of In_2S_3 and ZnS Thin Films Deposited by Ultrasonic Spray Pyrolysis and Chemical Deposition. 2009.

85. **Veljo Sinivee**. Portable Spectrometer for Ionizing Radiation "Gammamapper". 2009.

86. **Jüri Virkepu**. On Lagrange Formalism for Lie Theory and Operadic Harmonic Oscillator in Low Dimensions. 2009.

87. **Marko Piirsoo**. Deciphering Molecular Basis of Schwann Cell Development. 2009.

88. **Kati Helmja**. Determination of Phenolic Compounds and Their Antioxidative Capability in Plant Extracts. 2010.

89. **Merike Sõmera**. Sobemoviruses: Genomic Organization, Potential for Recombination and Necessity of P1 in Systemic Infection. 2010.

90. **Kristjan Laes**. Preparation and Impedance Spectroscopy of Hybrid Structures Based on $CuIn_3Se_5$ Photoabsorber. 2010.

91. **Kristin Lippur**. Asymmetric Synthesis of 2,2'-Bimorpholine and its 5,5'-Substituted Derivatives. 2010.

92. **Merike Luman**. Dialysis Dose and Nutrition Assessment by an Optical Method. 2010.

93. **Mihhail Berezovski**. Numerical Simulation of Wave Propagation in Heterogeneous and Microstructured Materials. 2010.

94. **Tamara Aid-Pavlidis**. Structure and Regulation of BDNF Gene. 2010.

95. **Olga Bragina**. The Role of Sonic Hedgehog Pathway in Neuro- and Tumorigenesis. 2010.

96. **Merle Randrüüt**. Wave Propagation in Microstructured Solids: Solitary and Periodic Waves. 2010.

97. **Marju Laars**. Asymmetric Organocatalytic Michael and Aldol Reactions Mediated by Cyclic Amines. 2010.

98. **Maarja Grossberg**. Optical Properties of Multinary Semiconductor Compounds for Photovoltaic Applications. 2010.

99. **Alla Maloverjan**. Vertebrate Homologues of Drosophila Fused Kinase and Their Role in Sonic Hedgehog Signalling Pathway. 2010.

100. **Priit Pruunsild**. Neuronal Activity-Dependent Transcription Factors and Regulation of Human *BDNF* Gene. 2010.

101. **Tatjana Knjazeva**. New Approaches in Capillary Electrophoresis for Separation and Study of Proteins. 2011.

102. **Atanas Katerski**. Chemical Composition of Sprayed Copper Indium Disulfide Films for Nanostructured Solar Cells. 2011.

103. **Kristi Timmo.** Formation of Properties of $CuInSe_2$ and $Cu_2ZnSn(S,Se)_4$ Monograin Powders Synthesized in Molten KI. 2011.

104. **Kert Tamm**. Wave Propagation and Interaction in Mindlin-Type Microstructured Solids: Numerical Simulation. 2011.

105. **Adrian Popp**. Ordovician Proetid Trilobites in Baltoscandia and Germany. 2011.

106. **Ove Pärn**. Sea Ice Deformation Events in the Gulf of Finland and This Impact on Shipping. 2011.

107. **Germo Väli**. Numerical Experiments on Matter Transport in the Baltic Sea. 2011.

108. **Andrus Seiman**. Point-of-Care Analyser Based on Capillary Electrophoresis. 2011.

109. **Olga Katargina**. Tick-Borne Pathogens Circulating in Estonia (Tick-Borne Encephalitis Virus, *Anaplasma phagocytophilum*, *Babesia* Species): Their Prevalence and Genetic Characterization. 2011.

110. **Ingrid Sumeri**. The Study of Probiotic Bacteria in Human Gastrointestinal Tract Simulator. 2011.

111. **Kairit Zovo**. Functional Characterization of Cellular Copper Proteome. 2011.

112. **Natalja Makarytsheva**. Analysis of Organic Species in Sediments and Soil by High Performance Separation Methods. 2011.

113. **Monika Mortimer**. Evaluation of the Biological Effects of Engineered Nanoparticles on Unicellular Pro- and Eukaryotic Organisms. 2011.

114. **Kersti Tepp**. Molecular System Bioenergetics of Cardiac Cells: Quantitative Analysis of Structure-Function Relationship. 2011.

115. **Anna-Liisa Peikolainen**. Organic Aerogels Based on 5-Methylresorcinol. 2011.

116. **Leeli Amon**. Palaeoecological Reconstruction of Late-Glacial Vegetation Dynamics in Eastern Baltic Area: A View Based on Plant Macrofossil Analysis. 2011.

117. **Tanel Peets**. Dispersion Analysis of Wave Motion in Microstructured Solids. 2011.